Cellular Forces

Adhering, Shaping, Sensing and Dividing

PROEFSCHRIFT

ter verkrijging van
de graad van Doctor aan de Universiteit Leiden,
op gezag van Rector Magnificus prof. mr. C.J.J.M. Stolker,
volgens besluit van het College voor Promoties
te verdedigen op 26 november 2014
klokke 10:00 uur

door

Hedde van Hoorn

geboren te Marum, Nederland
in 1983

Promotiecommissie

Promotor:	Prof. dr. T. Schmidt
Overige leden:	Dr. E.H. Danen
	Prof. dr. E.R. Eliel
	Prof. dr. B. Ladoux (Université Paris Diderot, France)
	Dr. ir. S.J.T. van Noort
	Prof. dr. H. Schiessel
	Dr. C. Storm (TU Eindhoven)

Cover: HeLa cell at the end of mitosis, visualized with tubulin-GFP and "Vitruvian Man" by Leonardo da Vinci.

Casimir PhD Series, Delft-Leiden, 2014-28
ISBN 978-90-8593-201-7
An electronic version of this thesis can be found at
https://openaccess.leidenuniv.nl

Het onderzoek beschreven in dit proefschrift is onderdeel van het wetenschappelijke programma van de Stichting voor Fundamenteel Onderzoek der Materie (FOM), die financieel wordt gesteund door de Nederlandse organisatie voor Wetenschappelijk Onderzoek (NWO).

"Through measurement to knowledge."
Heike Kamerlingh Onnes

Voor Bart, Melissa, Inez, Peter en Vivian.

Contents

Chapter 1

Introduction [1]

abstract

This chapter gives an overview of recent advances in the field of cell mechanics. Mechanical cues influence many biological processes and a wide range of stiffnesses is present in different parts of the body. Powerful new experimental tools have expanded our understanding of constitutive processes at a single cell level. In particular, a combination of imaging and micro-fabrication techniques provide valuable insights into the differential cellular response to extracellular stiffness on a subcellular level.

[1] This chapter is based on: H. van Hoorn and T. Schmidt, A closer look at cellular forces - inversion improves resolution, to be submitted

1.1 Mechanics matters

The human body continually applies deformative stresses and strains while performing a multitude of functions [1–5]. Deformation takes place on a range of length scales and stiffnesses. Blood is pumped through the vasculature, muscles are flexed in sarcomeric multicellular structures, and single cells (such as fibroblasts and neutrophils) exert significant forces on the extracellular matrix (ECM) while performing their task. In order to properly function at these different length scales, biological matter exhibits a great variety in mechanical characteristics.

The mechanics in such processes has been quantified in a wide range of previous studies. For example, endothelial cells lining blood vessels need to withstand the significant shear flow of 0.1-7 Pa throughout the vasculature [5]. An aggregate of approximately 500 contracting cardiomyocytes can produce periodic forces of $\sim$10 μN with a stress accumulation $\sim$1 kPa [6]. And individual neutrophils exert nN forces on the ECM to invade [7] and adapt their membrane tension to phagocytose [8]. The mechanical behavior of cell aggregates, tissues and single cells is vital to their functioning in an organism. To gain a quantitative fundamental understanding of cell mechanics, we view a single cell as the basic building block. We aim to measure and understand how constitutive cellular processes contribute to cellular deformation and force exertion. This biophysical behavior in turn expands our understanding of a wide range of biological functions.

Several crucial processes in cell biology have been shown to depend on mechanical cues. Stem cell differentiation [9–11], cell migration [12, 13] and cancer progression [14, 15] have been directly linked to stiffness, force exertion and deformation. At a single cell level, contractile forces are typically exerted in the order of 1 - 100 nN at a single adhesion site [16–19]. All higher order structures making up tissues and other multi-cellular systems, are comprised of these basic building blocks. Constitutive cell mechanics is given by a cell's ability to deform and exert forces in relation to intracellular protein localization and activation.

Still, the relevance of quantified cell mechanics to its biological niche needs to be taken into account. Therefore, we first discuss the variation of stiffness throughout an organism providing a framework for the relevance of extracellular stiffness. Next, we discuss recently developed methods to probe cell mechanics. Experimental approaches have been developed on a global or local scale that measure cellular mechanics ei-

ther through active perturbation or passive observation. We then discuss possible mechanical mechanisms that can influence biological behaviour and how cellular force exertion and deformation can be inferred from biological processes. Finally, we make a case that high-resolution imaging combined with new technology probing mechanics can provide answers to many crucial biophysical questions.

1.2 Stiffness varies

To properly compare the stiffness in the body, it must be described by a common variable. While a variety of moduli have been used in prior studies, we transferred all previous results to the common stiffness characteristic denoted by the Young's modulus [20]. This modulus describes a linear response between applied stress and strain thus giving a measure for stiffness, as given in equation (1.1). When studies reported a shear modulus, we directly translated this into a Young's modulus assuming incompressability of the material (i.e. a Poisson ratio ν of 0.5 with $E = 2(1 + \nu)G$). To enable comparison between various results, we consistently denoted here the stiffness by the Young's modulus or an equivalent measure.

$$\sigma = E \cdot \varepsilon \tag{1.1}$$

Diversity in the mechanical environment of a cell is best described by quantification of the stiffness. Next to the important assumption of linear elasticity, another difficulty in interpreting results is the length scale at which stiffness is probed. This is especially important since the length scale at which cells probe their environment remains a subject of debate [17, 21, 22]. We will discuss this in section 1.5. Furthermore, the stiffness found *in vivo* at various lengthscales has proven to vary by several orders of magnitude [23].

The length scale that is probed depends on the technique that is used. In previous studies, excised organs or reconstituted organ systems were probed either by a nano-scale indenter (typically using a probe with an Atomic Force Microscope - AFM) at a very local scale. The curvature of an AFM-tip is $\sim$ 10-100 nm. A larger $\sim$ 1-100 μm micron-sized probe has also been used to measure stiffness, as well as an optical cell stretcher [24], to measure stiffness. In some studies, a macro-scale measurement was performed, typically using a rheometer, a tensile test apparatus or a

macro-indenter. We collected the results from measurements at different length scales and methods and discuss variations among different data sets - if they were observed - and relate them to length scale and/or experimental technique. Overall, we assumed linear elasticity, a similar and homogeneous stiffness for the different tissues in mammals and an identical local and global stiffness. It should be noted that for large deformations, simple linear elasticity does not hold for many biological networks [25, 26]. With these considerations in mind, we collected experimental data to show the diversity of stiffness in a (human) body.

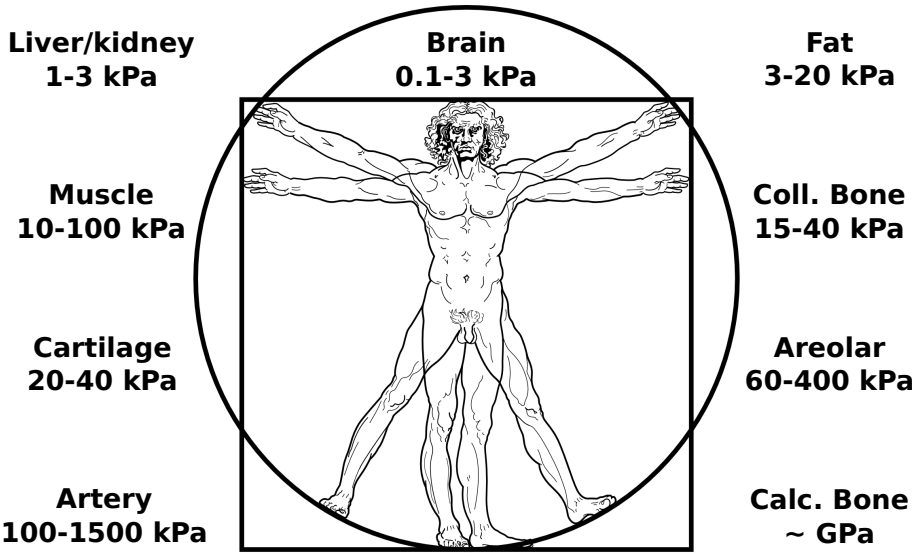

Figure 1.1
Stiffness varies throughout the human body. Stiffness is quantified through the Young's modulus and spans multiple orders of magnitude throughout the human body, as probed by experiments over various length scales. [2]

Figure 1.1 shows an overview of the wide range of measured stiffnesses throughout the body (see also recent reviews [5, 27, 28]). The softest region is the brain, where stiffnesses ranging from 0.1 to 3 kPa have been reported [29–32]. Interestingly, these measurements were mostly performed in macro-scale experiments that showed a relatively higher

[2] Image adapted from stock photo at www.freepik.com

stiffness. The only microscale AFM indentation study [29] showed a stiffness of the rat hippocampus of 0.1-0.4 kPa. The stiffness of brain tissue at a smaller length scale may thus be even smaller, though this is technically a difficult experiment to perform.

Both macroscale rheometer measurements on freshly excised liver [33] and microscale measurements on the glomerular capsule of the kidney [34] showed a similar stiffness range of 1-3 kPa. Fat has been reported to have a stiffness of 3 kPa [11]. In another study the stiffness of fat tissue has been quantified only by means of ultrasonic measurement on a macroscale [35] and was found to be (20±10) kPa. The broadest interpretation of the stiffness of fat is thus a range of 3-20 kPa. Similar difficulties arose when looking for the stiffness of lungs [36] and the endothelium [37], where values ranging from 1 to 100 kPa could be found, but were not always clear in their interpretation.

More experimental data is available for the stiffness of muscle tissue and cells. Excised mouse muscle showed a stiffness of (12±4) kPa [38]. AFM indentations on (skeletal) muscle cells showed a larger range of stiffnesses of 10-40 kPa [37, 39]. One of these studies also addressed the stiffness of cardiac muscle, which was found to be 100 kPa [37]. Another study which measured the stiffness of excised heart found the Young's modulus to be (18±2) kPa [40]. From this we conclude that muscle stiffness spans a wide range of 10-100 kPa.

Stiffness measurements of cartilage (from human tissue) showed a stiffness of 20-40 kPa, using both micropipette aspiration and AFM indentation techniques [23, 41]. Variations in these results can largely be explained by a difference in microscale versus nanoscale stiffness. One previous study [23] showed that the nano-indentation results on mouse tissue probed the individual collagen fibrils. In the same study, however, microscale indentations could not resolve the fibrils and yielded very different results, where the large scale stiffness was 2 orders of magnitude larger. The nanoscale indentation results corresponded well to the previous measurements. We thus conclude that a reasonable estimate for the stiffness of cartilage is 20-40 kPa.

Through nanoscale AFM indentations, collagenous (not calcified-) bone was found to be (27±10) kPa [9]. Global stiffness measures (tensile tests) on fibroblast-populated reconstituted matrices showed that areolar tissue could obtain stiffnesses of 60-400 kPa [42, 43]. Rat arteries showed an even larger stiffness of 100-1500 kPa [44]. The stiffness of calcified

bone was determined to be much larger still, with stiffnesses measured in the order of GPa [9, 27].

Throughout an organism a huge variety in stiffness is present. Without calcified bone, biological functionality is carried out over 5 orders of magnitude of stiffness. Stiffness is likely an emergence of evolution through diversification of biological material. Further evolution undoubtedly also guided functional responses to this diversification of stiffness. Biological matter has accordingly developed a coupling between biological and mechanical behavior at a cellular level. Understanding of the biological-mechanical coupling in the function of living matter is therefore crucial when dissecting many of life's processes. Precise tools to control- and measure the mechanics of cells are vital in this research.

1.3 Techniques advance

For a quantitative understanding of cell mechanics we need to probe forces and measure deformations while monitoring relevant biological processes. In recent years, many technical steps forward have been taken that enable the accurate measurement of cellular forces and deformations. Active perturbation of cells yields new information about the outside-in coupling and response to a physical stimulus. This stimulus is often physiologically relevant, such as the deformation of heart muscle cells during the beating of a heart or the active deformation that expands lungs during breathing. In other processes, it is interesting to observe the inside-out coupling of a cell through a passive measurement. One can observe the local movement of vesicles, beads or fluorescently labeled proteins inside a cell, for instance. The extracellular deformation caused by a cell also povides important information in processes such as cancer cell migration to form metastasic sites. Figure 1.2 gives an impression of techniques that actively deform or passively quantify cell mechanics on a local or global cellular scale.

1.3.1 Active deformation

Techniques actively probing cell mechanics include the application of atomic force microscopy (AFM), magentic tweezers (MTs) and a substrate stretcher [5, 45]. Local stiffness mapping of fibroblasts on substrates of different rigidities with an AFM showed that the stiffness of

fibroblasts corresponded to the stiffness of their substrate up to a stiffness of 20 kPa [46]. Using MTs, it was possible to quantify the dynamic stiffness moduli of the cellular membrane [47]. These exciting developments allow one to measure local mechanical characteristics by actively perturbing a cell.

Since the intracellular organization is comprised of many components, it is also interesting to examine the cell-wide response to perturbation. An important and physiologically relevant perturbation is the physical stretching of whole cells through the ECM. Physical cell stretching occurs, for instance, when muscle cells contract or lungs expand. Several setups have been designed that enable the deformation of cells on a substrate [48–50]. Cells can also be stretched by trapping in a focussed optical beam [24], enabling mechanical characterization of cells in suspension. The effect of disease on the force exertion characteristics by muscle cells is often quantified using dynamic force transducers, for instance to elucidate the effect of hypoxia [51].

In recent years, whole-cell active deformation has provided many valuable insights. Global alignment of the actin cytoskeleton was shown to occur when cells were stretched at mHz frequencies [49]. Organ level functions of a lung were even obtained by actively stretching a layered device with different cell types by mimicking functional alveoli [50]. Cell division, which is guided through a massive re-organization of the microtubule network, was shown to occur preferentially in the direction in which cells were stretched [52]. And a clue for a local mechanosensory mechanism was provided by global stretching of an intact cellular cytoskeleton that showed stretch-dependent phosphorylation of the putative mechanosensor p130Cas [53]. By globally deforming a whole cell on a stretchable membrane, the response of a cell can thus yield important new insights in the relation between active deformation and biological function.

1.3.2 Passive cell mechanics

Instead of actively deforming a cell, much can be learned from passively observing cell mechanics. Several intriguing techniques have been developed, among which the incorporation of submicron-particles into cells [54]. By performing tracking and (nano-)rheology experiments mechanical properties of cells are quantified. Using this technique, the role of the keratin intermediate filament network was investigated in determining

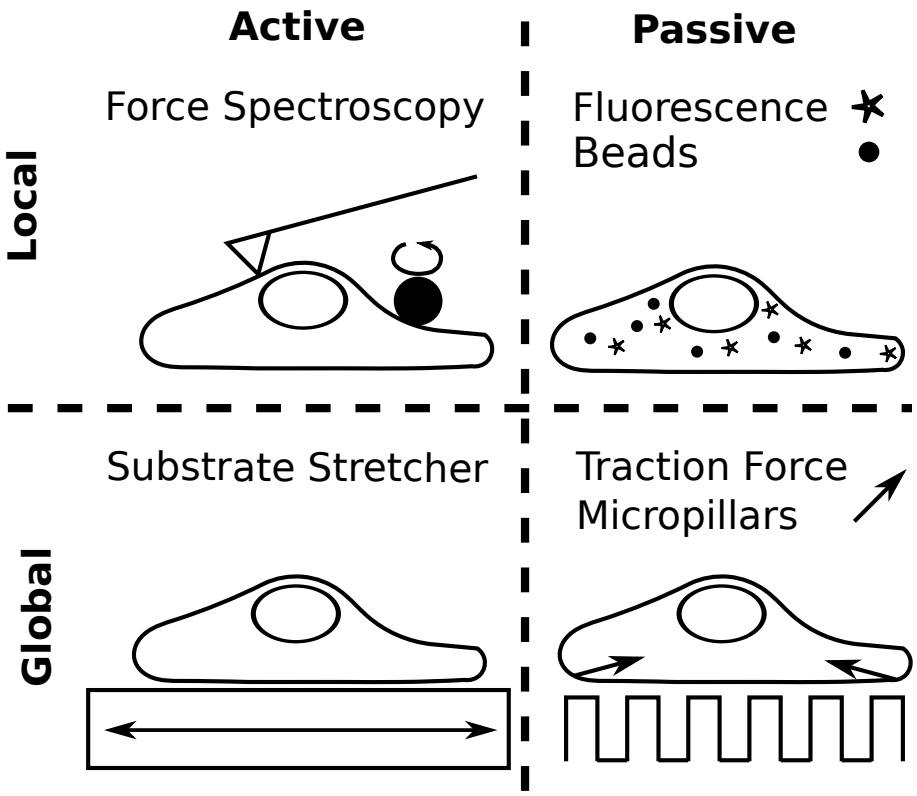

Figure 1.2
Approaches to probing Cell Mechanics. Active probing is done on a local scale by force spectroscopy techniques such as atomic force microscopy, magnetic tweezers or optical tweezers. Global active cellular deformation is achieved by stretching a substrate to which cells are attached. Passive- and local mechanics is probed by tracking beads or through fluorescence methods. On a global scale, cell mechanics is quantified by traction force microscopy or micropillars with which one can measure cellular force exertion.

subcellular stiffness [55]. In fibroblasts, the effect of actomyosin contractility on intracellular stiffness was measured [56]. Using a dual-labeling technique it was shown that stretch of a single talin molecule was dependent on myosin activity [57]. A FRET-based intracellular force sensor was designed by attaching to fluorophores onto either side of a spider-silk protein, for which force and distance were calibrated [58]. These techniques provide information on the local intracellular mechanics through

an optical readout.

Instead of locally probing cell mechanics, passive measurement of how cells deform their enivronment is a topic of increasing interest. This approach has been the main focus of our research. In such studies mechanics is typically probed passively and on a cell-wide scale. Cell-wide force exertion was first quantified by tracking the wrinkles on a stretchable silicon substrate [59, 60]. This technique was adapted to include fluorescent beads [61] or regular patterns [16, 62] that could track the deformation field caused by a cell with higher accuracy and was termed traction force microscopy (TFM). This technique can yield a high-resolution force map [63] and was recently expanded to also quantify the out-of-plane force exerted locally at a site of adhesion [64]. TFM has provided many important insights in the way cells deform their environment and forces are transmitted. However, the effect of a varying extracellular stiffness remains difficult to investigate, since changing the stiffness of a substrate used in TFM invariably changes the local molecular architecture (i.e. connectivity, pore-size and active groups) of the substrate. Through this disadvantage, TFM cannot decouple the global extracellular stiffness and the local adhesion stoichiometry.

1.3.3 Micropillars

After the development of TFM, micropillar substrates were developed [65, 66]. With etching techniques on silicon wafers, a template for replica-molding with Poly(DiMethyl-)Siloxane (PDMS) was constructed [67, 68]. PDMS can be activated through oxidation which enables the direct binding of ECM proteins onto the surface. When the micropillars are functionalized through micro-contact printing [69] and the remaining PDMS is passivated, cells only attach to the very tops of the micropillars. Since cells mainly exert in-plane forces, this makes the pillar force-deflection relationship relatively easy to solve. Calculating back from a continuous substrate strain field to local force exertion sites (as is needed for TFM) is possible, but not straightforward [62]. Furthermore, variation in etch depth and thus pillar height provides direct control over the bending modulus of a single pillar and the global extracellular stiffness.

By measuring the deflections imposed onto micrometer-sized posts, the force a cell locally exerts is directly quantified. A disadvantage to micropillars relative to TFM is that the substrate is no longer continuous since the individual pillars need space to deform. Advantages to micropil-

lars are the more straightforward interpretation of the force-deflection relationship and the possibility to change the global extracellular stiffness (i.e. the pillar bending modulus) without changing the local site of attachement. Increasing the micropillar height decreases the global stiffness, while decreasing the height increases the stiffness.

The typical approximation for the force-deflection relationship is given by the well-known Euler-Bernoulli beam theory [20], as given for a circular beam in equation (1.2). The force F relates to the pillar deflection δ through the bulk material stiffness E, the pillar diameter d and pillar height h. Both diameter and height greatly influence the bending modulus through a fourth power and third power, respectively. The diameter of our pillars was 1 or 2 μm with a center-to-center distance of 2 or 4 μm, respectively. The range of diameter and spacing is limited since the dimensions need to be large enough to be accurately engineered and its deflection needs to be detected, while it needs to be small enough to be able to probe the force exerted by a cell at multiple locations. Importantly, the local stiffness E does not need to change, while the cell-wide global stiffness does change, decoupling the local extracellular environment from the global stiffness. In the current debate on whether cellular mechanosensing takes place on a local [21, 22, 70] or cell-wide global scale [11, 17], decoupling of these parameters can provide important insights.

$$F = \frac{3\pi}{64} \cdot E \cdot \frac{d^4}{h^3} \cdot \delta \tag{1.2}$$

Micropillar arrays have been used in a variety of ways since their development. It has been shown that asymmetric micropillars guide cell migration [71], heart muscle cells have been suspended between pillars to examine their mechanical function [72] and individual micropillars have been actively deflected using a magentic probe to exert a local force on a cell [73]. It has even been shown that stem cell differentiation depends on the global stiffness of the cellular environment as it is changed by pillar height [10, 68] The advent of micropillars, and microstructured materials in general, has much promise to elucidate many of the outstanding questions in cell mechanics. However, to directly relate local cellular mechanics to biology, high-resolution optical microscopy must be possible simultaneously.

1.4 Combining imaging and mechanics

Next to cell mechanics techniques, optical microscopy has undergone a transformation as well in recent years. Breakthroughs were first made in single molecule spectroscopy [74] and sub-diffraction limit [75] localization of the intensity profile emitted by single molecules in live cells [76], enabling the localization of single fluorescent molecules. By localizing many molecules in rapid succession, super-resolution microscopy was developed less than a decade ago. Simultaneously, STochastic Optical Reconstruction Microscopy (STORM) [77], PhotoActivated Localization Microscopy (PALM) [78] and fluorescence PhotoActivation Localization Microscopy (fPALM) [79] were developed, all adhering to the same principle. Rapid switching of either fluorescent dyes or photo-convertible fluorophores provides a reconstruction of a labeled structure with a resolution better than the fundamental diffraction limit [75]. STORM microscopy was simplified by introducing a reducing agent and by using standard fluorescent dyes [80, 81]. This innovation was termed direct STORM (dSTORM) and made the experiment easier to perform.

Super-resolution techniques can answer many open questions in cell mechanics. Processes in cell mechanics often take place beyond the diffraction limit through local molecular interactions. Especially when we consider mechanosensory mechanisms (further elaborated on in section 1.5) where a single or a few molecules localize differentially depending on mechanical features (e.g. extracellular stiffness). To enable the combination of the measurement of cell mechanics and single-molecule microscopy we needed to advance current techniques.

Limiting in the detection of single molecules is the amount of light one can detect. The localization precision of a molecule scales with the inverse square-root of the number of photons observed [82]. However, in super-resolution microscopy this light also needs to be obtained within a limited timespan. Drift in the setup or the physical movement of a structure can blurr a reconstructed image. Furthermore, approximately 10,000 - 100,000 single molecules need to be detected. These practical conditions set limits to the design of a super-resolution imaging technique. To detect sufficient photons from a single molecule, the angle under which light is collected through the objective needs to be as large as possible. An objective with a high Numerical Aperture (NA) is therefore a prerequisite for super-resolution microscopy (see figure 1.3A).

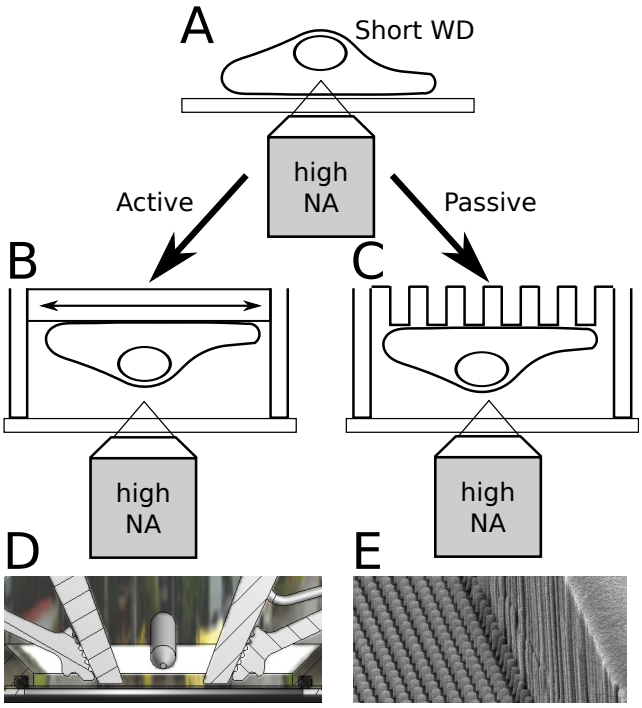

Figure 1.3
Imaging cell mechanics at high resolution. (A) High resolution imaging requires the use of a high-NA objective with a short working distance (WD). (B) Active- and (C) passive probing of cell mechanics can be achieved simultaneously with high-resolution imaging by inverting a substrate stretcher and micropillar array, respectively (A-C not to scale). (D) Clamps holding a 100 μm thin PDMS sheet (distance between clamps is 8 mm) can stretch a substrate and (E) spacers with a height of 50 μm on the side of a micropillar array (pillar diameter is 2 μm) both keep cells within the short WD of a high-NA objective.

1.4.1 Inversion improves resolution

The fundamental difficulty with a high-NA objective is the short working distance. Since light under a large angle is observed, the distance at which objects are in focus is small, typically 100-170 μm. Many techniques that probe cell mechanics, however, involve microfabricated structures that make approaching the sample at such distances impossible. In these cases, imaging is either performed through this microfrabricated structure or using a water-dipping objective. In both cases, it

is not possible to use a high-NA objective. Furthermore, devices that probe cell mechanics are typically made of Poly-Acrylamide (PA) or Poly(DiMethyl-)Siloxane (PDMS) that have a refractive index of 1.45 and 1.4, respectively [69, 83]. Imaging through structures with a different refractive index from glass (n=1.515) and water (n=1.333) further complicates high-resolution imaging.

Recently, we have been able to adapt techniques that either actively deform cells or probe cellular force exertion to enable the use of a high-NA objective. We adapted a substrate stretcher so the mechanical stretching was inverted and close to the coverslip (see figure 1.3B and D). The mechanical clamps are held in place $\sim$ 50 µm above a 100 µm coverslip, keeping the total distance from objective to cell and substrate within the desired WD. A thin PDMS sheet was used as a membrane of only 100 µm thickness, so the transverse strain would not shrink the sheet out of range of the WD. We have quantified the strain field of this device and performed succesful initial experiments stretching live cells. Experiments with the inverted substrate stretcher are out of the scope of this thesis and will be discussed elsewhere.

In a similar inversion-approach, we adapted micropillars by adding flanking 50 µm spacers so we could invert them onto a 100 µm coverslip (see figure 1.3C and E). Cells remained viable on these inverted micropillar arrays and their mechanical behaviour seemed unaltered. This approach allowed us to measure cellular force exertion and perform super-resolution microscopy simultaneously [19] (chapter 2). With the potential to probe cell mechanics and carry out high-resolution microscopy, we further focussed on fundamental cellular processes.

1.5 From mechanics to biology (and back)

The basic principle of a mechanical feature (e.g. deformation or stiffness) that influences a biological process has been termed mechanosensing (see figure 1.4). It is most clearly envisioned by the mechanical activation of a protein which induces a conformational change that leads to biological activity. This process can occur in several different ways, as will be described by means of individual examples. Mechanical activation can be caused by physical stretching, as was measured for p130Cas and talin [53, 57]. More well-studied are mechanosensitive channels, in particular in bacteria where the structure of the large-conductance mechanosensitive

channel MscL [84] for instance shows a large complex that opens when the membrane tension changes.

After mechanical activation, molecular adaptation is needed. This can be physical stretching (as is the case for p130Cas and talin) or opening of a pore complex (as is the case for mechanosensitive channels). Conformational changes of a mechanosensory protein or -structure finally activate a biological pathway. This cascade of events can be performed through activation of a kinase, or by enabling a protein to bind to the mechanosensory protein and form a multi-protein complex (for p130Cas and talin, respectively). Mechanosensitive channels typically allow the influx of ions that in turn influence a wide range of biological processes. Kinase activation or protein binding in turn activates downstream biological signalling pathways. As many biological pathways are cascades with positive feedback, a mechanosensory mechanism can also further amplify the mechanosensory response through such a mechanism.

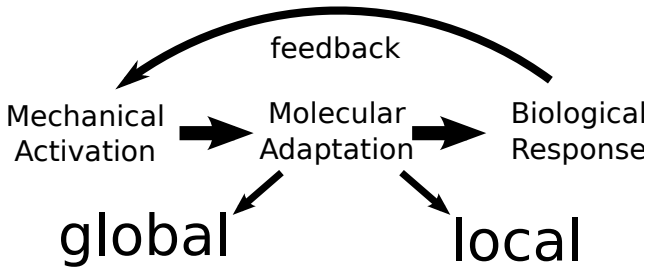

Figure 1.4
Mechanosensing as a direct molecular mechanism. A mechanical activation causes a molecular adaptation. This can occur globally (cell-wide) through network adaptation or locally (at single- or several protein level) through direct molecular response. Finally a biological response changes functionality that feeds back onto the activation.

1.5.1 Mechanosensing through network reorganization

Manifestation of a biological phenotype is thus observed as a result of varying stiffness. However, the exact molecular mechanism that mediates mechanosensing is often not understood. The most striking mechanosensory observation was the stiffness-dependent differentiation of mesenchymal stem cells (MSCs) on poly-acrylamide gels [9]. MSCs showed a myosin-dependent response on substrates with a stiffness of 0.1 - 1 kPa,

10 kPa and 30-40 kPa with markers for neurogenic, myogenic and osteogenic differentiation, respectively. A follow-up experiment showed that it was not the local extracellular stiffness, but the global cell wide micron-scale stiffness that induced differentiation as confirmed by experiments on micropillars [10, 68]. More recently it was shown that the lamin-network around the cell nucleus adapted especially the laminA-content to changes in the extracellular stiffness [11]. Notably, a correlation between laminA:laminB ratio was found with tissue microelasticity *in vivo*. These observations imply that the ECM stiffness can cause a global cellular network adaptation as a mechanosensory response. A further fundamental understanding of how forces are transmitted throughout cellular networks is thus vital to understanding these mechanosensory processes.

Another striking global cellular mechanosensing response was termed mechanotaxis, in which cells migrate depending on mechanical cues. Mechanotaxis was observed by differential migration depending on shear flow [85]. Durotaxis is the most well-known subset of mechanotaxis that describes how cells migrate depending on the stiffness of their extracellular environment or substrate [86]. Again using micropillars, it was recently shown that durotaxis in fact depends on the global extracellular stiffness [17]. At a barrier where micropillars changed their diameter, the effective global stiffness greatly increases with micropillar diameter (see equation (1.2)). Indeed, at this barrier, fibroblasts migrated towards the stiffer micropillars, demonstrating the effect of another global mechanosensing mechanism. This phenomenon can be directly explained by the fact that fibroblasts [17–19], epithelial cells [18, 87] and muscle cells [18, 88] exert pulling forces towards the cell body that increase with extracellular stiffness.

Changing the stiffness of the extracellular environment thus causes a fundamentally different response in cellular mechanics. Cellular mechanotransduction is mainly mediated by myosin-dependent contraction of the actin cytoskeleton [89]. To gain further insight into how forces are transmitted and shape the cell, we examined the effect of actin cytoskeletal orientation at the cellular periphery in relation to cell geometry and force exertion (chapter 3). Such insights in the force balance of cellular networks provide important cues into how cellular forces are transmitted globally.

1.5.2 Local activation through force

Another mechanism through which a cell can respond to extracellular mechanical cues is through direct local changes in molecular conformation. We and others have observed that cells in stiffer environments typically exert larger force [17, 18] (chapter 4). Of particular interest in this respect is the focal adhesion (FA) complex [90, 91]. A schematic of intracellular forces transmitted through the FA to the ECM is depicted in figure 1.5. The cytoskeletal structure inside the cell comprises of intermediate filaments, microtubules and actin filaments. The actin cytoskeleton is connected to the FA, which comprises of a multitude of biologically functional interactions [92]. Integrin heterodimers then span the cell membrane, connecting the FA complex to ECM proteins (e.g. fibronectin, collagen or laminin). One can imagine that mechanosensing through protein localization or -activation takes place in the FA, as forces are transmitted in this co-localization of mechanical stress and biological functionality.

The FA complex as a whole grows with local force exertion and its global assembly is force-dependent [16–19]. The reported size distribution of FAs does not increase accordingly with stiffness, so the force per protein increases with increasing stiffness. Mechanosensitive activity has already been indicated or reported for multiple FA proteins. An intriguing observation was made in the force-dependent unfolding of talin which enables binding of vinculin [57]. Recently, single-molecule force spectroscopy and binding assays confirmed the unfolding of talin, and binding of vinculin upon forces of $\sim$5 pN, with a differential role for higher and lower forces [93]. Forces in the range of 10 pN per protein are likely typical for the adhesion complex, as a minimum of 30-40 pN per integrin is the minimum force needed for cell spreading [94].

1.5.3 P130Cas as a mechanosensor

The mechanosensitive protein of our interest is the multi-functional scaffolding protein p130Cas [95]. When fixed cell cytoskeletons were stretched on a substrate, it was observed that p130Cas would phosphorylate, indicating stretch-dependent signalling activation [53]. The intrinsically disordered substrate domain [96] has 15 YxxP motifs that can be tyrosine phosphorylated by Src. In cancer progression, it was shown that p130Cas promotes invasiveness in Src-transformed cells [97], giving this

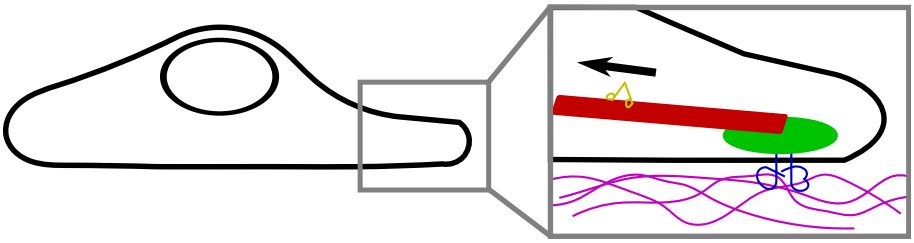

Figure 1.5
Local cellular force exertion. Zoomed in on an adhesion site, cellular contractile force (arrow) is exerted towards the cell body through myosin-motor activity (yellow) on the actin cytoskeleton and stress fibers (red). The actin cytoskeleton attaches to focal adhesion complexes (green) through many molecular interactions. Force is transmitted through integrin heterodimers (blue) that connect intracellular proteins to the extracellular matrix (pink).

biophysical process added relevance. In further studies it was shown that p130Cas directly influences actin polymerization and branching as well as FA dynamics [98, 99].

To further investigate the response of p130Cas in live cells and on varying stiffnesses, we performed experiments on Mouse Embryonic Fibroblasts (MEFs) lacking p130Cas (chapter 4). We compared MEFs with p130Cas-YFP reintroduced at endogenous levels to MEFs without p130Cas or without its two FA-targeting domains. We found that p130Cas does indeed have a mechanosensory function in a physiological stiffness range of 40-150 kPa, within the range of areolar tissue stiffness [42, 43]. Differential localization to FAs depends on the global extracellular stiffness. Furthermore, we found that this differential localization had an effect on the local force exertion characteristics on a single micropillar. Cells expressing truncated p130Cas (inhibiting localization to FAs) showed different force exertion characteristics, directly demonstrating the role of p130Cas in force exertion. P130Cas thus not only acts as a sensor, but also directly influences the mechanical response.

1.5.4 Force exertion during cell division

Finally, we investigated the cell mechanics implications of cell division. The process is evidently ubiquitous in life and development, and as such the mechanical progression is important to study. We characterized pro-

gression through the cell cycle (chapter 5) and found that the typical pulling force toward the cell center on a substrate was released. Instead, cells went through progressive steps in outward pushing forces that consistently preceded a well-known biological phenotype. We hypothesized a force balance that is set up by reorganizing the internal cytoskeleton and in particular the mitotic spindle and alignment of chromosomes.

A force-dependent role for kinetochore activation to continue through mitosis with kinase Aurora B was previously proposed [100]. We observed mitotic disturbance with a tripolar spindle coinciding directly with a lack of outward pushing and thus a disturbance of the force balance. These results show the need for mechanical integrity for progression through mitosis and direct proof of a mechanosensory effect in division.

1.6 Outline of this thesis

In **chapter 2** our adaptation to micropillars that enables the use of high-resolution optical microscopy is presented. Simultaneous measurement of cellular force exertion on the ECM and high resolution live- and fixed cell microscopy shows normal cellular morphology and mechanics. Using direct STochastic Optical Microscopy FAs are super-resolved and shown to be smaller structures than previously quantified. The connection between the intra- and extracellular matrix thus is shown to bear a high concentration of cellular forces.

In **chapter 3** micropillar force measurements and fluorescence microscopy on live 3T3 fibroblasts show how extracellular force exertion correlates to the intracellular actin cytoskeleton. Locally, actin fibers co-orient with force exertion and globally the cellular shape shows circular arcs, described by a local mechanical equilibrium. The local orientation of the actin cytoskeleton influences curvature of arcs spanning the cell membrane and the guidance of force exertion.

In **chapter 4** the response in function of p130Cas to variations in extracellular stiffness is described. Over an extracellular stiffness of poly-Acrylamide gels of 42-87 kPa, the presence of p130Cas changes FA formation. In fact, p130Cas localizes to FAs predominantly on micropillar arrays with a global stiffness larger than 47.2 kPa. Its differential localization also changes the force exertion dynamics on single micropillars, changing cell mechanics. P130Cas thus couples not just from mechanics to biological activity but also changes cellular forces.

In **chapter 5** the cell division cycle is related to extracellular force exertion. For the first time, a passive extracellular force measurement of the evolution of a force balance throughout mitosis is quantified. Outward pushing forces from the cell center to the ECM increase throughout mitosis. The observed force balance proves vital in maintaining integrity of the mitotic spindle and succesful cell division.

Bibliography

[1] Dennis E Discher, Paul Janmey, and Yu-Li L Wang. "Tissue cells feel and respond to the stiffness of their substrate." In: *Science* 310.5751 (2005), pp. 1139–1143.

[2] Viola Vogel and Michael Sheetz. "Local force and geometry sensing regulate cell functions." In: *Nat. Rev. Mol. Cell Bio.* 7.4 (2006), pp. 265–275.

[3] Bruce Alberts et al. *Molecular Biology of the Cell.* 5th ed. Garland Science, 2008.

[4] Jeroen Eyckmans et al. "A hitchhiker's guide to mechanobiology." In: *Dev. Cell* 21.1 (2011), pp. 35–47.

[5] William J Polacheck et al. "Microfluidic platforms for mechanobiology." In: *Lab Chip* 13.12 (2013), pp. 2252–2267.

[6] Thomas Boudou et al. "A microfabricated platform to measure and manipulate the mechanics of engineered cardiac microtissues." In: *Tissue Eng. Pt. A* 18.9-10 (2012), pp. 910–919.

[7] Aleksandr Rabodzey et al. "Mechanical forces induced by the transendothelial migration of human neutrophils." In: *Biophys. J.* 95.3 (2008), pp. 1428–1438.

[8] Marc Herant, Volkmar Heinrich, and Micah Dembo. "Mechanics of neutrophil phagocytosis: experiments and quantitative models". In: *J. Cell Sci.* 119.9 (2006), pp. 1903–1913.

[9] Adam J Engler et al. "Matrix elasticity directs stem cell lineage specification." In: *Cell* 126.4 (2006), pp. 677–689.

[10] Jianping Fu et al. "Mechanical regulation of cell function with geometrically modulated elastomeric substrates." In: *Nat. Methods* 7.9 (2010), pp. 733–736.

[11] Joe Swift et al. "Nuclear lamin-A scales with tissue stiffness and enhances matrix-directed differentiation". In: *Science* 341.6149 (2013), p. 1240104.

[12] Ryan D Sochol et al. "Unidirectional mechanical cellular stimuli via micropost array gradients". In: *Soft Matter* 7 (2011).

[13] Sergey V Plotnikov et al. "Force fluctuations within focal adhesions mediate ECM-rigidity sensing to guide directed cell migration." In: *Cell* 151.7 (2012), pp. 1513–1527.

[14] Christopher C DuFort, Matthew J Paszek, and Valerie M Weaver. "Balancing forces: architectural control of mechanotransduction." In: *Nat. Rev. Mol. Cell Bio.* 12.5 (2011), pp. 308–319.

[15] Melody A Swartz and Amanda W Lund. "Lymphatic and interstitial flow in the tumour microenvironment: linking mechanobiology with immunity." In: *Nat. Rev. Cancer* 12.3 (2012), pp. 210–219.

[16] Nathalie Q Balaban et al. "Force and focal adhesion assembly: a close relationship studied using elastic micropatterned substrates." In: *Nat. Cell Bio.* 3.5 (2001), pp. 466–472.

[17] Lea Trichet et al. "Evidence of a large-scale mechanosensing mechanism for cellular adaptation to substrate stiffness." In: *Proc. Natl. Acad. Sci. USA* 109.18 (2012), pp. 6933–6938.

[18] Sangyoon J Han et al. "Decoupling substrate stiffness, spread area, and micropost density: a close spatial relationship between traction forces and focal adhesions." In: *Biophys. J.* 103.4 (2012), pp. 640–648.

[19] Hedde van Hoorn et al. "The nanoscale architecture of force-bearing focal adhesions". In: *Nano Lett.* 14.8 (2014), pp. 4257–4262.

[20] William D Callister and David G Rethwisch. *Fundamentals of materials science and engineering: an integrated approach.* John Wiley & Sons, 2002.

[21] Saba Ghassemi et al. "Cells test substrate rigidity by local contractions on submicrometer pillars." In: *Proc. Natl. Acad. Sci. USA* 109.14 (2012), pp. 5328–5333.

[22] Britta Trappmann et al. "Extracellular-matrix tethering regulates stem-cell fate." In: *Nat. Mater.* 11.7 (2012), pp. 642–649.

[23] Martin Stolz et al. "Early detection of aging cartilage and osteoarthritis in mice and patient samples using atomic force microscopy". In: *Nat. Nanotechnol.* 4.3 (2009), pp. 186–192.

[24] Kristin Seltmann et al. "Keratins significantly contribute to cell stiffness and impact invasive behavior". In: *Proc. Natl. Acad. Sci. USA* 110.46 (2013), pp. 18507–18512.

[25] Cornelis Storm et al. "Nonlinear elasticity in biological gels". In: *Nature* 435.7039 (2005), pp. 191–194.

[26] Yi-Chia Lin et al. "Control of non-linear elasticity in F-actin networks with microtubules". In: *Soft Matter* 7.3 (2011), pp. 902–906.

[27] Simon W Moore, Pere Roca-Cusachs, and Michael P Sheetz . "Stretchy Proteins on Stretchy Substrates: The Important Elements of Integrin-Mediated Rigidity Sensing". In: *Dev. Cell* (2010).

[28] Amnon Buxboim, Irena L Ivanovska, and Dennis E Discher. "Matrix elasticity, cytoskeletal forces and physics of the nucleus: how deeply do cells 'feel'outside and in?" In: *J. Cell Sci.* 123.3 (2010), pp. 297–308.

[29] Benjamin S Elkin et al. "Mechanical heterogeneity of the rat hippocampus measured by atomic force microscope indentation". In: *J. Neurotraum.* 24.5 (2007), pp. 812–822.

[30] Penelope C Georges et al. "Matrices with compliance comparable to that of brain tissue select neuronal over glial growth in mixed cortical cultures". In: *Biophys. J.* 90.8 (2006), pp. 3012–3018.

[31] Karol Miller et al. "Mechanical properties of brain tissue in-vivo: experiment and computer simulation". In: *J. Biomech.* 33.11 (2000), pp. 1369–1376.

[32] Karol Miller and Kiyoyuki Chinzei. "Mechanical properties of brain tissue in tension". In: *J. Biomech.* 35.4 (2002), pp. 483–490.

[33] Penelope C Georges et al. "Increased stiffness of the rat liver precedes matrix deposition: implications for fibrosis". In: *Am. J. Physiol.-Gastr. L.* 293.6 (2007), G1147–G1154.

[34] Hans M Wyss et al. "Biophysical properties of normal and diseased renal glomeruli". In: *Am. J. Physiol.-Cell Ph.* 300.3 (2011), pp. C397–C405.

[35] J Ophir et al. “Elastography: ultrasonic estimation and imaging of the elastic properties of tissues”. In: *P. I. Mech. Eng. H* 213.3 (1999), pp. 203–233.

[36] Stephen J Lai-Fook and Robert E Hyatt. “Effects of age on elastic moduli of human lungs”. In: *J. Appl. Physiol.* 89.1 (2000), pp. 163–168.

[37] Anshu B Mathur et al. “Endothelial, cardiac muscle and skeletal muscle exhibit different viscous and elastic properties as determined by atomic force microscopy”. In: *J. Biomech.* 34.12 (2001), pp. 1545–1553.

[38] Adam J Engler et al. “Myotubes differentiate optimally on substrates with tissue-like stiffness pathological implications for soft or stiff microenvironments”. In: *J. Cell Biol.* 166.6 (2004), pp. 877–887.

[39] Amy M Collinsworth et al. “Apparent elastic modulus and hysteresis of skeletal muscle cells throughout differentiation”. In: *Am. J. Physiol.-Cell Ph.* 283.4 (2002), pp. C1219–C1227.

[40] Mark F Berry et al. “Mesenchymal stem cell injection after myocardial infarction improves myocardial compliance”. In: *Am. J. Physiol.-Heart C.* 290.6 (2006), H2196–H2203.

[41] Farshid Guilak et al. “Zonal uniformity in mechanical properties of the chondrocyte pericellular matrix: micropipette aspiration of canine chondrons isolated by cartilage homogenization”. In: *Ann. Biomed. Eng.* 33.10 (2005), pp. 1312–1318.

[42] JF Chapuis and P Agache. “A new technique to study the mechanical properties of collagen lattices”. In: *J. Biomech.* 25.1 (1992), pp. 115–120.

[43] Tetsuro Wakatsuki et al. “Cell mechanics studied by a reconstituted model tissue”. In: *Biophys. J.* 79.5 (2000), pp. 2353–2368.

[44] Hope D Intengan et al. “Resistance artery mechanics, structure, and extracellular components in spontaneously hypertensive rats effects of angiotensin receptor antagonism and converting enzyme inhibition”. In: *Circulation* 100.22 (1999), pp. 2267–2275.

[45] Gang Bao and Subra Suresh. “Cell and molecular mechanics of biological materials.” In: *Nat. Mater.* 2.11 (2003), pp. 715–725.

[46] Jérôme Solon et al. “Fibroblast adaptation and stiffness matching to soft elastic substrates.” In: *Biophys. J.* 93.12 (2007), pp. 4453–4461.

[47] Matthias Irmscher et al. “Probing the cell membrane by magnetic particle actuation and Euler angle tracking”. In: *Biophys. J.* 102.3 (2012), pp. 698–708.

[48] Michael J Yost et al. “Design and construction of a uniaxial cell stretcher”. In: *Am. J. Physiol.-Heart C.* 279.6 (2000), H3124–H3130.

[49] Uta Faust et al. “Cyclic stress at mHz frequencies aligns fibroblasts in direction of zero strain.” In: *PLoS. One* 6.12 (2011).

[50] Dongeun Huh et al. “Reconstituting organ-level lung functions on a chip.” In: *Science* 328.5986 (2010), pp. 1662–1668.

[51] Hans Degens et al. “Changes in contractile properties of skinned single rat soleus and diaphragm fibres after chronic hypoxia”. In: *Pflug. Arch. Eur. J. Phys.* 460.5 (2010), pp. 863–873.

[52] Jenny Fink et al. “External forces control mitotic spindle positioning.” In: *Nat. Cell Bio.* 13.7 (2011), pp. 771–778.

[53] Yasuhiro Sawada et al. “Force sensing by mechanical extension of the Src family kinase substrate p130Cas.” In: *Cell* 127.5 (2006), pp. 1015–1026.

[54] Pei-Hsun Wu et al. “High-throughput ballistic injection nanorheology to measure cell mechanics”. In: *Nat. Protoc.* 7.1 (2012), pp. 155–170.

[55] Sivaraj Sivaramakrishnan et al. “Micromechanical properties of keratin intermediate filament networks”. In: *Proc. Natl. Acad. Sci. USA* 105.3 (2008), pp. 889–894.

[56] Christopher M Hale, Sean X Sun, and Denis Wirtz. “Resolving the role of actoymyosin contractility in cell microrheology”. In: *PLoS. One* 4.9 (2009), e7054.

[57] Felix Margadant et al. “Mechanotransduction in vivo by repeated talin stretch-relaxation events depends upon vinculin”. In: *PLoS. Biol.* 9.12 (2011), e1001223.

[58] Carsten Grashoff et al. “Measuring mechanical tension across vinculin reveals regulation of focal adhesion dynamics.” In: *Nature* 466.7303 (2010), pp. 263–266.

[59] Albert K Harris, Patricia Wild, and David Stopak. “Silicone rubber substrata: a new wrinkle in the study of cell locomotion”. In: *Science* 208.4440 (1980), pp. 177–179.

[60] W Mark Leader, David Stopak, and Albert K Harris. “Increased contractile strength and tightened adhesions to the substratum result from reverse transformation of CHO cells by dibutyryl cyclic adenosine monophosphate”. In: *J. Cell Sci.* 64.1 (1983), pp. 1–11.

[61] Micah Dembo and Yu-Li Wang. “Stresses at the cell-to-substrate interface during locomotion of fibroblasts”. In: *Biophys. J.* 76.4 (1999), pp. 2307–2316.

[62] Ulrich S Schwarz et al. “Calculation of forces at focal adhesions from elastic substrate data: the effect of localized force and the need for regularization”. In: *Biophys. J.* 83.3 (2002), pp. 1380–1394.

[63] Benedikt Sabass et al. “High resolution traction force microscopy based on experimental and computational advances.” In: *Biophys. J.* 94.1 (2008), pp. 207–220.

[64] Wesley R Legant et al. “Multidimensional traction force microscopy reveals out-of-plane rotational moments about focal adhesions.” In: *Proc. Natl. Acad. Sci. USA* 110.3 (2013), pp. 881–886.

[65] John L Tan et al. “Cells lying on a bed of microneedles: an approach to isolate mechanical force.” In: *Proc. Natl. Acad. Sci. USA* 100.4 (2003), pp. 1484–1489.

[66] Olivia du Roure et al. “Force mapping in epithelial cell migration.” In: *Proc. Natl. Acad. Sci. USA* 102.7 (2005), pp. 2390–2395.

[67] Alexandre Saez et al. “Is the mechanical activity of epithelial cells controlled by deformations or forces?” In: *Biophys. J.* 89.6 (2005), pp. L52–L54.

[68] Michael T Yang et al. “Assaying stem cell mechanobiology on microfabricated elastomeric substrates with geometrically modulated rigidity.” In: *Nat. Protoc.* 6.2 (2011), pp. 187–213.

[69] Younan Xia and George M Whitesides. “Soft lithography”. In: *Ann. Rev. Mater. Sci.* 28.1 (1998), pp. 153–184.

[70] Alex G de Beer et al. "Force-induced destabilization of focal adhesions at defined integrin spacings on nanostructured surfaces." In: *Phys. Rev. E* 81.5 Pt 1 (2010).

[71] Alexandre Saez et al. "Rigidity-driven growth and migration of epithelial cells on microstructured anisotropic substrates." In: *Proc. Natl. Acad. Sci. USA* 104.20 (2007), pp. 8281–8286.

[72] A Kajzar et al. "Toward physiological conditions for cell analyses: forces of heart muscle cells suspended between elastic micropillars." In: *Biophys. J.* 94.5 (2008), pp. 1854–1866.

[73] Jimmy le Digabel et al. "Magnetic micropillars as a tool to govern substrate deformations." In: *Lab Chip* 11.15 (2011), pp. 2630–2636.

[74] Orrit and Bernard. "Single pentacene molecules detected by fluorescence excitation in a p-terphenyl crystal." In: *Phys. Rev. Lett.* 65.21 (1990), pp. 2716–2719.

[75] Ernst Abbe. "Beiträge zur Theorie des Mikroskops und der mikroskopischen Wahrnehmung". In: *Arch. Mikrosk. Anat.* 9.1 (1873), pp. 413–418.

[76] T Schmidt et al. "Imaging of single molecule diffusion." In: *Proc. Natl. Acad. Sci. USA* 93.7 (1996), pp. 2926–2929.

[77] Michael J Rust, Mark Bates, and Xiaowei Zhuang. "Sub-diffraction-limit imaging by stochastic optical reconstruction microscopy." In: *Nat. Methods* 3.10 (2006), pp. 793–795.

[78] Eric Betzig et al. "Imaging intracellular fluorescent proteins at nanometer resolution." In: *Science* 313.5793 (2006), pp. 1642–1645.

[79] Samuel T Hess, Thanu P Girirajan, and Michael D Mason. "Ultra-high resolution imaging by fluorescence photoactivation localization microscopy." In: *Biophys. J.* 91.11 (2006), pp. 4258–4272.

[80] Mike Heilemann et al. "Super-resolution imaging with small organic fluorophores." In: *Angew. Chem. Int. Edit.* 48.37 (2009), pp. 6903–6908.

[81] Sebastian van de Linde et al. "Direct stochastic optical reconstruction microscopy with standard fluorescent probes." In: *Nat. Protoc.* 6.7 (2011), pp. 991–991009.

[82] Norman Bobroff. "Position measurement with a resolution and noise-limited instrument". In: *Rev. Sci. Instrum.* 57.6 (1986), pp. 1152–1157.

[83] "Data sheet". In: Sigma Aldrich, 2014.

[84] Elizabeth S Haswell, Rob Phillips, and Douglas C Rees. "Mechanosensitive channels: what can they do and how do they do it?" In: *Structure* 19.10 (2011), pp. 1356–1369.

[85] Song Li et al. "The role of the dynamics of focal adhesion kinase in the mechanotaxis of endothelial cells". In: *Proc. Natl. Acad. Sci. USA* 99.6 (2002), pp. 3546–3551.

[86] Chun-Min Lo et al. "Cell movement is guided by the rigidity of the substrate". In: *Biophys. J.* 79.1 (2000), pp. 144–152.

[87] Alexandre Saez et al. "Traction forces exerted by epithelial cell sheets." In: *J Phys.-Condens. Mat.* 22.19 (2010).

[88] Adrian R West et al. "Bioengineering the Lung: Molecules, Materials, Matrix, Morphology, and Mechanics: Development and characterization of a 3D multicell microtissue culture model of airway smooth muscle". In: *Am. J. Physiol.-Lung C.* 304.1 (2013), p. L4.

[89] Ulrich S Schwarz and Margaret L Gardel. "United we stand - integrating the actin cytoskeleton and cell-matrix adhesions in cellular mechanotransduction." In: *J. Cell Sci.* 125.Pt 13 (2012), pp. 3051–3060.

[90] Alexander Bershadsky, Michael Kozlov, and Benjamin Geiger. "Adhesion-mediated mechanosensitivity: a time to experiment, and a time to theorize." In: *Curr. Opin. Cell. Biol.* 18.5 (2006), pp. 472–481.

[91] Benjamin Geiger, Joachim P Spatz, and Alexander D Bershadsky. "Environmental sensing through focal adhesions." In: *Nat. Rev. Mol. Cell Bio.* 10.1 (2009), pp. 21–33.

[92] Ronen Zaidel-Bar and Benjamin Geiger. "The switchable integrin adhesome." In: *J. Cell Sci.* 123.Pt 9 (2010), pp. 1385–1388.

[93] Mingxi Yao et al. "Mechanical activation of vinculin binding to talin locks talin in an unfolded conformation". In: *Sci. Rep.* 4 (2014).

[94] Xuefeng Wang and Taekjip Ha. "Defining single molecular forces required to activate integrin and notch signaling." In: *Science* 340.6135 (2013), pp. 991–994.

[95] Nadezhda Tikhmyanova, Joy L Little, and Erica A Golemis. "CAS proteins in normal and pathological cell growth control." In: *Cell. Mol. Life Sci.* 67.7 (2010), pp. 1025–1048.

[96] Chen Lu et al. "P130Cas substrate domain is intrinsically disordered as characterized by single-molecule force measurements". In: *Biophys. Chem.* 180 (2013), pp. 37–43.

[97] Jan Brábek et al. "CAS promotes invasiveness of Src-transformed cells". In: *Oncogene* 23.44 (2004), pp. 7406–7415.

[98] Dominique M Donato et al. "Dynamics and mechanism of p130Cas localization to focal adhesions." In: *J. Biol. Chem.* 285.27 (2010), pp. 20769–20779.

[99] Leslie M Meenderink et al. "P130Cas Src-binding and substrate domains have distinct roles in sustaining focal adhesion disassembly and promoting cell migration." In: *PLoS. One* 5.10 (2010).

[100] Michael A Lampson and Iain M Cheeseman. "Sensing centromere tension: Aurora B and the regulation of kinetochore function". In: *Trends Cell Biol.* 21.3 (2011), pp. 133–140.

Chapter 2

The nanoscale architecture of force-bearing focal adhesions[1]

[1]This chapter is based on: H. van Hoorn, R. Harkes, E.M. Spiesz, C. Storm, D. van Noort, B. Ladoux and T. Schmidt, The nanoscale architecture of force-bearing focal adhesions, *Nano Lett.*, **14** (8), 4257-4262 (2014)

abstract

The combination of micropillar array technology to measure cellular traction forces with super-resolution imaging allowed us to obtain cellular traction force maps and simultaneously zoom in on individual focal adhesions with single-molecule accuracy. We achieved a force detection precision of 500 pN simultaneously with a mean single-molecule localization precision of 30 nm. Key to the achievement was a two-step etching process that provided an integrated spacer next to the micropillar array that permitted stable and reproducible observation of cells on micropillars within the short working distance of a high-magnification, high numerical aperture objective. In turn, we used the technology to characterize the super-resolved structure of focal adhesions during force exertion. Live-cell imaging on MCF-7 cells demonstrated the applicability of the inverted configuration of the micropillar arrays to dynamics measurements. The smallest structural features of focal adhesions, however, could not be resolved by diffraction-limited microscopy. Forces emanated from a molecular base that was localized on top of the micropillars. What appeared as a single adhesion in conventional microscopy were in fact multiple elongated adhesions emanating from only a small fraction of the adhesion on the micropillar surface. Focal adhesions were elongated in the direction of local cellular force exertion with structural features of 100-280 nm in 3T3 Fibroblasts and MCF-7 cells. The combined measure of nanoscale architecture and force exerted shows a high level of stress accumulation at a single site of adhesion.

2.1 Introduction

It has come as a surprise recently that cells respond not only to biochemical cues but also to the mechanical properties of their local environment [1–4]. Studies showed the stiffness-dependent differentiation of stem cells [5], stiffness-directed cell motility (durotaxis) [6], and the importance of the environmental mechanical properties in disease like cancer [7, 8]. While these phenomena may have different biological relevance, all start at a common origin: the measurement of the mechanical response of the microenvironment performed by the cell, followed by some unexplored mechano-chemical coupling that finally leads to a cellular phenotype.

The cellular structures at which mechanical signals could be measured and analyzed are the focal adhesions (FA). At these sites, the physical connection between the internal contractile cytoskeleton and the extracellular matrix is made through integrin-dimers spanning the cell membrane. On the cytosolic side of the integrins a huge multi-protein complex is formed which attaches to the actin cytoskeleton. The latter forms an active cellular mechanical network contracted by myosin-motor activity. More than 100 proteins have been identified in FAs, that define a biological network with a multitude of interactions [9]. Several FA proteins have been suggested to potentially serve as mechano-chemical transducers that alter their biochemical function according to the amount of mechanical force exerted. These mechanosensors include talin [10], vinculin [11], p130Cas [12], zyxin [13] and paxillin [14]. It has been proposed that upon force exertion on those mechanosensors, specific binding sites become available that promote further biochemical interaction. However, it remains unclear whether the FA complex undergoes enough deformation and force exertion to physically stretch such proteins to perform their mechanosensing activity. We should thus examine on what length scale deformations occur and how much force is carried by FA proteins to enable a comparison to *in vitro* studies. Knowledge about the nanostructured organization of a FA relative to a local site of force exertion has the potential to address these open issues and to provide novel insights about the physical interpretation of local mechanosensory mechanisms.

The lack of knowledge is in part due to a lack of experimental methodology that permits direct measurement of the locally exerted force and simultaneously quantify the local molecular stoichiometry inside a FA complex. Here, we present methodology that combines two high-resolution

optical imaging techniques that enabled us to directly correlate molecular arrangements and cellular forces. In our approach, micropillar array technology was used to quantify sub-nN local cellular forces [15–17]. We show the ability to combine this technique with fixed- and live-cell fluorescence microscopy, giving diffraction limited results comparable to previous work [18–20]. Simultaneously, we employed super-resolution optical microscopy [21–23] with a localization precision of 30 nm to quantify the nanostructure of paxillin and phosphorylated paxillin in focal adhesions.

Prior studies have demonstrated that super-resolution microscopy yields insights into the dynamics and composition of focal adhesion complexes [24, 25]. To those super-resolution studies we here add the simultaneous readout of cellular forces at high resolution in an inverted micropillar arrangement. First, we show that inversion of the micropillar array to an upside-down configuration on an optical microscope with high-sensitivity multi-color fluorescence imaging capability allows us to accurately measure whole-cell mechanics in both fixed- and live cells. Second, we demonstrate that simultaneous super-resolution microscopy allows us to zoom in onto FAs to generate a molecular density map of phosphorylated paxillin stained by antibodies as well as two-color super-resolution on actin and paxillin. Taken together, our approach provides a sub-nN force precision map of cellular force exertion together with a super-resolved paxillin density map which directly measures the nanoscale architecture of force-bearing focal adhesions. Finally, our measurements demonstrate that multiple small, elongated FAs with dimensions of 100-280 nm carry forces of 10-20 nN, which leads to local stress accumulation up to 300 nN/μm^2. Force is thus carried through smaller structures than could be quantified using diffraction-limited microscopy and the diffraction limited stress measured on the same micropillar arrays was an order of magnitude smaller. Quantification of the stress accumulation at a focal adhesion site indeed provides the potential to check whether specific FA proteins can act as mechanosensors.

2.2 Methods

2.2.1 Cell biology

3T3 fibroblasts were cultured in high-glucose Dulbecco's Modified Eagle's Medium (DMEM) supplemented with 10% calf serum (Thermo Scientific), 2 mM glutamine and 100 µg/ml pennicilin/streptomycin. MCF-

7 cells stably expressing a paxillin-GFP fusion construct (a gift from Erik Danen at Leiden University) were cultured in DMEM supplemented with 10% fetal calf serum (Thermo Scientific), 2 mM glutamine and 100 µg/ml pennicilin/streptomycin. Cells were seeded at single cell density directly on the micropillar array. Cells were allowed to spread for 8 to 24 hours. Micropillar arrays were subsequently inverted onto #0, 25 mm diameter, round coverslips (Menzel Glaser). The micropillar arrays were kept from floating using a support weight of glass. Live-cell measurements were performed in overnight time-lapse measurements on a confocal spinning-disk setup with a home-built focus-hold system. The temperature was kept at 37 °C with constant 5% CO_2 concentration in a stage-top incubator (Tokai Hit, Japan). Cells were fixed in 4% Paraformaldehyde 16-24 hours after seeding for immunolabeling.

2.2.2 Confocal microscopy

All diffraction-limited fixed and live-cell imaging was performed on a home-built setup based on an Axiovert200 microscope body (Zeiss). An in-house focus-hold system performing feedback on the reflected light from a 850 nm laser-diode at the glass-water interface assured overnight experiments with axial drift <1 µm. Confocal imaging was achieved by means of a spinning disk unit (CSU-X1, Yokogawa). The confocal image was acquired on an emCCD camera (iXon 897, Andor). IQ-software (Andor) was used for basic setup-control and data acquisition. Specifically developed software (Labview, National Instruments) controlled the autofocus and automated XY positioning (Marzhauser XY-stage). Illumination was performed with five different lasers of wavelength 405, 488, 514, 561 and 642 nm (CrystaLaser, Coherent, Cobolt (2x) and Spectra Physics, respectively). Accurately controlled excitation intensity and excitation timing was achieved using an acousto-optic tunable filter (AA Opto-electronics). Light was coupled into the confocal spinning-disk unit by means of a polarization maintaining single-mode fiber.

2.2.3 Force measurement on micropillar arrays

A hexagonal array of poly-di-methyl-siloxane (PDMS, Sylgard 184, Dow Corning) micropillars of 2 µm diameter, 2 µm spacing and with a height of 6.9 µm were produced using replica-molding from a silicon wafer into which the negative of the structure was etched by deep reactive-ion

etching (for details see Supplemental methods). The pillar arrays were flanked by integrated 50 μm high spacers (shown in figure 2.1A and E) such that pillar tops and hence cells attaching to them were within the limited working distance of a high-NA objective (<170 μm) on an inverted microscope. The use of a high-NA objective is a prerequisite for any high-resolution optical imaging. Further, such objectives provide the high collection-efficiency which is essential to super-resolution imaging.

The tops of the micropillars were coated with a mixture of Alexa405-labeled and unlabeled fibronectin (1:5) using micro-contact printing. This approach ensured that cells were solely attached to the tops of the micropillars as confirmed by confocal microscopy (data not shown). Finite element analysis that was fed the exact micropillar dimensions (figure S1) as measured by in-situ scanning electron microscopy (SEM, FEI nanoSEM) allowed us to precisely calibrate the force-deflection relation (for details see Supplemental methods). Pillars on the array had a characteristic spring constant of 16.7 nN/μm. The position of the pillar tops was observed by fluorescence microscopy at 405 nm excitation. From those fluorescence images (figure 2.1B, pillar array without cells) the exact pillar-centroid positions were determined down to 30 nm accuracy using specifically designed software (Matlab, Mathworks). The deflection precision of 30 nm, that is solely limited by the fluorescence signal from an individual pillar, corresponded to a force accuracy of 500 pN (figure 2.1C).

Experimental results are presented with at least 3 independent experiments per graphical representation, performed on at least 4 different cells per experiment. When fitting was performed to results, R^2 analysis gives the accuracy of the fit. An example of a fixed and dehydrated cell on pillars when imaged in a low-vacuum mode SEM is shown in figure 2.1D. It should be noted that the deflections of the pillars in this image are larger than in live-cell measurements due to the de-hydration procedure needed for electron-microscopy.

2.2.4 Super-resolution imaging on micropillar arrays

The upside-down micropillar approach with integrated spacers and high-NA fluorescence imaging on an inverted microscope allowed us to combine force measurements with super-resolution imaging (for details see Supplemental methods). In brief, we labeled paxillin-GFP in the MCF-7 cells with Alexa647-labeled GFP-traps (Chromotek) and phosphorylated

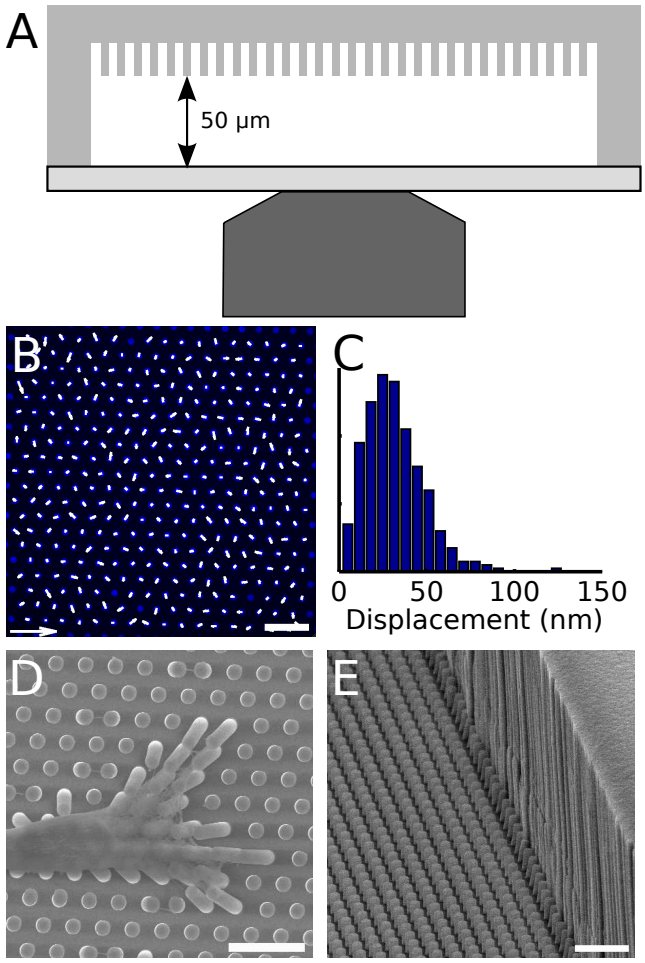

Figure 2.1
Inverted micropillars with well-defined spacers provide simultaneous super-resolution fluorescence- and force measurements. (A) Schematic overview of configuration during microscopy (not to scale). With a 100 µm coverslip and 50 µm spacer next to the array, micropillars and cells are within working distance of a high-NA objective. (B) A fluorescence image of the micropillars is analyzed to show the resolution of the deflection field (scalebar in lower left is for the pillar deflections corresponding to 500 nm, lower right is for the fluorescence image corresponding to 10 µm). (C) Histogram of the absolute deflections in (B) shows a mean deflection of 30 nm, giving the one-dimensional localization precision. (D) Scanning electron microscopy (SEM) of a 3T3 fibroblast spread on a micropillar array shows deflected pillars. (E) One 50 µm high spacer - as seen with SEM - flanking the micropillar array. (Scalebars in D and E correspond to 10 µm)

paxillin with Alexa647-labeled anti-rabbit antibody (donkey-anti-rabbit, Jackson Immunoresearch) to recognize the primary paxillin pY118 antibody (Invitrogen). Alexa647 was reported to show favorable switching properties to employ direct STochastic Optical Reconstruction Microscopy (dSTORM) [23].

Imaging was performed in 100 mM mercaptoethylamine (MEA, Sigma Aldrich) and a glucose oxygen scavenging system (for details see Supplemental methods). By sequential re-activation with 405 nm light from a diode laser (Crystalasers) at 1-20 W/cm^2 and imaging with 642 nm light from a diode laser (Spectra Physics) at 1.5 kW/cm^2, we localized individual molecules to a precision of 30 nm, limited by the signal from an individual molecule of 630 counts per 10 ms of illumination. For simultaneous two-color imaging of the actin structure we stained with Alexa532-phalloidin (Invitrogen) and adapted the buffer conditions by removing the oxygen-scavenging system to facilitate favorable switching conditions for Alexa532. The 405 nm switching light also excited the Alexa405-labeled fibronectin on the pillar tops, such that we simultaneously obtained high-resolution information of local cellular forces with each activation step. The combined single-molecule and micropillar approach yielded both a molecular density map of focal adhesion proteins and the local forces exerted by the cell.

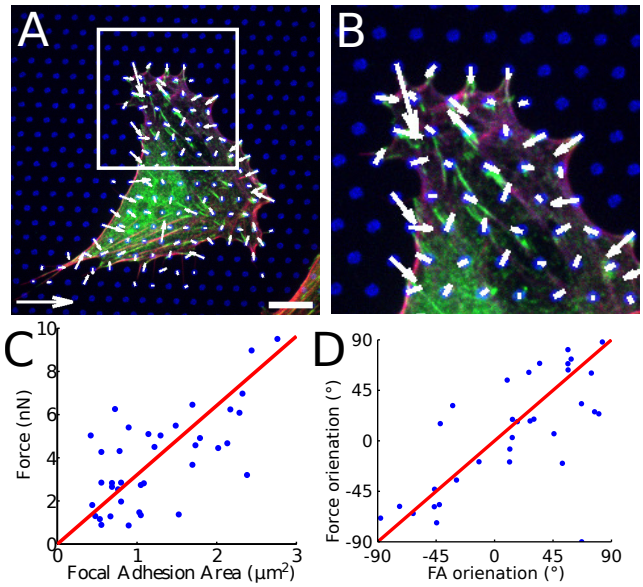

Figure 2.2
Force exertion is guided from actin stress fibers through focal adhesions. (A) 3T3 fibroblast on hexagonal pillar array micro-contact printed with fibronectin (blue), immunostained for paxillin (green) and actin (red) and (B) zoomed in on forces exerted with focal adhesions and actin (in A lower left arrow scalebar corresponds to 20 nN force, lower right scalebar corresponds to 10 μm). (C) The force exerted locally increases with focal adhesions size, a fit to the data gives (3±1) nN/ μm² (R^2 = 0.459). (D) Focal adhesions co-orient with the direction in which the force is exerted, a correlation of 1 deg/deg is shown in red (a histogram of the co-orientation gives a standard deviation of 10° around a mean difference in orientation of 0°).

2.3 Results

2.3.1 High-resolution measurement of cellular forces.

First, we assured that cell behavior on inverted pillar arrays did not differ from cell behavior in upright chambers. Phenomenologically we found that cells showed a healthy morphology, migrated and divided as expected. We further performed both live-cell and fixed-cell imaging on 3T3 fibroblasts to confer the phenomenological findings. We found that force exertion evolved from the cell periphery, and was largely aligned with actin stress fibers (figure 2.2A). After careful calibration of the micropillars using finite-element analysis, the total vectorial force per

cell was zero within experimental uncertainty. The absolute force per pillar in each cell varied over a large range from 0 to 10 nN (figure 2.2B) with a mean of 4±3 nN (mean±std). Typically, most of the large forces were localized on a few (5-10) pillars per cell.

Multi-color imaging of paxillin and actin confirmed that cellular forces emerged from focal adhesions (FAs) with their edges attached to the top of the pillars as shown in figure 2.2A-B (figure S2 shows seperate channels). The FAs were detected by an antibody that recognizes phosphorylated paxillin. The focal adhesion area was distributed between 0.5 to 3 μm^2 with a mean of (1.4±0.7) μm^2 (figure 2.2C). Larger-sized FAs were able to support larger forces as indicated by the correlation between FA area and force displayed in figure 2.2C. Assuming a linear relationship the local force increased by (3±1) $nN/\mu m^2$ of FA area. A similar range of forces and FA area was previously found for Human Foreskin Fibroblasts [18] and REF52 Fibroblasts [19].

Shapes and sizes of FAs were quantified using custom software to detect the edges of focal adhesions (figure S3). Those quantities were correlated to local cellular traction forces. Actin stress fibers (mostly cortical fibers) were formed throughout the cell and emerged from force-bearing FAs (figures 2.2A-B). Throughout all cells, we observed a homogeneous distribution of orientation for both forces and focal adhesion elongation. This was predicted, since there is no preferential orientation for cells on hexagonal pillar arrays. However, we found a clear correlation between the direction of force and the direction of FA elongation. FAs were oriented within 10° (standard deviation) with respect to the direction of force (figure 2.2D).

Live-cell imaging of FAs in MCF-7 cells stably expressing a paxillin-GFP fusion construct in the inverted configuration further confirmed the ability to perform live-cell experiments in the inverted configuration and local force-FA area correlations. In figure 2.3A snapshots of a migrating cell on micropillars (blue) expressing paxillin-GFP (green) are shown. FA dynamics were directly quantified. The local FA area followed the force again in an apparent linear relationship. For two individual pillars (figure 2.3B) force and FA area correlated over time as one decreased in force and FA area and the other increased in force at an approximately constant small FA area. The force in live-cell experiments increased with FA area with (13±2) $nN/\mu m^2$ (figure 2.3C).

Our measurements of FA characteristics, cellular forces and their cor-

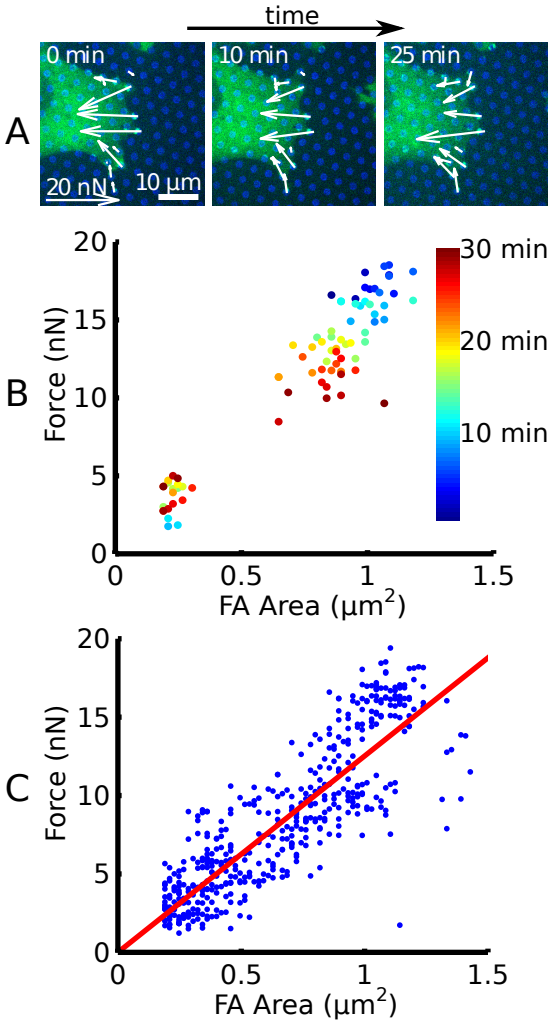

Figure 2.3
Live-cell dynamics of focal adhesions and force. (A) Live MCF-7 cell expressing paxillin-GFP on a micropillar array exerts significant forces locally where focal adhesions (FAs) are present. (B) Force and FA area correlate over time, from two individual pillar locations. Color correlates to time, indicating FA and Force decrease for one pillar, while another grows in force at a constant small FA size. (C) Over multiple focal adhesions and sites of force exertion on live MCF-7 cells, a clear correlation is given by a linear fit with (13±2) nN/µm² (R^2 =0.711).

relations corroborate previous observations of fibroblast-behavior when grown in the upright configuration [18–20]. Using our inverted approach we can furthermore characterize live-cell force and FA area dynamics at the highest possible diffraction-limited resolution. Hence, we conclude that cells that are spread on inverted pillar arrays remain viable and their phenotypic and mechanical behavior is unaltered with repect to other situations.

2.3.2 Super-resolution imaging of focal-adhesion proteins on micropillar arrays.

In order to relate cellular forces to the molecular structure of focal adhesion complexes, we performed super-resolution imaging of the FA protein paxillin in cells that pulled on micropillar arrays[23]. After adhesion, cells were fixed and immunostained for phosphorylated paxillin (pY118) using the primary rabbit-anti-pY118Paxillin antibody. Subsequently, a secondary Alexa647-anti-rabbit antibody was used for fluorescence-labeling. Cells were imaged in phosphate-buffered saline at pH 8 supplemented with 100 mM mercapto-ethylamine and a glucose-oxidase oxygen-scavenging system. After pre-bleach, Alexa647 was re-activated with 405 nm light for 10 ms every 20 frames with increasing intensity (1-20 W/cm^2) such that a constant 10 to 20 Alexa647 molecules were observed in each image. Individual Alexa647 molecules were identified and localized when excited at 642 nm for 10 ms with an intensity of 1.5 kW/cm^2. In total 15,000 images were recorded within 5 minutes. From those data we reconstructed a super-resolved image of FAs on pillars with a mean one-dimensional localization-precision of 30 nm. Figure 2.4A exemplifies the largely increased resolution of the super-resolved image (right) in comparison to the image taken at diffraction-limited resolution (left, the full diffraction-limited image is depicted in figure S4). Note the scalebar of 2 μm in this image when comparing to the image in figure 2.2B. FAs that appear as elliptical globular structures in the diffraction-limited images (figure 2.2B) appear rather as elongated stretches of 100-500 nm by 1-5 μm in the super-resolved image.

Labeling the micropillars with Alexa405-fibronectin allowed us to overlay the super-resolution images of FAs with diffraction-limited images of the micropillar arrays resulting in high-resolution force-maps. Figure 2.4B shows such overlay in which the pillar indicated by an arrow was deflected significantly with a force of 6.5 nN, which is carried by two

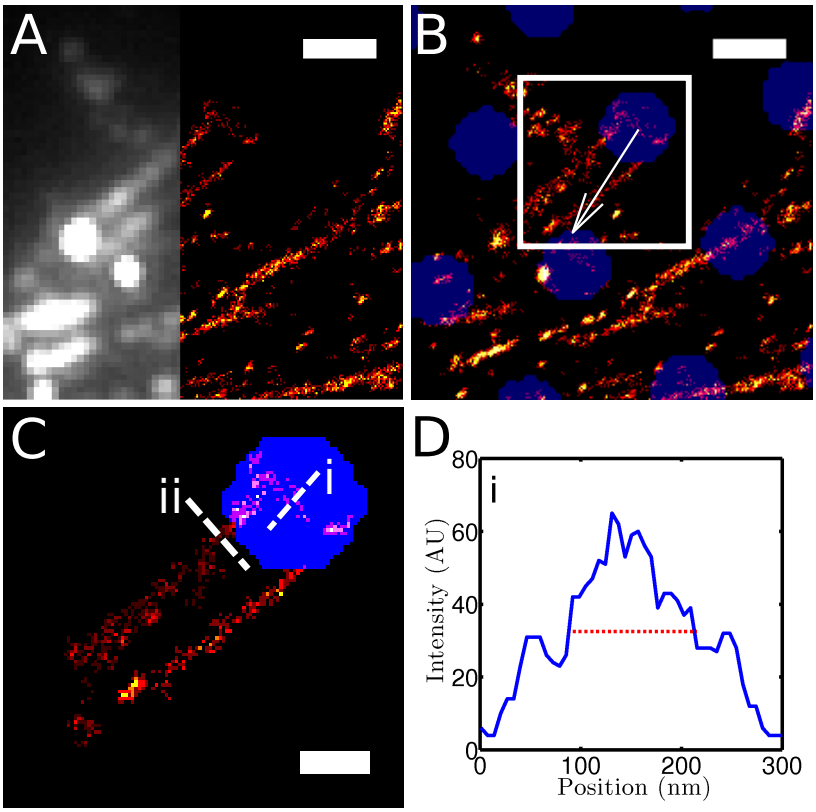

Figure 2.4
Nanoscale architecture of force bearing focal adhesions (FAs). (A) Super-resolved structure of phosphorylated paxillin using dSTORM. The diffraction limited image (left side) cannot resolve the small structural features of focal adhesions, but the super-resolved image (right side) reveals smaller features. (B) Micropillar locations are correlated to the super-resolved FAs through direct observation of the Alexa405-labeled fibronectin in blue during dSTORM re-activation. The arrow corresponds to a force of 6.5 nN. (C) A closer look at a single site of force exertion reveals a super-resolved image of a force-bearing FA. (scalebars in A-B correspond to 2 μm and in C to 1 μm) (D) Collapsed histogram of multiple line profiles along the FA base, as denoted by i in C. The base of the elongated FAs is only 125 nm wide and is perpendicular to two elongated FA structures.

individual elongated FAs. From such images it becomes obvious that the cell's major forces emerge from elongated FAs that end on pillars, and that FA elongation is parallel to force exertion (as we observed in figure 2.2D). However, in the super-resolved image the attachment region of FAs to fibronectin is more clearly resolved. The FA is elongated, but also clearly localized on the very top of the pillars. Furthermore, we observe that the FA cluster extends several micrometers beyond the pillar. Fibroblasts produce fibronectin by which they model a fibrous network left behind when cells move forward (staining for fibronectin is shown in figure S5). The elongated FA in figure 2.4B attached to fibronectin left behind by the cell leading to the elongated growth of FAs towards the cell center.

With super-resolved imaging we further characterized the nanoscale architecture of the focal adhesions bearing the force exerted on a single pillar, as exemplified in figure 2.4C. In this case, two focal adhesions emerged in parallel at a distance of 1 μm and carried a force of 6.5 nN. The two parallel focal adhesions each measured a width of 280 nm at the full-width of half-maximum (FWHM, see figure S6). Strikingly, the base of contact in figure 2.4C on top of the pillar shows an additional structure 125 nm wide (FWHM, figure 2.4D) perpendicular to the two elongated FAs. In all super-resolution images analyzed, we found that force-exertion clearly emerged from the top of the pillars and from localized FA structures that had a width of 125-280 nm FWHM for 3T3 fibroblasts.

We also examined the super-resolved structure of paxillin in the MCF-7 cells used for live-cell microscopy (see figure 2.3). Directly labeled Alexa647-nanobodies recognizing the beta-barrel of GFP on the paxillin and Alexa532-labeled phalloidin were used to reconstruct a two-color super-resolution image (see figure 2.5). The structure of the FAs (figure 2.5A) appeared similar to what we obtained from super-resolved phosphorylated paxillin in figure 2.4C. Actin bundles preceded the elongated FAs carrying the exerted force (figure 2.5B). Again, multiple elongated stretches emanated from the top of the micropillars bearing forces in the order of 0-20 nN (zoom in on a single pillar in figure 2.5C) with a width of 100-150 nm.

With the super-resolved structure of FAs carrying a local force, we measured the FA area more accurately as compared to diffraction-limited microscopy. For both cell types it was apparent that the local force

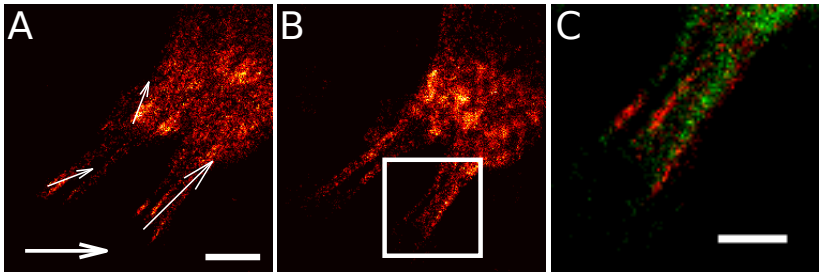

Figure 2.5
Super-resolved focal adhesions and actin correlated to force. Fixed MCF-7 cells show super-resolved paxillin using Alexa647-nanobody staining directly to paxillin-GFP and Alexa532-phalloidin to actin. (A) Paxillin molecular density and (B) actin molecular density through dSTORM imaging relative to force exertion. (C) A closer look at the location of one pillar shows multiple elongated FAs that emanate into actin bundles with a width of 100-150 nm. (Scalebars in A, also valid for B: lower-left corresponds to 20 nN and lower-right to 2 μm. Scalebar in C corresponds to 1 μm)

exerted was distributed over small FAs, consisting of multiple elongated 100-280 nm wide stretches. From these smaller FA areas, the actual force per area amounted to 10-300 nN/μm^2. The stress accumulated is thus approximately one order of magnitude higher as compared to the values we and others [18–20] obtained using diffraction-limited experiments. The individual sites of attachment as in the enlargement in figure 2.5C thus carried an even larger force per FA area, making it a locally highly stress-bearing state.

2.4 Discussion and conclusion

With one additional step in the micropillar fabrication procedure, we achieved simultaneous high-resolution cellular traction force measurements and super-resolution imaging. The precisely fabricated and integrated spacers next to the microfabricated pillar array allowed us to perform microscopy using high-NA objectives that are required for super-resolution microscopy. With our approach it became possible to measure local focal adhesion molecule-densities and the local force exerted by the cell at the same location. The ability to perform super-resolution measurements further makes our approach an attractive technique to address the question of a global versus local mechanosensory mechanism.

Cells that were attached on inverted micropillar arrays remained viable, as observed by proliferation and mechanical characteristics. Cellular force maps with high resolution down to the sub-nN force precision were obtained for fixed 3T3 fibroblasts and live MCF-7 cells. Simultaneously, we were able to image the nanostructural organization of the focal adhesion protein paxillin. Our method further allowed us to characterize exact adhesion size and localization relative to forces. Focal adhesions in 3T3 fibroblasts and in MCF-7 cells were elongated parallel to the direction of force exertion and had a typical witdth of 100-280 nm. The approximate stress carried by a FA complex was one order of magnitude higher as compared to the diffraction-limited case, since the FA actually consisted of multiple narrow elongated structures. Our measurements thus revealed a higher stress accumulation compared to previous measurements on cellular adhesion sites.

With the ongoing developments to quantify the exact number of molecules in super-resolution imaging [26], our approach can be directly used to quantify the amount of specific force-bearing molecules in a FA. We estimated that the focal adhesion structures localized on the pillar presented in figure 2.4C contained about 780 paxillin molecules. Combined with the measure of the local force we may in the future be able to complete our image of how forces are transmitted through the multifaceted focal adhesion complex. It will be interesting to investigate, using our methodology, the structure-force responses of potential mechanosensory proteins like talin, vinculin, p130Cas and zyxin. Such experiments may shed light on how a cell structurally alters its adhesion organization depending on its mechanical behaviour.

2.5 Supplemental methods

2.5.1 Micropillar fabrication and coating

Micropillar arrays were prepared by replica molding from a microfabricated master produced by a two-step Si-technology process following described methods [16, 17, 27, 28]. In the initial step a hexagonal pattern of 2 µm diameter holes and 2 µm spacing was etched into a flat Si-wafer. Roughness of the sidewalls was minimized by an alternating SF6 etching and C4F8 passivation Bosch process in an inductively-coupled deep reactive-ion etcher. In a second step we etched 50 µm deep spacers at two sides of the 1x1 cm micropillar arrays. The etching process resulted in silicon-wafer masters with the negative mold of pillars and spacers.

The masters were cleaned in 100% ethanol, then 100% isopropanol, and finally silanized with trichloro(1H,1H,2H,2H-perfluorooctyl) silane (Sigma Aldrich) for 16 hours. Polydimethyl siloxane (PDMS, Dow Corning) was mixed with 1:10 crosslinker:prepolymer ratio, degassed, poured over the master wafers, and cured for 20 hours at 110 °C. The cured micropillar arrays with spacers were peeled from the wafers.

Subsequently, micro-contact printing with fluorescently labeled fibronectin was performed. A flat PDMS stamp was incubated for 1 hour with a 40 µl drop of 50 µg/ml fibronectin and 10 µg/ml fibronectin-Alexa405 (NHS-labeled with approximately 10 dyes per fibronectin). After two washing steps with ultrapure water, most liquid was adsorbed using a tissue and left to dry in a laminar flow hood. Prior to labeling the micropillars were activated using a UV-ozone cleaner (Jelight) for 10 minutes. The stamp was applied 2-5 minutes. Finally, the PDMS micropillars were blocked for 1 hour with 0.2% pluronic (Sigma) in phosphate buffered saline.

2.5.2 Force-deflection calibration

We first accurately assessed the pillar dimensions and their bulk material properties. We measured the stress-strain behavior of bulk PDMS in a uni-axial test using a dynamic mechanical analyzer (TA Instruments). From those experiments the Young's modulus of the pillar bulk material was determined to be 2.5±0.1 MPa with a negligible Loss Modulus. Subsequently, scanning electron microscopy (FEI nanoSEM) was used to directly quantify the dimensions of the non-conductive PDMS micropil-

lars. Images were taken in low vacuum mode at a partial water vapour pressure of 0.7 mbar, such that coating with a conductive material was not necessary. At the base of the micropillars a notch due to undercutting during the etching process is visible. The pillars shown in figure S7 had a height of 6.9±0.2 μm and a diameter of 2.0±0.1 μm (see figure S8) and were homogeneously arranged in a hexagonal array of 10x10 mm.

In most previous work, a perfect linear elastic beam is assumed for the force-deflection relationship. Schoen et al. [29] showed in their experiments that base-deformation has to be considered. They therefore developed an analytical extension to linear elastic beam theory that includes tilting of the base, shear in the base as well as base displacement. This led to a more accurate relation between force at the pillar top and displacement of the pillar, but still a linear relationship. Because of the more complicated shapes of our pillars we employed finite element modelling (FEM) to give a precise measure of the force-deflection behavior and to account for the effect of the notch at the base of the pillar (see figure S7).

In our FEM model the base of the micropillar was assumed to be an elastic, deformable material of the same stiffness as the pillar (see figure S1), to facilitate base-deformation. FEM analysis confirmed that the small notch on our pillars indeed influences the result from a perfect cylinder modeled with FEM. It further showed that the force-displacement relationship was linear even up to deflections of 2 μm for the relatively high pillars (6.9 μm) used in the experiments presented here, while a non-linear response occurs only for larger deflections. The linear elastic bending, base-tilting, cylindrical FEM and notch FEM bending moduli are given in table 2.1. The force-deflection behaviour over the relevant range of 0 - 2 μm deflection was determined to be 16.7 nN/μm with R^2=0.999.

	Analytical		FEM	
	Bending	Model [29]	Cylindrical	With notch
Base deformation	-	+	+	+
k (nN/μm)	17.9	14.3	18.0	16.7

Table 2.1
Linear force-deflection response for pure bending, the extended model by Schoen et al. [29], the cylindrical- and notched FEM pillar.

2.5.3 Deflection map

Fluorescence imaging of Alexa405-labeled fibronectin shows the homogeneous application of non-fibrous fibronectin to only the top of the micropillars. We determined the micropillar positions with sub-pixel accuracy by fitting a Gaussian or cone-profile to the cross correlation of the measured pillar intensity map and a circle of identical radius. Doing so we were able to obtain a mean deflection precision of 30 nm solely determined by the signal-to-noise ratio of pillar detection. Subsequently we corrected the positions for optical aberrations. In general objectives are perfectly corrected for aberrations only in terms of diffraction limited imaging. As SEM measurements showed with very high precision that pillars were arranged in a perfectly hexagonal array (see figure S8) this knowledge was used to correct positions of an undeflected pillar array that in turn was used to obtain a position correction-field to account for optical aberrations (figure S9). In summary, the high positional accuracy in determination of the pillar positions, including aberration correction and our finite element modeling of the pillar stiffness, allowed us to reliably determine cellular forces at a precision of 500 pN.

2.5.4 Focal adhesion analysis

Automated image analysis of the focal adhesion fluorescence images provided measures for focal adhesion size in the diffraction-limited images. Specifically designed software provided us with the detection and further characterization of discrete focal adhesion patches (see figure S3). Focal adhesion patches were analyzed in terms of area, elongation, angle of elongation towards force, and were assigned to its respective pillar on which force exertion emerged.

2.5.5 Super resolution imaging

For the dSTORM single-molecule measurements, we took a similar approach as in van de Linde et al. [23]. Primary antibodies recognized paxillin that is phosphorylated at site Y118 (Invitrogen). Secondary antibodies were labeled with the dye Alexa647 (Jackson Immunoresearch). We labeled paxillin-GFP in the MCF-7 cells using Alexa647-labeled GFP-trap (Chromotek) with 1.6 dyes per trap. Actin was directly stained using Alexa532-phalloidin (Invitrogen). Imaging was performed with 100

mM MEA in PBS at pH 8 supplemented with an oxygen scavenging system, containing 10% w/v glucose, 0.5 mg/ml glucose oxidase and 40 μg/ml catalase (all from Sigma Aldrich). The oxygen-scavenging system was not added for the two-color experiments, as it greatly decreased the blinking of Alexa532. The sample was sealed between two coverslips with grease during the measurement, to minimize the influence of oxygen. The sample was imaged on a wide-field single-molecule setup equipped with a 100X, NA 1.4 objective (Zeiss) onto a back-illuminated emCCD camera (Cascade). In the two-color experiments a sCMOS Orca Flash camera (Hamamatsu) was used on the same setup. The illumination intensity of a 642 nm diodelaser (Spectra Physics) was kept at 1.5 kW/cm^2, while re-activation of molecules was performed every 20 frames with a 405 nm laser (Crystalaser) at an increasing intensity of 1-20 W/cm^2. The mean localization precision of the single molecules in both x- and y-direction was 30 nm (see figure S10).

2.6 Supplemental figures

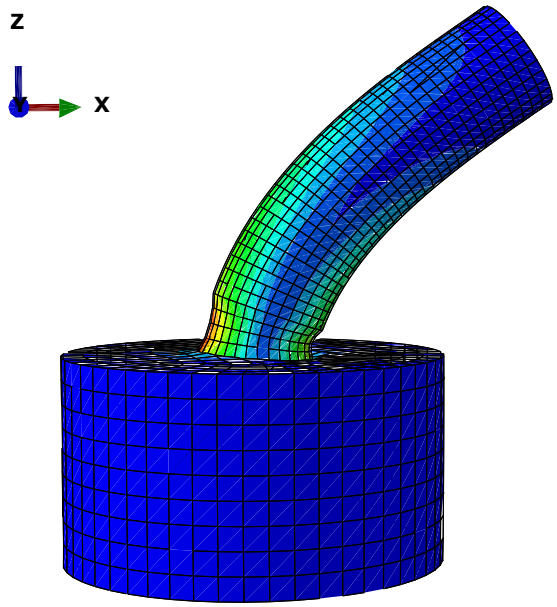

Figure S1
Finite element analysis of a single micropillar. The exact pillar shape and size were taken into account: including a notch at the base and the base-tilting effect (both pillar and base had the same properties), to provide a precise force-deflection relationship.

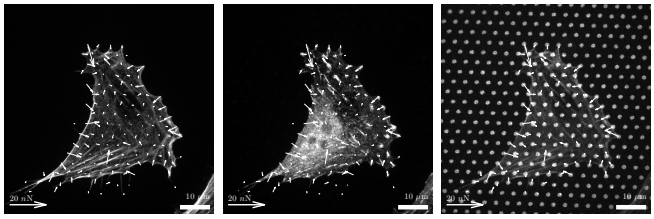

Figure S2
Diffraction limited imaging of actin, focal adhesions and micro-contact printed fibronectin. Forces exerted by a 3T3 Fibroblast are plotted with staining for actin (left), paxillin (middle) and micro-contact printed fibronectin (right). Arrow corresponds to 20 nN and scalebar to 10 μm in fluorescence images.

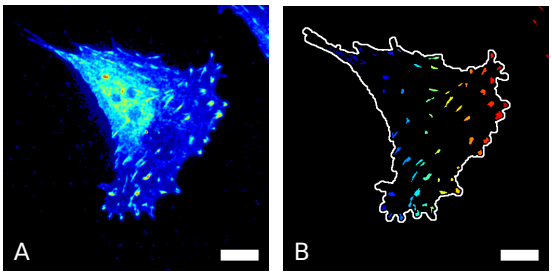

Figure S3
Automated analysis gives all focal adhesion properties after spatial frequency filtering of the background (left image, after background substraction). The resulting focal adhesions (color-coded in the right image) are detected using Canny-edge detection. This yields the cellular outline and pixel-limited geometrical information on the focal adhesion sites (e.g. area, orientation). Scalebar corresponds to 10 μm.

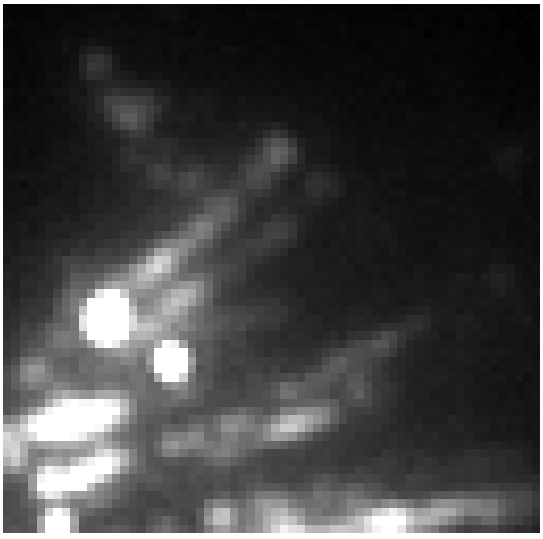

Figure S4
Diffraction limited close-up image of paxillin. Focal adhesions appear as rounded objects and structural features below 200 nm cannot be clearly seen (image size is 10x10 μm).

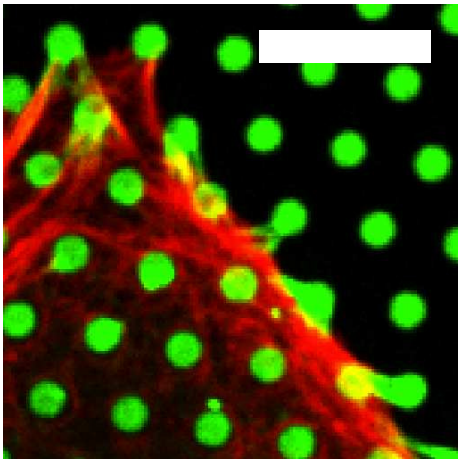

Figure S5
3T3 Fibroblast spread on micropillars stained for Fibronectin (green) and actin (red). Micro-contact printed fibronectin is present only on the pillar tops, while the fibronectin produced by the cell is visible at the edge of the pillars where the cell attaches (scalebar corresponds to 10 μm).

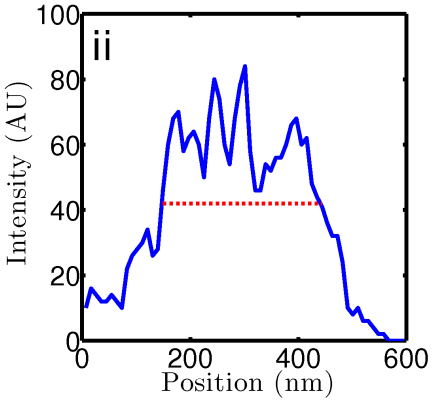

Figure S6
Sum of collapsed line profiles of a single focal adhesion in figure 4B. Full Width at Half Maximum of elongated focal adhesions is 280 nm.

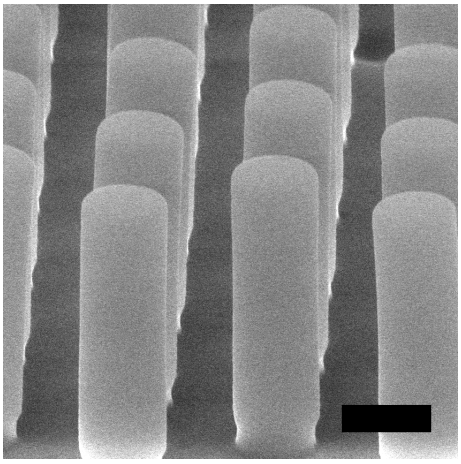

Figure S7
Scanning electron microscopy image sideview of PDMS micropillars. These micropillars have a height of 6.9 µm *and diameter of 2* μ*m. The force-deflection behaviour is calibrated including the notch at the base using Finite Element Analysis (scalebar bottom right corresponds to 2* μ*m).*

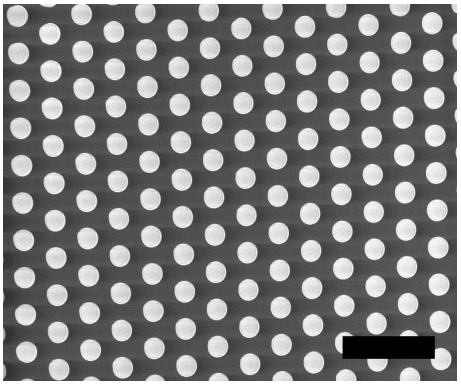

Figure S8
Scanning electron microscopy topview of PDMS micropillars. All SEM was performed using Low-Vacuum Mode, which enabled the imaging of non-conductive samples. Replica-molding from the etched Silicon wafers yields perfectly hexagonal arrays with precision beyond the fluorescence imaging resolution (scalebar corresponds to 10 μ*m).*

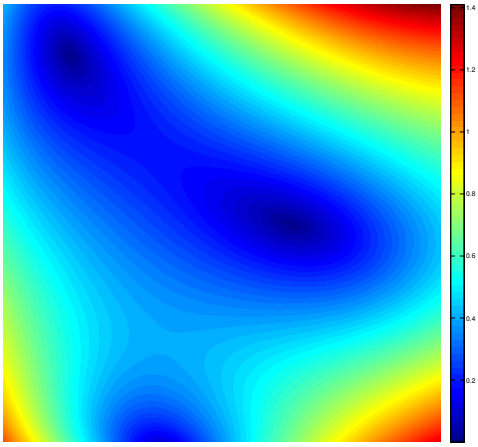

Figure S9

High resolution imaging reveals subpixel astigmatism. The micropillar arrays are perfectly hexagonal (see figure S8) below the optical pillar localization precision (30 nm) and an imperfect hexagonal map was observed larger than this precision. This was corrected for in the pillar localization using a two-dimensional mapping as depicted here with deflections corrected up to approximately 1 pixel (corresponding to 138 nm). The correction map is color coded corresponding to the colorbar in pixels.

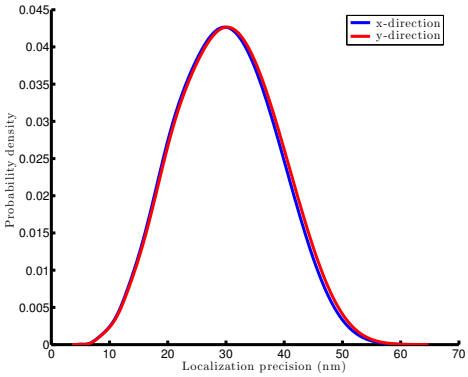

Figure S10

Localization precision of single molecules. Histogram of localization precision of single molecules from dSTORM as observed on inverted micropillar array in x- and y-direction. Mean localization precision is approximately 30 nm.

Bibliography

[1] Dennis E Discher, Paul Janmey, and Yu-Li L Wang. "Tissue cells feel and respond to the stiffness of their substrate." In: *Science* 310.5751 (2005), pp. 1139–1143.

[2] Viola Vogel and Michael Sheetz. "Local force and geometry sensing regulate cell functions." In: *Nat. Rev. Mol. Cell Bio.* 7.4 (2006), pp. 265–275.

[3] Benjamin Geiger, Joachim P Spatz, and Alexander D Bershadsky. "Environmental sensing through focal adhesions." In: *Nat. Rev. Mol. Cell Bio.* 10.1 (2009), pp. 21–33.

[4] Joe Swift et al. "Nuclear lamin-A scales with tissue stiffness and enhances matrix-directed differentiation". In: *Science* 341.6149 (2013), p. 1240104.

[5] Adam J Engler et al. "Matrix elasticity directs stem cell lineage specification." In: *Cell* 126.4 (2006), pp. 677–689.

[6] Ryan D Sochol et al. "Unidirectional mechanical cellular stimuli via micropost array gradients". In: *Soft Matter* 7 (2011).

[7] Christopher C DuFort, Matthew J Paszek, and Valerie M Weaver. "Balancing forces: architectural control of mechanotransduction." In: *Nat. Rev. Mol. Cell Bio.* 12.5 (2011), pp. 308–319.

[8] Melody A Swartz and Amanda W Lund. "Lymphatic and interstitial flow in the tumour microenvironment: linking mechanobiology with immunity." In: *Nat. Rev. Cancer* 12.3 (2012), pp. 210–219.

[9] Ronen Zaidel-Bar et al. "Functional atlas of the integrin adhesome." In: *Nat. Cell Bio.* 9.8 (2007), pp. 858–867.

[10] Felix Margadant et al. "Mechanotransduction in vivo by repeated talin stretch-relaxation events depends upon vinculin". In: *PLoS. Biol.* 9.12 (2011), e1001223.

[11] Carsten Grashoff et al. "Measuring mechanical tension across vinculin reveals regulation of focal adhesion dynamics." In: *Nature* 466.7303 (2010), pp. 263–266.

[12] Yasuhiro Sawada et al. "Force sensing by mechanical extension of the Src family kinase substrate p130Cas." In: *Cell* 127.5 (2006), pp. 1015–1026.

[13] J. Colombelli et al. "Mechanosensing in actin stress fibers revealed by a close correlation between force and protein localization". In: *J. Cell Sci.* 122 (2009).

[14] Ronen Zaidel-Bar et al. "A paxillin tyrosine phosphorylation switch regulates the assembly and form of cell-matrix adhesions." In: *J. Cell Sci.* 120.Pt 1 (2007), pp. 137–148.

[15] John L Tan et al. "Cells lying on a bed of microneedles: an approach to isolate mechanical force." In: *Proc. Natl. Acad. Sci. USA* 100.4 (2003), pp. 1484–1489.

[16] Olivia du Roure et al. "Force mapping in epithelial cell migration." In: *Proc. Natl. Acad. Sci. USA* 102.7 (2005), pp. 2390–2395.

[17] Jianping Fu et al. "Mechanical regulation of cell function with geometrically modulated elastomeric substrates." In: *Nat. Methods* 7.9 (2010), pp. 733–736.

[18] Nathalie Q Balaban et al. "Force and focal adhesion assembly: a close relationship studied using elastic micropatterned substrates." In: *Nat. Cell Bio.* 3.5 (2001), pp. 466–472.

[19] Lea Trichet et al. "Evidence of a large-scale mechanosensing mechanism for cellular adaptation to substrate stiffness." In: *Proc. Natl. Acad. Sci. USA* 109.18 (2012), pp. 6933–6938.

[20] Sangyoon J Han et al. "Decoupling substrate stiffness, spread area, and micropost density: a close spatial relationship between traction forces and focal adhesions." In: *Biophys. J.* 103.4 (2012), pp. 640–648.

[21] Michael J Rust, Mark Bates, and Xiaowei Zhuang. "Sub-diffraction-limit imaging by stochastic optical reconstruction microscopy." In: *Nat. Methods* 3.10 (2006), pp. 793–795.

[22] Bo Huang et al. "Three-dimensional super-resolution imaging by stochastic optical reconstruction microscopy." In: *Science* 319.5864 (2008), pp. 810–813.

[23] Sebastian van de Linde et al. "Direct stochastic optical reconstruction microscopy with standard fluorescent probes." In: *Nat. Protoc.* 6.7 (2011), pp. 991–991009.

[24] Olivier Rossier et al. "Integrins b1 and b3 exhibit distinct dynamic nanoscale organizations inside focal adhesions." In: *Nat. Cell Bio.* 14.10 (2012), pp. 1057–1067.

[25] Pakorn Kanchanawong et al. "Nanoscale architecture of integrin-based cell adhesions." In: *Nature* 468.7323 (2010), pp. 580–584.

[26] Paolo Annibale et al. "Identification of clustering artifacts in photoactivated localization microscopy." In: *Nat. Methods* 8.7 (2011), pp. 527–528.

[27] Alexandre Saez et al. "Rigidity-driven growth and migration of epithelial cells on microstructured anisotropic substrates." In: *Proc. Natl. Acad. Sci. USA* 104.20 (2007), pp. 8281–8286.

[28] Michael T Yang et al. "Assaying stem cell mechanobiology on microfabricated elastomeric substrates with geometrically modulated rigidity." In: *Nat. Protoc.* 6.2 (2011), pp. 187–213.

[29] Ingmar Schoen et al. "Probing cellular traction forces by micropillar arrays: contribution of substrate warping to pillar deflection." In: *Nano Lett.* 10.5 (2010), pp. 1823–1830.

Chapter 3

Orientation of the actin cytoskeleton determines cell shape and force exertion [1]

[1] This chapter is based on: H. van Hoorn, W. Pomp and T. Schmidt, Orientation of the actin cytoskeleton determines cell shape and force exertion, to be submitted

abstract

Characterization of cellular contractility is key to understanding many of the processes governing cellular function. With live-cell measurements of actin organization and cellular force exertion, we observed actin fibers to orient preferentially in the direction of force exertion. Since circular arcs provided a good fit to cortical actin in these fibroblast cells, we used the theoretical description of a mechanical equilibrium. We directly observed the local balance between internal stress, line tension, radius of curvature and external forces. However, the resulting internal stress did not give a constant result over different cells, as would be expected for a homogeneously contractile cell. We therefore developed an analytical model to describe the relationship between contractile stress and orientation of the actin cytoskeleton. Local stress fiber density and -force guidance were sufficient to explain our results. This yielded a quantitative description of the local force balance along the actin cortex. Our observed ten-fold increase in contractile stress is attributed to local actin orientation, showing that cell shape and force exertion are guided through directed contractility of the actin cytoskeleton.

3.1 Introduction

In recent years, the importance of the mechanical characterization of cellular behavior has attracted increasing attention [1, 2]. This interest has developed since processes like directed cell migration [3], stem-cell differentiation [4, 5] and metastatic development [6, 7] have been found to be controlled by a significant stiffness-dependent component. However, how cells probe the mechanical properties of the environment is largely unknown. The process of mechanosensing likely involves a step in which the cell pulls on its environment, followed by a biochemical stiffness-dependent readout. Cellular pulling forces in the nanoNewton range have been observed by various techniques [8–10]. These forces are generated by the actomyosin cytoskeleton. Actin with myosin contractility forms the active network allowing to pull on the environment via specific membrane-spanning proteins. For many cells and extended periods of the cellular lifecycle the cytoskeletal network was found to be fairly homogeneous. This observation has spurred the development of models that seek a quantitative description of cell-generated forces [11–13]. In particular, active solid theory [11] directly links internal forces to cell-shape and succesfully describes observations that allow one to estimate the force exerted by the network.

However, for many cells, forces are highly directional and the organization of the cytoskeleton is far from homogeneous. Here we developed a description of cellular force generation building on those earlier models, including effects emerging from inhomogeneity in the network. To our surprise we found that the earlier result of a direct relation between cellular stress and cell shape [11, 14, 15] was fully recovered when the global cellular stress is interchanged by a local stress from an oriented stress-fiber (SF) network. We developed a model that takes relative SF density along the actin cortex and the fractional guidance along the network orientation into account. Using quantification of the network orientation, cortex curvature and a direct measurement of local cellular force exertion we validated our hypothesis. Further our model allowed us to obtain an estimation for the ratio between the stress developed from the cell's homogeneous cytoskeletal network in comparison to the stress emerging from the oriented network. We showed for fibroblasts that the stress from the oriented SF network outgrows that of the homogeneous network by approximately one order of magnitude.

3.2 Methods

3.2.1 Cell biology

3T3 fibroblasts were cultured in high-glucose DMEM medium supplemented with 10% newborn bovine serum (Thermo Scientific), 2 mM glutamine and 100 µg/ml pennicilin/streptomycin. Using virus transduction, a stable cell line expressing LifeAct-mCherry was created and kept in culture. Lentiviral particles using construct pRRL-Lifeact-mCherry (a gift of O. Pertz, University of Basel, Basel, Switzerland) were isolated from the supernatant of HEK293T cells. They were transiently transfected with third-generation packaging constructs and lentiviral expression vectors. 3T3 Fibroblasts were infected with the supernatant containing lentiviral particles in the presence of 4 µg/ml polybrene overnight. Cells were continuously selected using 1 µg/ml puromycin in culture.

After micropillar array preparation (see next section), cells were seeded at single cell density at approximately 100,000 cells per micropillar array. They were allowed to spread for 6 to 16 hours. Micropillar arrays were then inverted onto #0, 25 mm diameter, round coverslips (Menzel Glaser). The arrays were kept from floating using a support weight of glass during imaging.

3.2.2 Force measurement

Cellular traction forces were quantified using micropillar arrays as previously described [10]. Briefly, PolyDiMethylSiloxane (PDMS) micropillars with 2 µm diameter, 6.9 µm height and 2 µm spacing were produced using replica-molding from a silicon wafer etched with reactive ion etching. Only the tops of the micropillars were micro-contact printed with 50 µg/ml Fibronectin and 10 µg/ml Fibronectin-Alexa405. The labeled Fibronectin was imaged to ensure a homogeneous substrate and to determine the micropillar center. Through calibration of the bulk PDMS stiffness, exact micropillar dimensions and Finite Element simulations, we obtained a precise force-deflection calibration [10]. From the deflection fields we obtained a pillar localization precision of 30 nm, corresponding to 500 pN. All analysis was performed using specifically designed software (Matlab, Mathworks).

3.2.3 Microscopy

Live-cell measurements were performed in overnight time-lapse measurements on a confocal spinning-disk setup based on a Axiovert 200 body (Zeiss) with a home-made focus-hold system. For imaging, a 405 nm laser (Crystalaser) and a 561 nm laser (Cobolt) were controlled with and Acousto-Optic Tunable Filter (AA Optoelectronics) and coupled into the confocal spinning-disk unit. Collimated 850 nm LED illumination was coupled into the backport of the microscope and aligned to reflect of the glass-water interface back out the backport via a dichroic mirror. Using a reference detector before incoupling and a high sensitivity detector (Thorlabs) after reflection, the sample was kept at constant distance from the objective. Simultaneously, the temperature was kept at 37 °C with constant 5% CO2 concentration in a stage-top incubator (Tokai Hit, Japan). In this configuration, time-lapse movies were recorded overnight on live cells on inverted micropillar arrays.

3.2.4 Cellular curvature fitting

On spread cells, a custom-made algorithm in Matlab was used to determine curvature of the actin cortex. For a two- dimensional description (the cells are spread on a surface), the line tension λ is equal to the force along the curved actin cortex. The local mechanical equilibrium at this curve can be described by the balance of the surface tension σ. This is given by the line tension λ and the radius R through $\sigma=\lambda/R$. When two arcs emanated from one site of force exertion, we decomposed the force vector along the tangent of the two. A combined measure of the curvature and the line tension thus gives the local surface tension.

3.2.5 Actin stress fiber orientation

Orientation and coherence of the actin cytoskeleton was determined using the OrientationJ [16] plugin in ImageJ. This plugin makes orientation and coherence maps based on the local gradient of an image. Analysis was done using a Gaussian gradient with a window of 5 pixels. Only pixels with a local coherence above a threshold of 0.4 (on a scale 0-1) were used. The results from the ImageJ analysis was imported into Matlab (Mathworks) and further image processing was done in specifically designed Matlab scripts.

For the comparison between cortical actin orientation and the cell edge only the pixels in an arc with a radius between 10 and 50 pixels (approximately 5 µm into the cell) beyond the fitted arc were taken into account. The average orientation of the edge was determined using the the coordinates of the endpoints of the edge. The resulting relative orientation of the actin with reference to the cell edge was determined to be the difference between the actin orientation and the edge orientation.

3.3 Results

3.3.1 Actin stress-fibers co-orient with local force exertion

Mouse 3T3 fibroblasts that were transformed with the actin label LifeAct-mCherry were spread on inverted micropillar arrays and observed on a high-resolution microscope. This approach allowed us to simultaneously observe cell shape, organization of the cortical actin and of the actin SFs, as well as to analyze the forces the cells applied to the substrate. Figure 3.1A shows a 3T3 fibroblast expressing LifeAct-mCherry (red) as it was spread on micropillars coated with labeled fibronectin (blue). Actin SFs inside the cell and the cortical actin fibers that stretch along the cell's perimeter were clearly visible. Forces, as determined from the deflections of the micropillars, are indicated by white arrows. They extend in a range of 0-10 nN as observed previously for fibroblasts [8–10]. These live-cell measurements provided simultaneous information on cellular force exertion and the actin cytoskeletal organization.

Already from the raw image a strong parallel correlation between SF orientation and the direction of the cellular force is obvious. To further quantitate this observation we analyzed the SF arrangement. The local orientation of the actin cytoskeleton was quantified by means of a structure-tensor approach that involves image thresholding and erosion [16] (figure S1A). Subsequently, the orientation-map was analyzed for areas of structural coherence (coherence map, figure S1B) that finally yielded an orientation map as shown in figure 3.1B. The actin meshwork orientation ranged from -90° to +90° with respect to the x-axis of the figure. Subsequently we quantified the direction of the cellular forces with respect to the direction of the SF directional map. The analysis yielded that forces largely align with the diection of the SFs. Figure 3.1C shows co-orientation (0±20)° of the actin cytoskeleton with the direction

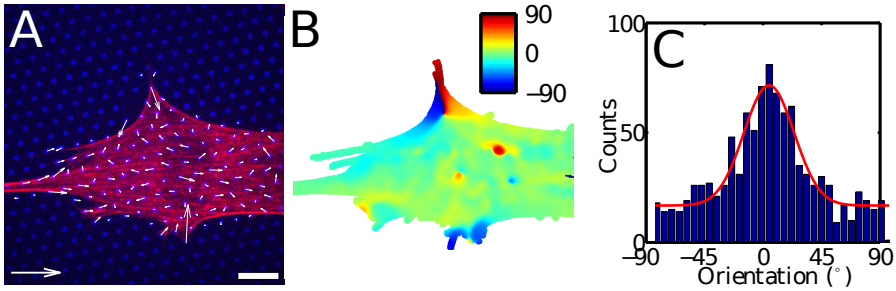

Figure 3.1
The orientation of actin stress fibers coincides with the direction of force exertion. (A) A 3T3 Fibroblast expressing lifeAct-mCherry (red) shows a polarized SF structure on top of micropillars with labeled fibronectin (blue). Cellular contractile forces are directed inward, but co-orient with the orientation of stress fibers (Arrow scalebar lower left corresponds to 20 nN, scalebar lower right corresponds to 10 µm). (B) Orientation map of actin fluorescence as depicted in (A), color coding from -90° (blue) to +90° (red). (C) Histogram of orientation difference of SFs relative to orientation of force exertion. Orientations of SFs and force exertion coincide within a distribution of standard deviation of 20° (24 cells, 997 orientations).

of force exertion for 997 displaced pillars in 24 cells. Our orientation analysis on the local scale of several micrometers corroborates earlier observations of directional cytoskeletal contractility [13] on the scale of the whole cell.

3.3.2 Cortical stress fibers suggest a homogeneous contractility

Next to the cytosolic SFs we analyzed the cortical SFs that align along the perimeter of the cell and contribute to the cellular integrity. Many of those cortical fibers were described by circular arcs to high accuracy as exemplified in figure 3.2B. For a mechanical system to display a deformation along a circular-arc one would predict a homogeneously distributed tension to act on the system [17]. The observation of a circlular arc-like cell perimeter has been reported earlier and has led to the homogeneous active solid theory of a cell [11]. In active solid theory the cell's contractility is characterized by an isotropic stress σ acting on the cortical actin leading to an outer circular arc of radius R. At the point of intersection between two arcs the cell exerts a force F on the environment that gives the line tension λ along the arc (see schematic figure 3.2A).

Indeed, our measurements showed that the highest forces emerged on pillars that were at the intersection of those circular arcs (see figure 3.2C). We therefore treat such a circular arc as a local mechanical equilibrium. This equilibrium follows Laplace's law, where internal contractile stress σ follows from the arc-radius R divided by the line tension λ:

$$\sigma = R/\lambda \tag{3.1}$$

Qualitatively our data followed the expected behavior for an increasing radius of curvature compared to spanning distance d. Previously [11], this behavior was explained by introducing an elastically-modified line tension. Even though the tension-elasticity model explains the observed variation in R-d dependence, it does not take a potential guidance of contractility along an inhomogeneous network into account. In our measurements we were able to directly quantify the line tension λ through the force exerted on the substrate. Independantly, we quantified the radius of curvature R by fitting a circle as depicted in figure 3.2B. Resulting from equation 4.1 we obtained a direct measure of the local contractile stress σ, which should be constant for a homogeneously contractile system. However, we observed variations between different circulars arcs, ranging from 0.1 to 1 $\mu N/\mu m$.

3.3.3 Contractile stress increases depending on the local stress fiber orientation

The shortcomings of the description of a cell as homogeneous system, together with our observation of the co-orientation of forces with the SF network motivated us to develop a cellular model that includes the orientation information. We use the observation that the SF orientation is nearly constant along each circular-arc. In our model, we take two distinct mechanisms into account that have consequences for both cell shape and force exertion. The first effect relates to the effective density of SFs at the cell periphery. When we assume the average distance δ between SFs to be constant, the density along the cortex depends on the local actin orientation θ. We propose that a more perpendicular orientation of SFs causes a higher local network density at the edge and thus a higher curvature:

$$\frac{1}{R} = \frac{1}{\delta} sin(\theta) \tag{3.2}$$

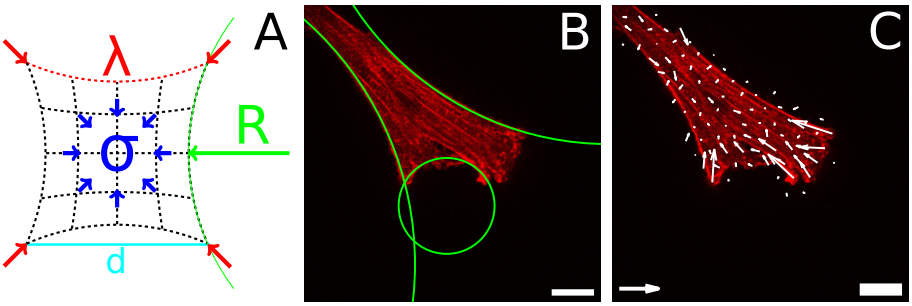

Figure 3.2
Cortical actin can be described by circular fits corresponding to an internal contractile stress. (A) Active solid theory describes how a continuum is contracted by an internal contractile stress σ. In a local mechanical equilibrium along the cortex the stress is given by the radius of curvature R and line tension λ. (B) Certain cellular edges can be fitted well by a circle, indicating an inward pulling force that is distributed over the entire cortex. (C) Micropillar deflections quantify the local force generated by the cell. The force is directed along the cortical actin and is large at the extremities of a circular arc, but mostly absent along the arc. The measured force gives a direct measure for the line tension λ. (scalebar in lower right in B and C indicates 10 μm, force scalebar in lower left in C indicates 10 nN)

Further we assummed that the force generated by SFs is transmitted through the cortical actin fibers. The second effect is described by the tangential part of the tension, $\lambda_{tan} = \lambda sin(\theta)$, which is the component of the force transmitted in the SFs. This reduced force is homogeneously distributed along the cortical actin. It should be noted that our model, although local directional information is included, still fulfills the strong requirement of a locally homogeneous medium that leads to circular-arc deformations of the cortical actin. As is schematically depicted in figure 3.3A, we assume forces exerted by the oriented SF network to be transmitted through a finer actin meshwork giving rise to the shape of the actin cortex. Finally, when the SFs are fully parallel along the edge we assume a basal level of homogeneous contractility σ_0. Taken together, the effect the contractile stress along the cell periphery can be described as:

$$\sigma = \frac{\lambda_{tan}}{R} = \frac{\lambda}{\delta} sin^2(\theta) + \sigma_0 \tag{3.3}$$

From our extended model predictions can be made for the cellular forces and concomittant cell shape which are confimed by our experiments. First, following equation 4.2 , the curvature should scale linearly

with $sin(\theta)$, depending on the orientation of the local actin network. The orientation of the actin cytoskeleton we defined along a region $\sim$ 5 μm into the cell along the curved actin cortex. In figure 3.3B the arc curvature (1/R) is shown as a function of SF orientation along the arc. Indeed, the data follow the predicted linear increase characterized by a slope of $\frac{1/R}{sin(\theta)}$=(0.12±0.01) μm^{-1} (R^2=0.8218). Hence, the curvature of cortical actin scale linearly with the direction of internal actin orientation.

In our experiments, we further quantified the local cellular force exertion and thus the local internal stress at a curved actin cortex. We quantified the line tension as the tangential force along the curved actin from the deflection of a pillar (see figure 3.3A). When we take this line tension into account and test our model, we observe a striking correspondence in figure 3.3C. Both curvature and force exertion together depend on the orientation of the actin network, which determines the local contractile stress. It is important to note here that we have three independent measurements for network orientation, curvature and line tension and all come together to corroborate our model. For a parallel orientation of actin SFs, i.e. $\sin(\theta)$=0, the fit to our model gives a basal contractile stress σ_0=(0.08±0.02) nN/μm. The contractile stress increases with more parralel SF orientation scaling with $\sin^2(\theta)$ at a rate of $\frac{\lambda}{\delta}$=(0.86±0.07) nN/μm (R^2=0.8179). Our quantitative model explains the increase in contractile stress from the local SF orientation over one order of magnitude.

3.4 Discussion and conclusion

Contractility of the actin cytoskeleton generates significant pulling forces which are at the basis of cellular function. We observed that local cellular force exertion co-orients with the actin cytoskeleton. The forces exerted along the edge were dominant at the extremities of curved edges. But the actin cortex is circular, implying a force distribution along these arcs. In this work, we have expanded on active solid theory to describe a model that takes inhomogeneous and directed contractility into account. To validate our model describing network spacing and force bearing SFs, we quantified actin organization, curvature of the cortex and cellular force exertion in live fibroblast cells.

Actin curvature increases with a locally more perpendicular actin cytoskeletal organization in a linear relation. When the forces exerted

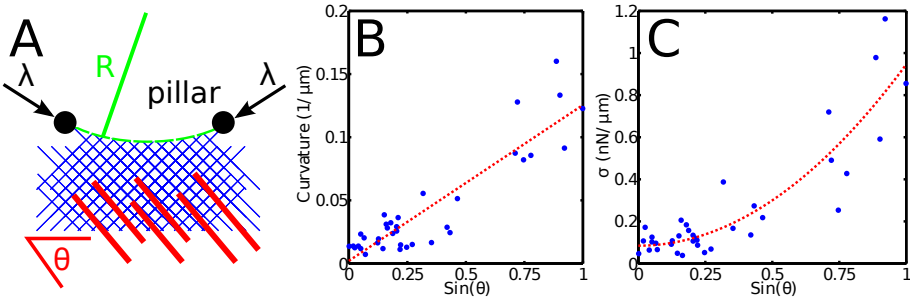

Figure 3.3
Local cortical actin curvature and force exertion increase depending on local actin orientation. (A) Schematic depiction of our model, indicating a relation between external force applied, curvature, SF orientation leading to contractile stress σ. θ is the angle of actin fibers relative to the cell cortex. Curvature and contractile stress are predicted to increase with sin(θ). (B) Experimental results (blue) show a good fit to the predicted linear increase in actin cortex curvature. In our model, this is attributed to decrease in SF spacing due to the angled oriented network. The linear fit (red line) describes an increase in curvature of 0.12 μm^{-1}. (C) Internal stress $\sigma=\lambda/R$ increases even more pronounced with larger θ. This can be explained by a co-operative effect of decreased local spacing and force exertion carried over SFs. The fitted model (red line) shows a quadratic increase from a contractile stress baseline σ_0=0.08 nN/µm with 0.86 nN/µm. This behaviour explains an increased contractile stress over one order of magnitude depending on SF orientation.

are taken into account an even more dramatic increase emerges. The measured values correspond well to the predicted theory, indicating that the orientation of actin SFs matters for both the density and the force transmission. From a baseline of homogeneous contractile stress of 0.08 nN/µm, perpendicular orientation of the actin cytoskeleton coincides with a ten-fold increase in contractility. These results imply a re-distribution of contractility along cortical actin and a strong dependence on a polarized actin structure of the contractile stress. The theoretical framework presented here provides a quantitative and qualitative description of the active mechanical directed behaviour of a single cell.

3.5 Supplemental figures

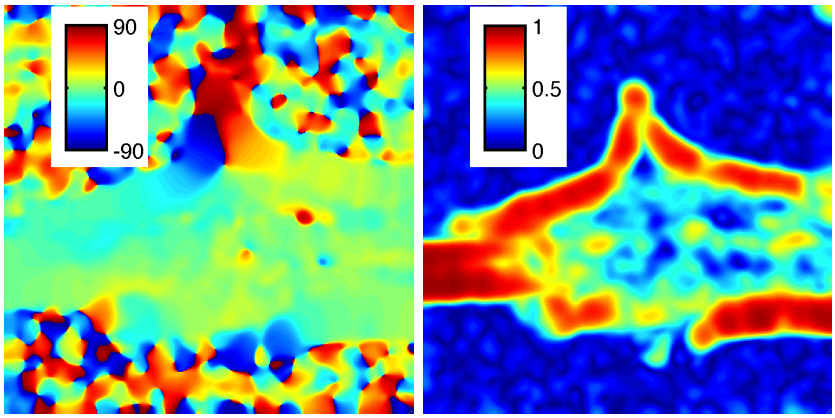

Figure S1
(A) Orientation map of a single cell and the surrounding noise. Orientation range over 180 degrees, with color coding from -90 (blue) to +90 (red) degrees. (B) Coherence map of the same cell with an arbitrary scaling from 0 (blue) to 1 (red). Only sufficiently coherent structures above a threshold of 0.4 are taken as significant values.

Bibliography

[1] Dennis E Discher, Paul Janmey, and Yu-Li L Wang. "Tissue cells feel and respond to the stiffness of their substrate." In: *Science* 310.5751 (2005), pp. 1139–1143.

[2] Viola Vogel and Michael Sheetz. "Local force and geometry sensing regulate cell functions." In: *Nat. Rev. Mol. Cell Bio.* 7.4 (2006), pp. 265–275.

[3] Ryan D Sochol et al. "Unidirectional mechanical cellular stimuli via micropost array gradients". In: *Soft Matter* 7 (2011).

[4] Adam J Engler et al. "Matrix elasticity directs stem cell lineage specification." In: *Cell* 126.4 (2006), pp. 677–689.

[5] Joe Swift et al. "Nuclear lamin-A scales with tissue stiffness and enhances matrix-directed differentiation". In: *Science* 341.6149 (2013), p. 1240104.

[6] Sanjay Kumar and Valerie M Weaver. "Mechanics, malignancy, and metastasis: the force journey of a tumor cell". In: *Cancer Metast. Rev.* 28.1-2 (2009), pp. 113–127.

[7] Melody A Swartz and Amanda W Lund. "Lymphatic and interstitial flow in the tumour microenvironment: linking mechanobiology with immunity." In: *Nat. Rev. Cancer* 12.3 (2012), pp. 210–219.

[8] Nathalie Q Balaban et al. "Force and focal adhesion assembly: a close relationship studied using elastic micropatterned substrates." In: *Nat. Cell Bio.* 3.5 (2001), pp. 466–472.

[9] Lea Trichet et al. "Evidence of a large-scale mechanosensing mechanism for cellular adaptation to substrate stiffness." In: *Proc. Natl. Acad. Sci. USA* 109.18 (2012), pp. 6933–6938.

[10] Hedde van Hoorn et al. "The nanoscale architecture of force-bearing focal adhesions". In: *Nano Lett.* 14.8 (2014), pp. 4257–4262.

[11] Ilka B Bischofs et al. "Filamentous network mechanics and active contractility determine cell and tissue shape." In: *Biophys. J.* 95.7 (2008), pp. 3488–3496.

[12] Daisuke Mizuno et al. "Nonequilibrium mechanics of active cytoskeletal networks." In: *Science* 315.5810 (2007), pp. 370–373.

[13] A Zemel et al. "Optimal matrix rigidity for stress fiber polarization in stem cells." In: *Nat. Phys.* 6.6 (2010), pp. 468–473.

[14] Ilka B Bischofs, Sebastian S Schmidt, and Ulrich S Schwarz. "Effect of adhesion geometry and rigidity on cellular force distributions." In: *Phys. Rev. Lett.* 103.4 (2009).

[15] A Zemel, IB Bischofs, and SA Safran. "Active elasticity of gels with contractile cells." In: *Phys. Rev. Lett.* 97.12 (2006).

[16] R Rezakhaniha et al. "Experimental investigation of collagen waviness and orientation in the arterial adventitia using confocal laser scanning microscopy". In: *Biomech. Model. Mechan.* 11.3-4 (2012), pp. 461–473.

[17] J.B. Marion and S.T. Thornton. *Classical Dynamics of Particles and Systems*. Thomson Learning, 1995.

Chapter 4

P130Cas is a mechanosensor that modulates force exertion at focal adhesions [1]

[1]This chapter is based on: H. van Hoorn, D.M. Donato, H.E. Balcioglu, E.H. Danen and T. Schmidt, p130Cas is a mechanosensor that modulates force exertion at focal adhesions, to be submitted

abstract

The Src substrate p130Cas plays a key role in regulating focal adhesion (FA) turnover and has previously been proposed as a direct mechanosensor. Proof of this principle and how p130Cas may influence force exertion remains unclear. Here we compared knockout cells (Cas -/-) to Cas -/- cells re-expressing either full-length p130Cas (Cas WT) or a mutant lacking the FA targeting domains (Cas ΔSH3/ΔCCH) on substrates of tunable stiffness. On poly-acrylamide gels of varying stiffness, we observed a differential response in FA formation dependent on the presence of p130Cas. On micropillar arrays of varying stiffness p130Cas only localized well to sites of force exertion on pillars with a stiffness larger than 47.2 kPa. Differential localization coincided with increased force exertion magnitude and decreased rate, as confirmed by comparison to the Cas ΔSH3/ΔCCH mutant that is known not to localize to FAs. Our results show that p130Cas is a mechanosensor that enables cells to sense stiffness in a physiologically relevant range and its differential localization directly influences a change in cellular force exertion.

4.1 Introduction

Tissues, cells and extracelullar matrix show a great variety in stiffness [1, 2]. In recent years, it has become apparent that these features not only emerge from but also dictate biological function [3–6]. Stiffness-dependent cellular behavior is attributed to a variety of molecular responses, such as transcription factor incorporation [7], remodeling of the nuclear envelope [3], and differential responses of Focal Adhesion (FA) protein signaling [8]. FAs are of particular interest in this respect, since they are the main site of force transmission by the cell on the extracellular matrix. As multi-molecular complexes, FAs contain a multitude of functional biological interactions [9]. The combination of force transmission and biological functionality observed at these sites has given rise to a variety of hypotheses on the stiffness-dependent mechanosensory role for FA proteins. Here, we address the mechanosensory role of the FA signaling protein p130Cas.

P130Cas is a member of the Cas (Crk associated substrate) family that regulates important cellular behavior such as migration, apoptosis, cell-cycle progression and differentiation [10]. Knocking out p130Cas constitutively leads to embryonic lethality 11.5-12.5 days post-fertilization. Moreover, p130Cas (also known as Breast Cancer Anti-Estrogen Resistance protein 1, BCAR1) has been associated with resistance to anti-estrogen treatment (the most commonly used treatment for breast cancer, i.e. Tamoxifen). Another study revealed that p130Cas overexpession predicts a poor prognosis in non-small-cell lung cancer [11].

The functional role of p130Cas is that of a scaffolding protein capable of initiating signaling cascades by recruiting proteins to multiple domains that act as protein-docking sites. These domains include a Src Homology 3 (SH3) domain on the N-terminus, a proline-rich domain, a central Substrate Domain (SD) containing 15 YxxP motifs, a serine-rich domain, a Src-Binding Domain (SBD) containing motifs for binding both the Src SH3 and SH2 domains, and a well conserved Cas-family C-terminal Homology (CCH) domain. A simplified schematic drawing of the p130Cas structure is shown in figure 4.1.

P130Cas promotes cell spreading in response to integrin engagement and was identified as an important driving force in cell migration through promotion of FA assembly and -turnover [12, 13]. Both the SH3 domain on the N-terminus and the CCH domain on the C-terminus localize the protein to FAs [14]. Phosphorylation of the SD directly influences migra-

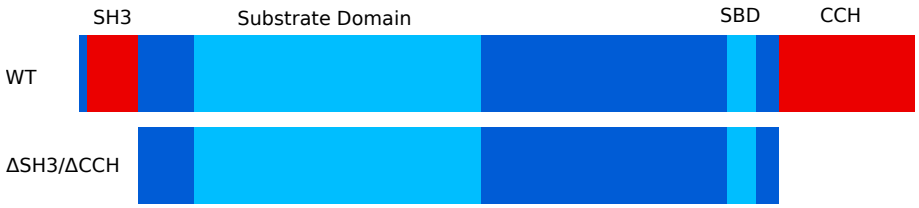

Figure 4.1
P130Cas structure and its domains. The ability of p130Cas to localize to FAs is mediated by the SH3 and CCH domains. The Substrate Domain (SD) contains 15 YxxP motifs that can be phosphorylated by Src. Src kinase can bind through the SBD or FAK bound via the SH3 domain [14]. Tyrosine phosphorylation of the SD is thought to depend on mechanical stretch [16]. Both the WT and ΔSH3/ΔCCH variants of p130Cas were used for this study.

tion, actin dynamics and FA dynamics [12, 14, 15].

In addition to its importance in cellular function and disease, a mechanosensory role has been proposed for p130Cas that remains unclear. Experiments on Triton-X extracted cytoskeletons of cells showed an increase in phosphorylation of p130Cas when cells were physically stretched [16]. Similar data have been gathered *in vitro* with a recombinant p130Cas substrate domain, demonstrating that its intrinsically disordered SD can be unfolded at pN forces leading to phosphorylation [17, 18]. This force range is expected to occur at the sites of integrins in FAs [19]. From these observations it was proposed that a large enough force to physically stretch the protein could make phosphorylation of the SD possible. It is unclear, however, whether physiological forces and extracellular stiffnesses have an impact on p130Cas localization and force exertion. Many functions of p130Cas have been characterized for cells grown on stiff glass and plastic substrates. Since p130Cas is involved in various biological and pathological functions, we performed experiments to understand whether p130Cas functions as a mechanosensor in a physiological stiffness range and how it might be involved in cellular mechano-regulation.

In this paper, we address the ability of p130Cas to sense and control forces in mouse embryonic fibroblasts (MEFs) grown on fibronectin coated substrates. We compared knock-out MEFs with p130Cas reintroduced at endogenous levels (Cas WT) to MEFs completely lacking p130Cas (Cas -/-) and MEFs expressing a variant of p130Cas without

the FA-targeting domains (Cas ΔSH3/ΔCCH) (see figure 4.1). Increase of FA size with increasing stiffness on poly-acrylamide (PA) gels occured at a stiffness of 42 kPa when p130Cas was present as compared to an increase in FA size at 87 kPa in Cas -/- cells. This shows that p130Cas plays a role in stiffness-dependent cell spread and FA formation. Using live-cell experiments, we observed that p130Cas localization to FAs increased where significant forces were exerted only on micropillars with a global stiffness larger than 47.2 kPa. With time-lapse microscopy we compared the dynamic force-exertion behavior of Cas WT cells to the Cas ΔSH3/ΔCCH mutant. This showed that p130Cas localization at high stiffness caused increased force exertion and decreased rates, making transient forces slower when p130Cas was present. As p130Cas localization occured before and during force exertion, we propose a mechanism where p130Cas functions as a mechano-chemical sensor and responder that changes cellular force exertion dependent on the global extracellular stiffness.

4.2 Methods

4.2.1 Cell biology

Cas -/- Mouse Embryonic Fibroblasts (MEFs) were used and adapted as previously described [14]. Briefly, p130Cas knockout MEFs were grown in Dulbeccos modified Eagles medium supplemented with 10% fetal bovine serum, 1% penicillin/streptomycin and 1% gluatamax. Cells were maintained in an incubator at 37°C, with 7% CO_2. p130Cas fused to YFP was re-introduced using retroviral transduction either in its full form or lacking both the CCH- and SH3-domains (for details see [14]. On PA gels, cells were seeded 1h prior to fixation with 4% ParaFormAldehyde in Phosphate Buffered Saline. On the micropillar arrays, cells were seeded 6h prior to overnight imaging in full medium. In both cases, cells were seeded at single-cell density.

4.2.2 PolyAcrylamide gels

PolyAcrylamide (PA) gels were prepared similarly to previous work [20]. Briefly, 12mm sterile coverslips were placed in 24-well plates, cleaned with 0.1 M NaOH, and then rendered hydrophilic by incubating with 0.5% 3-aminopropyl-

trimethoxysilane (3-APTMO, Sigma-Aldrich). The coverslips were then washed thoroughly with sterile distilled water and incubated in 0.5% glutaraldehyde and dried overnight in laminar flow. Coverslips of 10 mm diameter were rendered hydrophobic by incubating with a solution of 10% Surfa-Sil in chloroform (Thermo Scientific), washed in 100% chloroform, then in methanol and dried under laminar flow. PA solutions were made with a mixture of Acrylamide and Bis-Acrylamide as given in table 4.1.

After mixing Acrylamide and Bis-Acrylamide, 1.5 µl TEMED and 5µl of 10% ammonium persulfate were added to start polymerization. On each 12 mm coverslip, 10 µl was applied and the 10 mm coverslips were placed on the top to make a flat layer and left to polymerize for 1 hour. After 15 minutes washing with 50mM 4-(2-hydroxyethyl)-1-piperazineethanesulfonic acid (HEPES), the top 10 mm coverslips were removed and washed once with 50 mM HEPES. Cross-links for fibronectin on PA gels were created by incubating 0.5 mM sulfosyccinimidyl-6-hexanoate (sulfo-SANPAH, Thermo Scientific) in 50mM HEPES on gels under UV light for 8 mins. The gels were washed with 50 mM HEPES, then incubated with sulfo-SANPAH again under UV light, and washed extensively with 50 mM HEPES before incubatingovernight at 4 °C in 10 µg/ml fibronectin and 50 µg/ml Alexa405-conjugated fibronectin in PBS. After removing the fibronectin solution by washing with PBS, PA-gels were allowed to equilibrate for one hour in complete culture media at 37 °C before seeding with 25,000 cells/well complete media. Cells were allowed to adhere and spread before fixation and imaging by incubating for one hour at 37 °C and 7 % CO2.

Acrylamide (%)	Bis-acrylamide (%)	G (kPa)	E (kPa)
7.5	0.2	9.3	28
7.5	0.5	14	42
12	0.6	29	87
20	0.7	74	222

Table 4.1
Different percentages of Acrylamide and Bis-Acrylamide corresponded to different shear moduli G, as directly quantified through measurement with a rheometer. With a Poisson ratio of 0.5 this could be related to the Young's modulus E.

	28 kPa	42 kPa	87 kPa	222 kPa	Glass
Cells:	12	15	11	24	196
FAs:	750	1014	766	2054	14006

Table 4.2
Measurements on PA gels of varying stiffness were done on these numbers of cells and FAs.

4.2.3 Substrate stiffness

The substrate stiffness was measured using an Anton-Paar MCR 501 rheometer with a 40 mm diameter conical plate geometry to obtain the shear modulus G. Both storage and loss modulus were quantified, confirming a negligible viscous behavior. Assuming a Poisson ratio of 0.5 for an incompressible material, the calibrated Young's modulus was then calculated for proper comparison with previous work and our micropillar experiments.

4.2.4 Immunostaining

After 1h spreading on PA gels, the cells were fixed using 4% PFA in PBS for 15 minutes, permeabilized using 0.1% TritonX for 10 minutes and blocked using 5% normal goat serum for 1 hour (all diluted in PBS). Antibodies were diluted in blocking buffer and paxillin was recognized using a mouse-anti-paxillin IgG (BD Biosciences) and labeled by Cy3-conjugated AffiniPure Goat Anti-Mouse IgG F(ab')2 (Jackson Immunoresearch) antibody. Cells on pillars were also fixed using the same method, but stained with rabbit-anti-phosphoPaxillin (pY118, Invitrogen) and secondary Alexa647-anti-rabbit (Jackson Immunoresearch).

4.2.5 FA analysis

Automated image analysis in Matlab (Mathworks) was used to quantify FAs and their spatial properties. Using frequency-filtering and edge-detection algorithms, the cell as a whole and the FAs were detected. An example of a cell edge and the detected FAs is given in Supplemental Figure S1.

4.2.6 Force measurement

Cellular traction forces were quantified as previously described [21]. Briefly, masters were fabricated in Silicon wafers using inductively-coupled deep reactive ion etching. A two step fabrication procedure produced 1x1 cm hexagonal arrays of micropillars with a 2 µm diameter, 2 µm interpillar spacing and a varying depth which yielded the variation in stiffness. In the second step, spacers with 50 µm depth were produced flanking two sides of the 1x1 cm array, each with an area of 10x2 mm. The flanking spacers were added to keep the array at a constant distance from a 100 µm- thick coverslip constant and within the working distance of a high-NA objective. This negative master was cleaned with 100 % Isopropanol and 100 % Ethanol and passivated with Trichlorosilane (Sigma Aldrich).

Poly(DiMethyl-)Siloxane (PDMS, Sylgard 184, Dow Corning) was mixed with 1:10 crosslinker:prepolymer ratio and poured over the Silicon wafer master. After 20h curing at 110 °C the arrays were peeled off and micro-contact printed with fibronectin and fibronectin labeled with Alexa647 (Invitrogen). Prior to printing, the PDMS was activated with a UV-Ozone cleaner (Jelight) for 10 minutes and afterwards the non-printed parts were passivated with 0.2 % Pluronic (F-127, Sigma Aldrich) in PBS. The substrates were thoroughly rinsed with PBS, submerged in full medium and 100,000 cells per array were seeded. After 6 hour spreading, the samples were mounted on the microscope and imaged overnight.

	11.6 kPa	47.2 kPa	137 kPa
Cells:	12	20	13
Force curves:	153	243	119

Table 4.3
Measurements on micropillar arrays of varying stiffness were done on these numbers of cells and their transient force exertion curves.

4.2.7 Microscopy

Both live- and fixed cell imaging were performed on a specifically adapted Zeiss microscope (AxioVert 200 body) with a Spinning Disk Confocal Unit (Yokogawa X-1) and a Back-Illuminated EMCCD camera (Andor DU-897) on the side-port. Multiple laser lines were combined, controlled

using an Acousto-Optic Tunable Filter (AOTF, AA Optoelectronics) and coupled into the Spinning Disk Unit using a polarization-maintaining fiber. From the back-port a home-built focus-hold system was coupled in, using a 850 nm laser diode, dichroic mirror (Chroma) and a photodiode detector (Thorlabs). A Marzhauser XY-stage controlled automated movement to various positions on the sample at specific focus positions.

The imaging was controlled using Andor IQ-software, while the focus-hold and positions were controlled using Labview (National Instruments). The samples were mounted in a home-designed stable coverslip holder that fitted directly in the microscope incubator (Tokai Hit) and kept at 37 °C and 5% CO_2. Overnight live-cell imaging was done by moving between approximately 12 positions at specific focus points on the inverted micropillar array.

4.2.8 Force measurement

Forces and deflections were analyzed as previously described [21]. Briefly, we determined the pillar bulk material to be 2.5 ± 0.1 MPa. Scanning electron microscopy (FEI nanoSEM) was used to quantify the dimensions of the PDMS micropillars. We calibrated the exact stiffness of the micropillars using Finite Element Modeling. The pillar centroids were determined using specifically designed Matlab (Mathworks) scripts from the fluorescence images of labeled fibronectin (with Alexa647). From the deduction of a perfect hexagonal grid we obtained the pillar deflections within an accuracy of 30 nm. The corresponding force accuracy increases with increasing stiffness proportional to the bending stiffness 16.7 nN/µm, 70.9 nN/µm and 206 nN/µm for the micropillars with a global stiffness of 11.6 kPa, 47.2 kPa and 137 kPa, respectively. From the deflections and the bending stiffnesses we constructed a force field. The final local force was taken in the direction of maximal deflection, giving noise around zero force (its standard deviation corresponding to the force precision) when nothing happens to the pillar and the amount of force in the direction of migration over time.

4.2.9 Force dynamics fitting

Increase and decrease of transient force dynamics were fitted using the logistic function initially developed for population dynamics [22]. The dynamics of logistic behavior can be described by equation 4.1. We

postulated that the build-up of force will increase with a constant rate for both assembly and disassembly r up to a certain maximum force F_{max}. The resulting function for force F over time as given by equation 4.2 with offset values for time and force were fitted to the dynamic force measurements. Finally, we solved the force exertion rate out of this fit relative to the time offset $t = 0$, which results in the expression for the half-time $t_{1/2}$ given in equation 4.3.

$$\frac{dF}{dt} = r \cdot F \cdot [1 - \frac{F}{F_{max}}] \tag{4.1}$$

$$F(t) = \frac{F_{max} \cdot F_0 \cdot e^{r \cdot t}}{F_{max} + F_0 \cdot (e^{r \cdot t} - 1)} \tag{4.2}$$

$$t_{1/2} = \frac{1}{r} \cdot ln[\frac{F_{max} - F_0}{F_0}] \tag{4.3}$$

4.2.10 Comparing stiffness of PA-gel and micropillars

The Young's modulus of PA-gels can be directly derived from the measurement of the shear modulus G'. Assuming a Poisson ratio of 0.5 for an incompressible material, the Young's modulus (using E = 2G(1+ν) of our PA-gels was found to be 28, 42, 87 and 222 kPa. The effective stiffness of the micropillar arrays was determined using a prior derivaton [23] and tested and validated recently [24]. The derivation yields an effective Young's Modulus of 11.6, 47.2 and 137 kPa for the low-, medium- and high-stiffness pillars, respectively.

4.2.11 Force and p130cas dynamics

Half-times of transient force increase on a single pillar and fluorescence increase of p130Cas were quantified using specifically designed Matlab (Mathworks) scripts. The difference between force exertion rates was denoted Δt and quantified for 42 curves. The resulting distribution was quantified as a probability density function in Figure 4.5B, the original histogram is given in Supplemental Figure S4.

4.3 Results

4.3.1 Stiffness-dependent FA formation depends on p130Cas

As p130Cas influences cell spreading and promotes FA turnover, we hypothesized that it could also influence stiffness-dependent cell spreading and FA formation. To test this hypothesis, we compared the initial spreading behavior of Cas -/- and Cas WT MEFs on PA gels. PA gel stiffness was varied by changing the ratio (acrylamide:bis-acrylamide) yielding a Young's modulus range from 28 to 222 kPa (Figures 4.2A and B). After 1 hour of spreading, cells were fixed and stained for the FA protein paxillin. All fixed- and live-cell imaging was performed using a spinning disk confocal microscope setup with multi-color, high-resolution fluorescence measurements. Cell and FA area were quantified using specifically designed algorithms (for details see Methods). With increasing stiffness, cell area approximately doubled and FA size increased significantly. At the highest stiffness, both cell lines were similar to their morphology on glass [25]. This general trend corroborates similar stiffness-dependent spreading and FA size increase as has been observed previously [20, 26].

Though cell and FA area still increased irrespective of the presence of p130Cas, we observed significant differences between Cas -/- and Cas WT cells on intermediate stiffnesses. Cas WT cells only spread fully on high stiffness (222 kPa) substrates. On intermediate stiffness substrates (42-87 kPa), their cell area remained in the same range as on the softest substrates of 28 kPa. However, Cas -/- cells showed an increase in cell area from 42 kPa to 87 kPa (see Figure 4.2C). Cell spreading thus increased at a higher stiffness when p130Cas was expressed compared to when p130Cas was not present.

In the absence of p130Cas, a differential FA response was measured in the same stiffness range where a switching behavior in cell area was observed (see Figure 4.2D). In the range from 42 kPa to 87 kPa, the mean FA area increased significantly from (0.84±0.03) μm^2 to (1.00±0.08) μm^2 (mean ± s.e.). In Cas -/- cells, switching in cell area thus coincided with stiffness switching from small to large FAs.

The trend for FA area increase with stiffness was very different when p130Cas was present. On low stiffness substrates, Cas WT cells showed very poor adhesion and no FA formation. However, FAs were clearly present on substrates with a stiffness of 42 kPa and higher (Figure 4.2A).

FA area was (0.92±0.05) μm^2 on a 42 kPa substrate and did not change with increasing stiffness, though the cell area showed an increasing trend from 87 to 222 kPa. In the presence of p130Cas, cells increased their FA area readily at a low stiffness (42 kPa), even though a higher stiffness was needed for full cell spread (222 kPa). In the absence of p130Cas, this step-wise progression from increasing FA area to increased cell spread was not visible and FA area increase followed cell area increase.

Cell spread and FA formation is known to depend on substrate stiffness [20, 26], but the role of specific proteins directly involved in that process is not well understood. Our results show that p130Cas influences stiffness-dependent FA-formation at early time points (after 1 hour) of cell adhesion. The mechanism behind this mechanosensory response is potentially related to local force exertion, since FA formation has been previously observed to co-localize with areas of force exertion. Furthermore, force exertion has been observed to increase with increasing stiffness [21, 24, 27, 28]. The p130Cas-dependent FA formation with increasing stiffness thus suggests a direct dependence of p130Cas function on force exertion.

4.3.2 P130Cas localization depends on stiffness

Since p130Cas influenced stiffness-dependent FA formation, we hypothesized that p130Cas may localize to sites of force exertion depending on stiffness. To gain further insight into this potential mechanism, we performed experiments on micropillar arrays. Micropillars allow one to measure local cellular forces, while controlling the global, cell-wide extracellular stiffness. Simultaneously, we quantified subcellular fluorescence localization of p130Cas-Venus YFP. Prior studies showed that global stiffness variation of the substrate through variation of micropillar height could influence biological processes. It was shown that differentiation of mesenchymal stem cells directly depended on micropillar stiffness [29]. Indeed, forces increase with increasing stiffness [24, 28] and the FA functions as a force transducer with a high concentration of stress [21]. Sparked by our initial observation of FA formation on PA-gels, we measured force exertion- and p130Cas dynamics on micropillar arrays of varying stiffness to elucidate its mechanosensory function. Our recently developed, inverted micropillar array approach allowed us to perform high resolution, live-cell microscopy simultaneously with measurements of cellular force exertion [21].

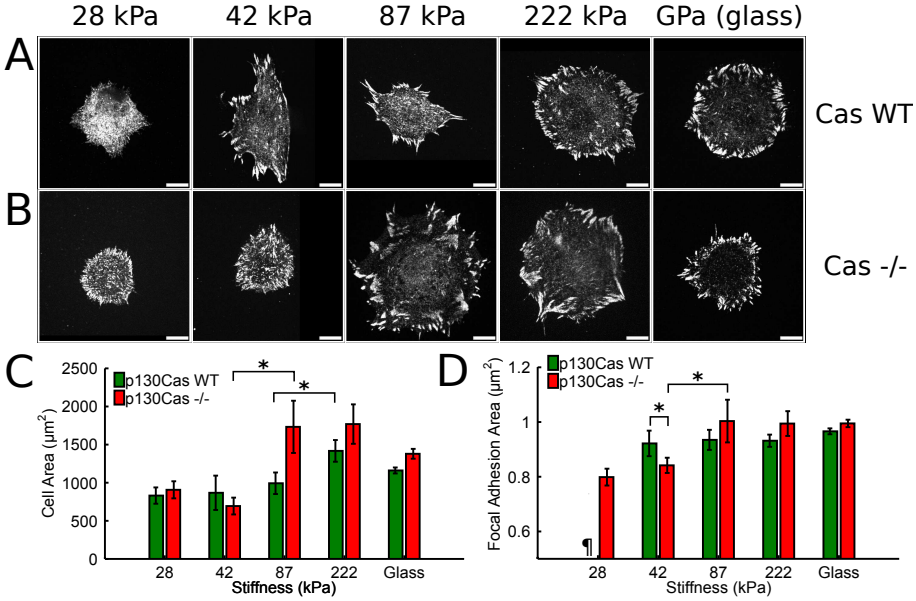

Figure 4.2
P130Cas expression influences cell spreading- and FA formation response to stiffness. (A) Cas WT and Cas -/- MEFs (B) were seeded on either on PA gels of varying stiffness (indicated in kPa) or on glass for 1 hour prior to fixation. Cells were immunostained for the common FA marker paxillin. All scale bars in B and C are 10 μm. Means and s.e.m for (C) cell area and (D) FA area were quantified for both cell types. No FAs were found for p130Cas WT cells on 28 kPa substrates (denoted by ¶). Asterisks indicate a significant difference by Kolmogorov-Smirnov test, $p<0.05$.

We tuned the global stiffness of the micropillar arrays by varying the height of the micropillars, while maintaining pillar diameter and interpillar spacing at 2 μms. Higher pillars resulted in a lower effective stiffness. Calibrated bending stiffnesses [21] yielded an effective Young's modulus as previously described [23, 24]. We tested micropillar arrays with a height of 6.9 μm, 4.1 μm and 3.2 μm, resulting in an effective Young's modulus of 11.6 kPa, 47.2 kPa and 137 kPa. The micropillar stiffness range was comparable to the stiffnesses used with the PA-gels. The tops of the micropillar arrays were functionalized with fibronectin through micro-contact printing. Pillar centroids were detected from the fluorescence signal of the fibronectin labeled with the dye Alexa647 at a localization precision of 30 nm. Deviations from the hexagonal pillar-

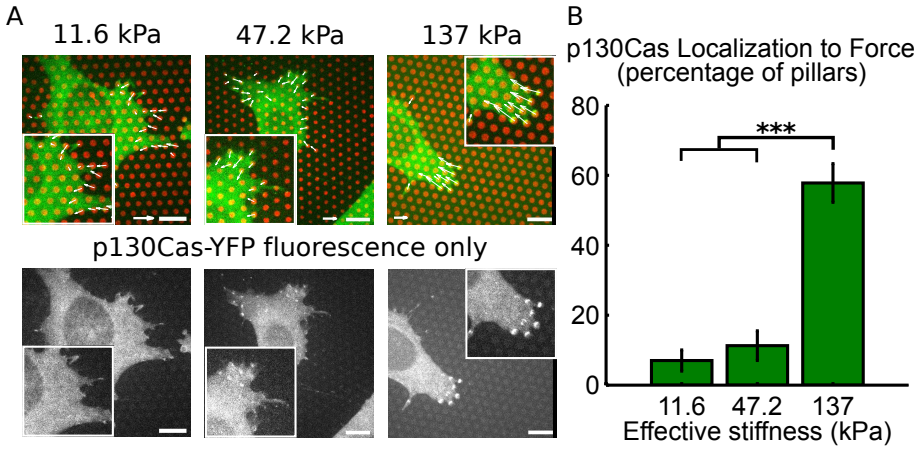

Figure 4.3
*P130Cas localizes to sites of force exertion dependent on stiffness. (A) MEFs expressing p130Cas-Venus YFP (green) at endogenous levels on micropillars (red) of varying stiffness, through variation of pillar height. Significant forces are given by white arrows, and grayscale images show p130Cas fluorescence only. Lower right fluorescence scalebar corresponds to 10 µm, lower left force scalebar corresponds to 20 nN (11.6 kPa and 47.2 kPa) and 50 nN (137 kPa). (B) The percentage of significantly deflected micropillars to which p130Cas fluorescence co-localized per cell is quantified in the bar graph with mean and s.e.m. (Significance by Kolmogorov-Smirnov test, *** $p<0.001$)*

grid provided the pillar deflections. Through calibrations from pillar dimensions and stiffness combined with Finite Element Analysis (see [21] and Methods), the local force exerted by the cell on the micropillars was derived.

Cas WT MEFs with p130Cas expressed at endogenous levels exerted significant forces on the micropillars. Cells attached only to the tops of the micropillars and were fully spread when we started the measurement 6 hours after seeding. These significant forces correspond to pillar deflections were on all different stiffnesses in the range of 0.1 - 1 µm. The magnitude of the corresponding forces increased with substrate stiffness, while the pillar deflections decreased with stiffness. Forces exerted on the micropillars were in the range of 1 - 60 nN. FA formation occurred directly on pillar-tops as we and others previously observed [21, 24, 28], where significant forces were measured (see supplemental figure S2 for staining for paxillin). We observed the localization of p130Cas simul-

taneously with local cellular force exertion. Figure 4.3A shows pillars in red, p130Cas fluorescence in green, micropillar deflections in white arrows and p130Cas fluorescence only in seperate grayscale images.

Interestingly, p130Cas localized to sites of force exertion predominantly on higher stiffness micropillar arrays as compared to the lower stiffnesses. We quantified this phenomenon through thresholding for significant pillar deflections and subsequent quantification of the fraction of those pillars with a patch of p130Cas fluorescence. Threshold values for force exertion of 10 nN, 20 nN and 30 nN were used for 11.6 kPa, 47.2 kPa and 137 kPa micropillar arrays, respectively. The resulting fraction of p130Cas localization to deflected pillars for the three stiffnesses is given in figure 4.3B. On the two lower stiffness micropillar arrays, 5-10 % of the deflected pillars showed p130Cas localization. At a global stiffness of 137 kPa, a significant increase in p130Cas localization to force exertion sites was observed: at approximately 60 % of the attachment sites where more than 30 nN of force was applied, p130Cas was localized to the tops of pillars. Localization on micropillars of 137 kPa closely resembled that of p130Cas localization to FAs on glass substrates [14].

These results directly demonstrate that p130Cas localizes to force exertion sites depending on stiffness. This local p130Cas response to FAs was in a similar stiffness range as we observed on the PA gels. On micropillars, however, the local stiffness (of the bulk PDMS) remained constant, while the pillar height varied the global stiffness. P130Cas thus responded to variations in the global extracellular matrix stiffness by differentially localizing to FAs.

4.3.3 Force exertion dynamics depend on substrate stiffness and p130Cas localization

Since p130Cas showed a clear mechanosensitive function in Cas WT cells, we hypothesized that its localization to FAs may also influence force exertion itself. P130Cas is a known docking protein that influences FA dynamics on glass [12, 14], so we investigated the dynamics of force exertion on micropillar arrays. Figure 4.4 shows still images from a time series movie of p130Cas-Venus YFP fluorescence in green and the tops of micropillars in red. As expected, random migration with an extended leading edge was visible after the cells were fully spread. Transient contractile forces opposite the direction of migration were visible at the leading edge of cells.

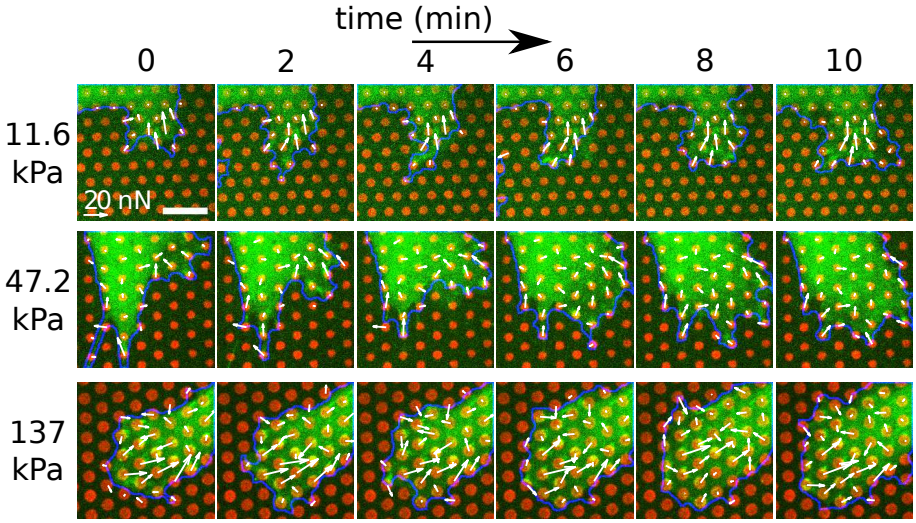

Figure 4.4
Time-lapse imaging of force exertion and p130Cas. MEFs expressing p130Cas-Venus YFP (green) at endogenous levels were imaged every two minutes to examine the dynamics of force exertion on micropillars (red). Pillar deflections (white arrows) close to the automatically detected cell edge (blue) are plotted. Time stamp is in minutes above still images, force scale bar corresponds to 20 nN and image scale bar corresponds to 10 μm (top-left image).

To test the effect of p130Cas localization to sites of force exertion, we quantified the force exertion characteristics of Cas -/- cells either re-expressing the full p130Cas-YFP (Cas WT) or a double-deletion mutant lacking both SH3 and CCH domains (ΔSH3/ΔCCH). This mutant has previously been characterized and was shown to lack FA localization while still being expressed at endogenous levels [14]. We confirmed that indeed, the truncated ΔSH3/ΔCCH version of p130Cas could not localize to FAs by fluorescence localization, whereas full-length p130Cas did localize to FAs on high-stiffness pillars as shown in Figure 4.3 and 4.4C. Cas ΔSH3/ΔCCH cells still showed transient contractile forces during random migration.

Typical curves for force over time for single pillars are shown in figure 4.5A (blue dots correspond to data) for micropillar stiffnesses of 11.6 kPa, 47.2 kPa and 137 kPa, respectively. These transient force dynamics were modeled with a logistic function (see Methods for details) that is

primarily described by two parameters: a maximum plateau force and a rate by which this maximum is obtained. The rate scales with the derivative of force over time but is independent of the plateau force. By fitting transient force exertion per pillar, we quantified the dynamics of local cellular force exertion. This model provided a good fit to the data, as shown in figure 4.5A (red line is the force increase fit and green line is the decrease fit).

The quantified plateau force (F_{max}) and rate of force exertion (r) are depicted in figures 4.5B and -C for all micropillar stiffness for both the Cas WT and Cas ΔSH3/ΔCCH cells. Cas WT cells on micropillar arrays of stiffness 11.6, 47.2 and 137 kPa showed a mean force plateau of (12.8±0.5) nN, (23.5±0.9) nN and (39±2) nN, respectively (figure 4.5B). The ΔSH3/ΔCCH mutant showed similar transient force exertion dynamics compared to the WT on 11.6 and 47.2 kPa micropillars. However, the force plateau was significantly higher for the WT in comparison to Cas ΔSH3/ΔCCH on pillars with a stiffness of 137 kPa. The mean maximum force decreased to (27±4) nN for the Cas ΔSH3/ΔCCH cells.

There was also a significant difference in the rate of force exertion for Cas ΔSH3/ΔCCH compared to Cas WT cells. On micropillars with an effective Young's modulus of 11.6 kPa and 47.2 kPa, there was no significant change in force exertion rate, for either Cas WT or Cas ΔSH3/ΔCCH cells. However, the rate of force exertion for Cas WT cells on 137 kPa pillars significantly decreased from (0.75±0.05) min^{-1} (on 47.2 kPa) to (0.45±0.03) min^{-1}. In the absence of functional p130Cas localization to FAs (ΔSH3/ΔCCH mutant), the rate on 137 kPa pillars increased to (1.72±0.45) min^{-1}.

The observed dynamics of transient force exertion were thus slower when p130Cas was present for cells on high stiffness micropillars. On low stiffness micropillars we found no significant effect on force exertion with the localization of p130Cas to FAs. The presence of p130Cas in FAs (figure 4.3) thus directly correlated to changes in force exertion, but only when the global extracellular stiffness was larger than 47.2 kPa. The force became significantly larger when p130Cas was present in FAs and the dynamics were significantly faster when p130Cas did not localize to FAs.

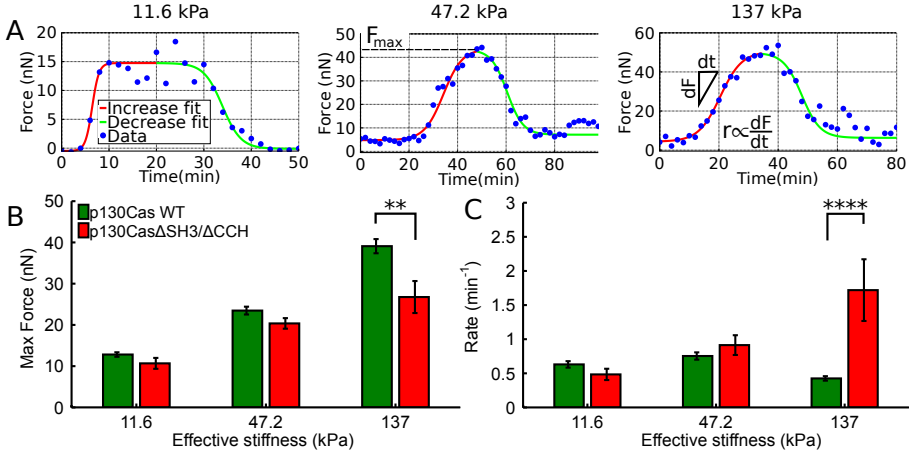

Figure 4.5

*Quantification of p130Cas-dependent force exertion dynamics. (A) Transient force exertion on a single pillar was quantified by fitting increase and decrease curves to a logistic function. From these fits the maximum force F_{max} and the rate of force exertion r were obtained. Force curves were fitted for both Cas WT- and Cas ΔSH3/ΔCCH MEFs. (B) In both cases, maximum force increased with increasing stiffness. Cas ΔSH3/ΔCCH MEFs exerted significantly less force on the high stiffness arrays. Bar represent the mean F_{max} with s.e.m. (C) The rate of force exertion also shows a significant difference only on high-stiffness micropillars. (Significance by Kolmogorov-Smirnov test, ** $p<0.01$ and **** $p<0.0001$)*

4.3.4 P130Cas localizes before and during force exertion

Since differential localization of p130Cas directly correlated to changes in force exertion, its localization may directly change local force exertion. Our experiments, as detailed in the previous paragraph, allowed us to further examine the cause and effect of p130Cas localization to FAs. We thus simultaneously quantified the time-course of p130Cas fluorescence on a pillar while a force was exerted over time. Figure 4.6A shows the force increase over time (blue) and the summed p130Cas fluorescence on top of the pillar (red, fluorescence in arbitrary units). Quantitative visualization of Cas-YFP fluorescence in a FA on the top of a single pillar through masking is given in supplemental figure S3. The time lag between force and fluorescence was quantified as the time difference between the half time of fluorescence increase and force increase.

The time-lag of force after fluorescence was quantified and shown

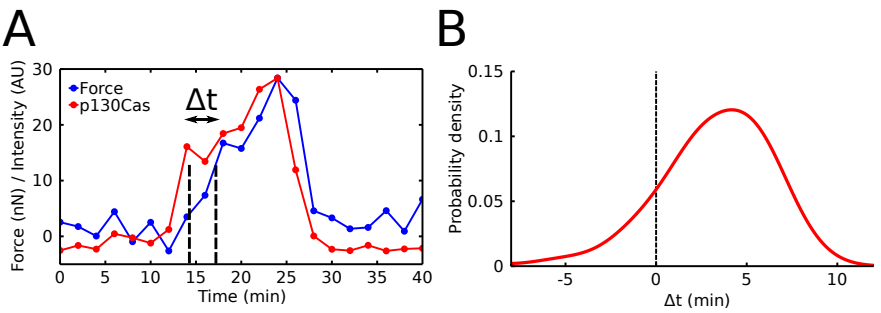

Figure 4.6
p130Cas localization precedes initial force exertion. (A) Force exertion over time on a single pillar was compared to the fluorescence intensity at the same pillar over time. Typically, p130Cas fluorescence increased just before force exertion, but continued to build up during force increase. (B) Probability density function of p130Cas fluorescence time-lag Δt. P130Cas fluorescence accumulated (3.2±0.7) minutes before force exertion.

as a probability density curve in Figure 4.6B. P130Cas preceded force exertion by (3.2±0.7) minutes and continued to increase with increasing force. The time increase up to maximal force exertion on these 137 kPa micropillar arrays was typically 10-20 minutes. Since p130Cas arrived prior to initial forces, it likely influenced biomolecular processes during build-up of force. These results indicate that p130Cas preceded force exertion and indeed influenced the rate and extent of force exertion directly.

4.4 Discussion and conclusion

Using two different kinds of substrates with similar stiffness ranges, we observed differential FA-formation, p130Cas localization, and changes in force exertion dynamics dependent on the presence of p130Cas. On PA-gels of varying stiffness we found that upon spreading for 1 hour, the presence of p130Cas in cells caused FA area to increase at a stiffness of 42 kPa where cells were not yet fully spread. Whereas in Cas -/- cells, FA area and cell area increased simultaneously at a higher stiffness of 87 kPa. This static quantification of a differential stiffness response showed that p130Cas played a role in stiffness-dependent FA formation. We proceeded to investigate the influence of p130Cas on force exertion dynamics. Differential localization of p130Cas to sites of local force exertion was only observed on micropillars with a stiffness larger than 47.2 kPa. The differential localization of p130Cas coincided with a change in magnitude- and rate of force exertion. Since p130Cas was present before and during force exertion, it could directly change the way cellular forces are exerted onto the extracellular matrix. The global stiffness of fibroblast-populated matrices mimicking connective tissue have been measured to be 60 - 400 kPa [30, 31]. To our knowledge, this is the first time that p130Cas has been shown to act as a mechanosensor in live cells and in a physiologically relevant stiffness range. Our results of a differential response on both PA gels and PDMS micropillars indicate that the mechanosensitivity of p130Cas depends on the cell-wide global stiffness.

As a molecular-mechanistic model, we envisage the mechanosensing process to take place as follows. On a higher stiffness substrate, cells exert larger forces regardless of the presence of p130Cas. For a given stiffness, FA area increases with force, but the approximate FA size remains similar for a given stiffness [21, 24, 28, 32]. The net effect over varying stiffness is thus a larger stress (force per area) on FAs, leading to a larger force carried by proteins inside the FA. This larger force per protein causes the stiffness-dependent incorporation of p130Cas in the FA complex. Inside the FA, p130Cas could thus be phosphorylated in a force-dependent manner, as proposed previously [16]. Phosphorylation occurs typically on a timescale of minutes [33], making a function for p130Cas to locally and directly influence force exertion possible. Localization of p130Cas to tops of pillars preceded force exertion by ~ 3 minutes making a causal relationship between phosphorylation and force exertion possible

(see figure 4.6). P130Cas phosphorylation is known to enhance leading edge actin flux and FA turnover [12, 14], which could in turn explain the higher force exertion and stabilized FAs we observed when p130Cas was incorporated at high stiffness. The hypothesis of force-dependent phosphorylation is thus supported by our findings. P130Cas thus acts as a mechanosensor both outside-in (it localizes depending on stiffness) and inside-out (it influences cellular force exertion). An overview of the sensing (outside-in) and responding (inside-out) mechano-chemical coupling is given in figure 4.7.

Physical deformation follows from molecular activity (i.e. actomyosin contractility) and the differential p130Cas localization in turn changes the extracellular force exertion. We propose this sensing and responding to take place together with several distinct FA proteins in the following intracellular biochemical response. It is known that both paxillin [21, 24] and vinculin [28] co-localize with sites of force exertion. It has recently been noted that tyrosine phosphorylation of p130Cas, as well as paxillin, vinculin, and FAK are upregulated on stiffer substrates as compared to low stiffness substrates [34]. This phenomenon was attributed to FAK/p130Cas/Rac mediated stiffening of the actin cytoskeleton, wherein p130Cas acts as a rigidity sensor in a Src-dependent manner. Based on our results, we propose a model where p130Cas differentially localizes to force-bearing FAs only on a substrate with a global stiffness larger than 47.2 kPa. Incorporation of p130Cas into the FA through FAK with paxillin, talin and vinculin then allows the central SD to become phosphorylated by Src. Independently, tyrosine phosphorylation of the p130Cas SD has been suggested as a physical link between the actin cytoskeleton and the FA, thereby regulating actomyosin contractility in migrating cells [35]. Phosphorylation of p130Cas can thus regulate the amount force exertion and the rate of force exertion as mediated by Rac. Our measurements and comparisons to previous work can explain the observed coupling from stiffness to biochemical activity to force exertion, mediated by p130Cas.

This mechanical-biological-mechanical coupling makes p130Cas not only a mechanosensor in a physiological stiffness range, it also directly influences the way cellular forces are transmitted. The insights provided by this study should aid in understanding the observed roles for p130Cas in many important cellular processes, especially malignant cancers. Increased metastasis and invasiveness in breast cancer has been

linked directly to p130Cas (also known as BCAR1) [10]. Invasion and podosome formation are upregulated in Src-transformed cells that expressed p130Cas [36]. In MCF10A-CA1d breast carcinoma cells, it has been shown that p130Cas localizes to podosomes that form preferentially on stiffer substrates. In these experiments, the percentage of area actively degraded by the cell on hard substrates compared to soft substrates was directly influenced by p130Cas expression [37]. Here, we provided the first live cell measurement of the constitutive biochemical-mechanical link through which cancer progression may be modulated by physical cues. It will be interesting in future studies to further dissect the other molecular players involved in this process and investigate the link between cancer progression and cellular mechanics.

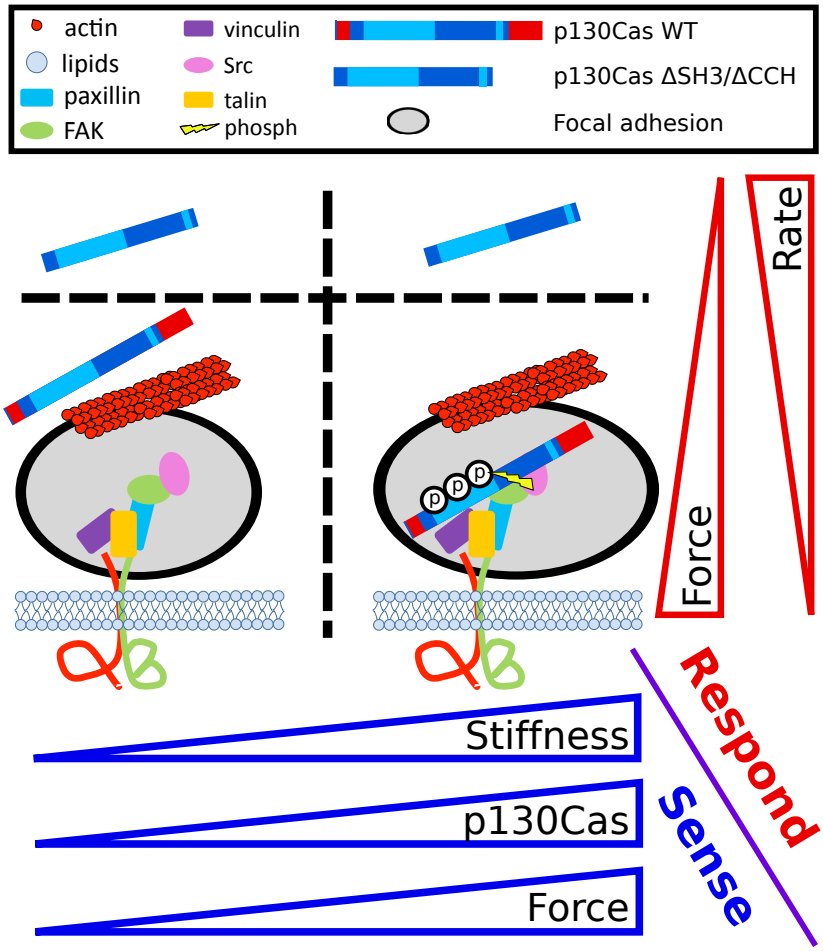

Figure 4.7
Mechanosensing and force exertion response at FAs via p130Cas. (Bottom bars in blue:) P130Cas shows increased accumulation at FAs with increased stiffness. Larger forces are exerted on higher stiffnesses, independent of the presence of p130Cas. (Right bars in red:) When p130Cas localizes to FAs, the cell responds by increasing forces and decreasing force exertion rates.

4.5 Supplemental figures

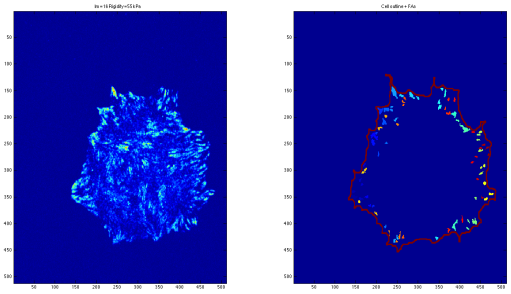

Figure S1
Matlab analysis provides the cell border and FAs. The fluorescence image is shown left, the results from cell- and FA-detection is shown right. The detection analysis gives information on cell area and FA area from the binary structure as shown here. For clarity, individual FAs are color-coded.

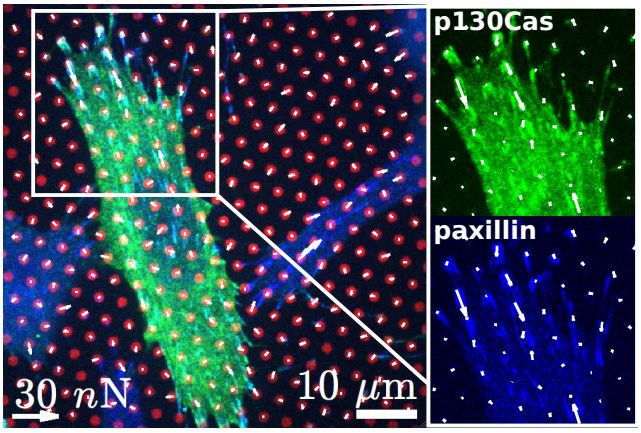

Figure S2
FAs localize onto pillars where force is exerted. P130Cas (green, YFP) localizes to FAs where force is exerted. Micropillars were stamped with Fibronectin (red, labeled with Alexa647). Immunostaining for paxillin (blue, alexa405) shows FA formation on micropillars even when p130Cas does not localize.

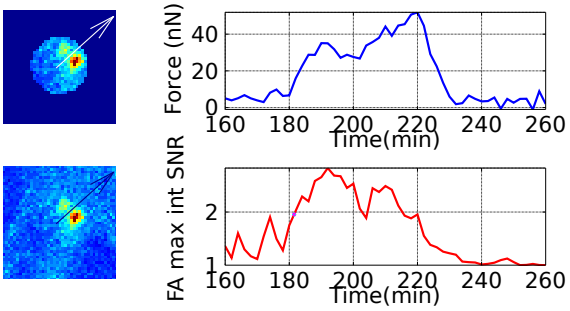

Figure S3

Quantification of p130Cas fluorescence over one pillar where a force is exerted. Over a radius of 1.2 µm around the pillar, the p130Cas fluorescence was summed (masked image in upper left and unmasked image in lower left). The force over time (upper right) exerted on this pillar was correlated to the fluorescence increase over time (lower right), giving direct information on the time-correlated dynamics of force exertion and p130Cas accumulation.

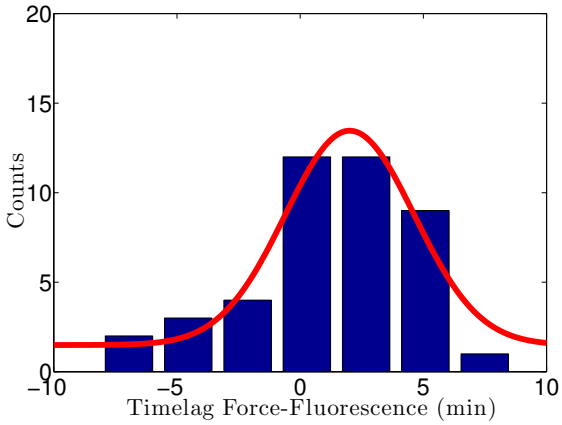

Figure S4

Histogram of measured timelags of p130Cas Fluorescence before force exertion. A probability density function shows the corresponding result in figure 4.5B.

Bibliography

[1] Simon W Moore, Pere Roca-Cusachs, and Michael P Sheetz . "Stretchy Proteins on Stretchy Substrates: The Important Elements of Integrin-Mediated Rigidity Sensing". In: *Dev. Cell* (2010).

[2] William J Polacheck et al. "Microfluidic platforms for mechanobiology." In: *Lab Chip* 13.12 (2013), pp. 2252–2267.

[3] Joe Swift et al. "Nuclear lamin-A scales with tissue stiffness and enhances matrix-directed differentiation". In: *Science* 341.6149 (2013), p. 1240104.

[4] Ryan D Sochol et al. "Unidirectional mechanical cellular stimuli via micropost array gradients". In: *Soft Matter* 7 (2011).

[5] Christopher C DuFort, Matthew J Paszek, and Valerie M Weaver. "Balancing forces: architectural control of mechanotransduction." In: *Nat. Rev. Mol. Cell Bio.* 12.5 (2011), pp. 308–319.

[6] Melody A Swartz and Amanda W Lund. "Lymphatic and interstitial flow in the tumour microenvironment: linking mechanobiology with immunity." In: *Nat. Rev. Cancer* 12.3 (2012), pp. 210–219.

[7] Sirio Dupont et al. "Role of YAP/TAZ in mechanotransduction." In: *Nature* 474.7350 (2011), pp. 179–183.

[8] Armando del Rio et al. "Stretching single talin rod molecules activates vinculin binding." In: *Science* 323.5914 (2009), pp. 638–641.

[9] Ronen Zaidel-Bar and Benjamin Geiger. "The switchable integrin adhesome." In: *J. Cell Sci.* 123.Pt 9 (2010), pp. 1385–1388.

[10] Nadezhda Tikhmyanova, Joy L Little, and Erica A Golemis. "CAS proteins in normal and pathological cell growth control." In: *Cell. Mol. Life Sci.* 67.7 (2010), pp. 1025–1048.

[11] Wei Huang et al. "BCAR1 protein plays important roles in carcinogenesis and predicts poor prognosis in non-small-cell lung cancer". In: *PLoS. One* 7.4 (2012), e36124.

[12] Leslie M Meenderink et al. "P130Cas Src-binding and substrate domains have distinct roles in sustaining focal adhesion disassembly and promoting cell migration." In: *PLoS. One* 5.10 (2010).

[13] Donna J Webb et al. "FAK–Src signalling through paxillin, ERK and MLCK regulates adhesion disassembly". In: *Nat. Cell Bio.* 6.2 (2004), pp. 154–161.

[14] Dominique M Donato et al. "Dynamics and mechanism of p130Cas localization to focal adhesions." In: *J. Biol. Chem.* 285.27 (2010), pp. 20769–20779.

[15] Nah-Young Shin et al. "Subsets of the major tyrosine phosphorylation sites in Crk-associated substrate (CAS) are sufficient to promote cell migration". In: *J. Biol. Chem.* 279.37 (2004), pp. 38331–38337.

[16] Yasuhiro Sawada et al. "Force sensing by mechanical extension of the Src family kinase substrate p130Cas." In: *Cell* 127.5 (2006), pp. 1015–1026.

[17] Chen Lu et al. "P130Cas substrate domain is intrinsically disordered as characterized by single-molecule force measurements". In: *Biophys. Chem.* 180 (2013), pp. 37–43.

[18] Kinya Hotta et al. "Biophysical Properties of Intrinsically Disordered p130Cas Substrate Domain—Implication in Mechanosensing". In: *PLoS. Comp. Biol.* 10.4 (2014), e1003532.

[19] Xuefeng Wang and Taekjip Ha. "Defining single molecular forces required to activate integrin and notch signaling." In: *Science* 340.6135 (2013), pp. 991–994.

[20] Tony Yeung et al. "Effects of substrate stiffness on cell morphology, cytoskeletal structure, and adhesion." In: *Cell Motil. Cytoskel.* 60.1 (2005), pp. 24–34.

[21] Hedde van Hoorn et al. "The nanoscale architecture of force-bearing focal adhesions". In: *Nano Lett.* 14.8 (2014), pp. 4257–4262.

[22] Pierre Verhulst. "Correspondance mathématique et physique". In: ed. by Jean Guillaume Garnier and Adolphe Quételet. Vol. 10. Gand. Impr. d' H. Vanderkeriehove, 1825-26; Bruxelles, M. Hayez, imprimeur, 1838. Chap. Notice sur la loi que la population suit dans son accroissement, pp. 113–121.

[23] Marion Ghibaudo et al. "Traction forces and rigidity sensing regulate cell functions". In: *Soft Matter* 4.9 (2008), pp. 1836–1843.

[24] Lea Trichet et al. "Evidence of a large-scale mechanosensing mechanism for cellular adaptation to substrate stiffness." In: *Proc. Natl. Acad. Sci. USA* 109.18 (2012), pp. 6933–6938.

[25] Hiroaki Honda et al. "Cardiovascular anomaly, impaired actin bundling and resistance to Src-induced transformation in mice lacking p130Cas". In: *Nat. Genet.* 19.4 (1998), pp. 361–365.

[26] Justin D Mih et al. "Matrix stiffness reverses the effect of actomyosin tension on cell proliferation." In: *J. Cell Sci.* 125.Pt 24 (2012), pp. 5974–5983.

[27] Nathalie Q Balaban et al. "Force and focal adhesion assembly: a close relationship studied using elastic micropatterned substrates." In: *Nat. Cell Bio.* 3.5 (2001), pp. 466–472.

[28] Sangyoon J Han et al. "Decoupling substrate stiffness, spread area, and micropost density: a close spatial relationship between traction forces and focal adhesions." In: *Biophys. J.* 103.4 (2012), pp. 640–648.

[29] Jianping Fu et al. "Mechanical regulation of cell function with geometrically modulated elastomeric substrates." In: *Nat. Methods* 7.9 (2010), pp. 733–736.

[30] JF Chapuis and P Agache. "A new technique to study the mechanical properties of collagen lattices". In: *J. Biomech.* 25.1 (1992), pp. 115–120.

[31] Tetsuro Wakatsuki et al. "Cell mechanics studied by a reconstituted model tissue". In: *Biophys. J.* 79.5 (2000), pp. 2353–2368.

[32] Ulrich S Schwarz and Margaret L Gardel. "United we stand - integrating the actin cytoskeleton and cell-matrix adhesions in cellular mechanotransduction." In: *J. Cell Sci.* 125.Pt 13 (2012), pp. 3051–3060.

[33] Christoph Ballestrem et al. "Molecular mapping of tyrosine- phosphorylated proteins in focal adhesions using fluorescence resonance energy transfer". In: *J. Cell Sci.* 119.5 (2006), pp. 866–875.

[34] Yong Ho Bae et al. "A FAK-Cas-Rac-Lamellipodin Signaling Module Transduces Extracellular Matrix Stiffness into Mechanosensitive Cell Cycling". In: *Science Sig.* 7.330 (2014), ra57.

[35] Hiroaki Machiyama et al. "Displacement of p130Cas from focal adhesions links actomyosin contraction to cell migration". In: *J. Cell Sci.* (2014), jcs–143438.

[36] Jan Brábek et al. "CAS promotes invasiveness of Src-transformed cells". In: *Oncogene* 23.44 (2004), pp. 7406–7415.

[37] Nelson R Alexander et al. "Extracellular matrix rigidity promotes invadopodia activity". In: *Curr. Biol.* 18.17 (2008), pp. 1295–1299.

Chapter 5

Outward force exertion is crucial for mitosis [1]

[1] This chapter is based on: H. van Hoorn, M. de Valois, C. Backendorf and T. Schmidt, Outward force exertion is crucial for mitosis, to be submitted

abstract

Cell division is tightly regulated by the kinetochore, a hierarchical assembly of nearly 100 proteins that connects DNA in chromosomes to the mitotic spindle to complete the mitotic cycle. Biochemical regulation of mitosis has been extensively studied, while its physical implications are not well understood. Here we show that throughout mitosis cells are mechanically coupled to their environment, heavily deform the extracellular matrix and an outward pushing force is needed for succesful division. We used fluorescently labeled HeLa cells to correlate chromosome- and microtubule dynamics directly to extracellular force exertion. Distinct successive hallmarks of force exertion correlated to well-known mitotic stages with an adaptation in force exertion consistently preceding cellular phenotype. These results illustrate the importance of cell mechanics next to biochemical interactions throughout a cellular lifecycle. Our novel experimental observations lead us to propose a force balance that proves crucial for succesful division and the mechanosensory function of checkpoints regulating progression through mitosis.

5.1 Introduction

Proper control over progression through the cell cycle and orientation of division is ubiquitous in life and vital in development. The importance of cell cycle control is evident from the large number of checkpoint-mechanisms, for instance in the formation of kinetochores and the multi-faceted spindle-assembly checkpoint mechanism [1–5]. The importance of cell cycle regulation is further exemplified from the observation that de-regulation of the centrosome cycle can lead to chromosome instabality and ultimately to the development of cancer [6, 7]. A multitude of proteins is involved in proper cell cycle progression and a great insight has developed over the past years [8, 9]. The main focus in past research has been on biochemical interactions and identification and localization of proteins. However, cell cycle progression is not just controlled biochemically, but is also greatly influenced by physical environmental cues.

How forces are transmitted through the mitotic spindle and progressively through the stages of cell division, has been investigated for decades [10, 11]. However, even in recent years it still remains a technical challenge to address the question of how cellular force exertion progresses throughout division [12, 13]. Tension-dependency in checkpoints was discovered nearly two decades ago, showing a direct tension-phosphorylation mechanosensitive mechanism [14, 15]. However, an insistent problem in this matter is the need for a physical disruption of cellular components in order to measure the forces exerted on them. Here, we try to gain insight in the force balance throughout mitosis by measuring extracellular forces simultaneously with internal re-organization of chromosomes and microtubules (MTs).

Several important extracellular insights during cell division in single eukaryotic cells have been discovered in recent years. The extracellular matrix (ECM) was modified to control the direction of cell division and it was shown that the ECM could guide the axis of cell division [16]. Further experiments using externally applied strain, ECM-patterning and laser-ablation showed that physical disruptions could also alter the direction of cell division [17]. An important role for retraction fibers was found for determination of the cell division axis. From these studies it became clear that externally applied spatial and mechanical cues (outside-in coupling) directly influenced cell division. However, the mechanical inside-out coupling due to forces generated by the cell transmitted onto the ECM is not well studied.

In previous studies, a large range of forces was quantified during cell division. Furthermore, force measurements throughout the full cycle with a functional correlation to local force exertion have not been reported. Local forces exerted directly on chromosomes were quantified using optical tweezers in the range of 1-10 pN [13]. The tension in retraction fibers was found to be in the order of 100-1000 pN [17]. A cell-wide, mitotic rounding pressure applied by the cell was found to be in the range of 100 nN, as measured by atomic force microscopy [18]. However, all previous measurements relied on an active perturbation, by impeding cellular behavior either with a bead or an AFM cantilever. To clarify the extracellular force balance, we aimed to investigate the locally exerted forces on the ECM dynamically with a passive measurement throughout the cell cycle.

We quantified extracellular forces using micropillar arrays of varying stiffness. Over time, we imaged fluorescently labeled HeLa cells and examined both chromosomes and tubulin using confocal microscopy. Inward pulling forces of 50-100 nN in interphase were released before chomosome condensation. Progression through prometaphase was accompanied by a build-up of outward pushing forces that culminated during metaphase. On a soft or hard substrate, outward pushing force amounted to 100-150 nN or 450-550 nN, respectively. Before succesful cell division, a force plateau was present through anaphase leading up to a peak in outward pushing force during telophase. After physical seperation, the two daughter cells spread and continued to exert inward pulling forces as is common for cells in interphase. However, not all cells exerted outward pushing forces throughout mitosis. Strikingly, a decrease in outward pushing forces during metaphase correlated to mitotic disturbance and the presence of three centrosomes instead of two leading to tripolar spindles. We thus conclude that the outward pushing force is crucial for spindle integrity and proper progression through cell division.

5.2 Methods

5.2.1 Cell culture

HeLa cells were cultured in high-glucose Dulbecco's Modified Eagle's Medium (DMEM) supplemented with 10% calf serum (Thermo Scientific), 2 mM glutamine and 100 μg/ml pennicilin/streptomycin at 37 °C with 5% CO2. Cells either expressed H2B-GFP stably or were trans-

duced with tubulin-GFP using baculovirus (BacMam 2.0, Invitrogen). Baculovirus transduction was performed overnight prior to the measurement at ∼70% confluency with 40 particles per cell. Cells were then seeded at single cell density directly on the micropillar array and allowed to spread ∼6 hours. Micropillar arrays were subsequently inverted onto #0, 25 mm diameter, round coverslips (Menzel Glaser) for imaging.

5.2.2 Micropillars

Hexagonal arrays of poly-di-methyl-siloxane (PDMS, Sylgard 184, Dow Corning) micropillars of 2 µm diameter, 2 µm spacing and with a height of 4.1 and 6.9 µm were produced using replica-molding from a silicon wafer into which the negative of the structure was etched by deep reactive-ion etching. The pillar arrays were flanked by integrated 50 µm high spacers (as described in [19] and shown in supplemental figure S2) such that pillar tops and hence cells attaching to them were within the limited working distance of our high-NA objective (<170 µm) on an inverted microscope. The use of a high-NA objective is a prerequisite for any high-resolution optical imaging. The micropillar arrays were kept from floating using a support weight of glass. Live-cell measurements were performed in overnight time-lapse measurements of 10-15 hours duration on a confocal spinning-disk setup with a home-built focus-hold system. The temperature was kept at 37 °C with constant 5% CO2 concentration in a stage-top incubator (Tokai Hit, Japan).

The tops of the micropillars were coated with a mixture of Alexa568-labeled and unlabeled fibronectin (1:5) using micro-contact printing. A 40 µl drop with 60 µg/ml fibronectin was incubated 1h on a flat piece of soft (1:30 PDMS, crosslinker:base ratio), washed with ultrapure water and left to dry under laminar flow. After 10 minutes UV-Ozone (Jelight) activation of the micropillars, micro-contact printing was performed 5 minutes and non-printed areas were blocked 1 hour with 0,2% Pluronic (F-127, Sigma) in PBS. Finite Alement Analysis (FEA) that was fed the exact micropillar dimensions as measured by in-situ scanning electron microscopy (SEM, FEI nanoSEM) allowed us to precisely calibrate the force-deflection relation. Short and tall micropillars on the array had a characteristic spring constant of 70.9 and 16.7 nN/µm, respectively. In the analysis, we consistently used a third order polynomial fit to the FEA results to obtain the force for a given deflection. The position of the pillar tops was observed by fluorescence microscopy at 561 nm excitation.

From those fluorescence images the exact pillar-centroid positions were determined down to 30 nm accuracy. The deflection precision of 30 nm corresponded to a force accuracy of 2 and 0.5 nN for the short and tall pillars, respectively. All analysis was done using specifically designed software (Matlab, Mathworks).

5.2.3 Microscopy

Imaging was performed on an inverted microscope (Zeiss Axiovert 200) with a 100X, 1.4 NA oil objective (Zeiss). The setup was expanded with a Confocal Spinning Disk unit (Yokogawa CSU-X1), an emCCD camera (Andor iXon DU897) and a home-built focus-hold system at the rear port. The focus-hold system consisted of a 850 nm diode laser that was coupled into the rear port reflected into the objective using a dichroic that only reflected light with a wavelength >800 nm (Chroma). The reflected light on the glass-water interface was collected at the back-port and positioned onto a Si-amplified photodetecter (PDA36A, Thorlabs). The relative signal was measured to a sample (90/10 splitter) of the signal of the incoupled diode laser to account for fluctuations of the diode laser. The position of the reflected light was a direct readout for the position of the glass-water interface relative to the objective over a range of 10-20 μm. A PID-controller programmed in Labview (National Instruments) controlled the objective positioning through its mounting on a PIFOC piezo (Physike Instrumente).

For each overnight measurement, multiple positions were recorded every 2 minutes. The positions were manually selected by moving the XY-stage (MarzHauser) and corresponding relative positions to the glass-water interface denoted the Z-position relative to the highest value for the derivative of the photodiode signal as a function of piezo-movement. Overnight, typically 8-14 positions were recorded. At each position, the focus-hold system determined the position of the coverslip-water interface and relative to that recorded the micropillar array with 561 nm laser light (Cobolt) and a z-stack 3-8 μm with 488 nm laser light (Coherent) below the micropillars for the chromosomes (for H2B-GFP cells) or microtubules (for tubulin-GFP cells). In all images shown, a maximum-intensity z-projection is constructed from this z-stack.

5.2.4 Radial force interpretation

A possible explanation for the apparent outward deflections of pillars would be an optical lensing effect caused by the rounding of the cell. We imaged the micropillars underneath the cell through the cell body, which has a different refractive index as compared to the medium surrounding the cell. A rounded dividing cell would then enable a lensing effect due to the higher refractive index inside the cell. This would indeed make the pillars appear deflected outward while they are are not deformed at all. In our measurements, however, this lensing effect does not play a significant role.

The refractive index of a HeLa cell has been accurately quantified [20] and is highly inhomogeneous rangin from 1.34 - 1.4. When we take the an extreme case of a full lens, where the refractive index is 1.38 everywhere in the cell compared to the surrounding medium, a rounded cell of 10 μm height with radius 15 μm would yield an apparent deflection of at maximum ∼150 nm (see supplemental figure S4). This is an upper limit, since the measurement in [20] shows high uniformity in the cell, which would severaly decrease the lensing ability. The actual deflections we measured were ∼300-400 nm per pillar. In a very extreme case, we would thus overestimate the outward pushing forces by a factor of 2, so the outward pushing is still significant in our measurement.

Finally, we observed a lack of outward pushing but random significant deflections in the case of cells that showed a mitotic disturbance during mitosis. If the lensing effect would have been significant, we would have seen outward pushing also in this case. However, there were significant deflections, but in all directions (not just radially outward). The difference in refractive index is attributed to an increased protein concentration in the cell, which would also be the case for the triplet division. We thus conclude that the deflections are a real measure of outward pushing forces and not an effect of lensing by the rounded cell.

It is important to note that the quantified deflections are only in-plane and thus parallel to the axis of division. Importantly our method can vary the global stiffness of the extracellular environment. With this variation we show that the cell indeed pushes harder when the outside is stiffer. With a significant variation of stiffness in organisms, it indeed makes sense that the extracellular force exertion can be increased so a certain deformation can be obtained.

5.3 Results

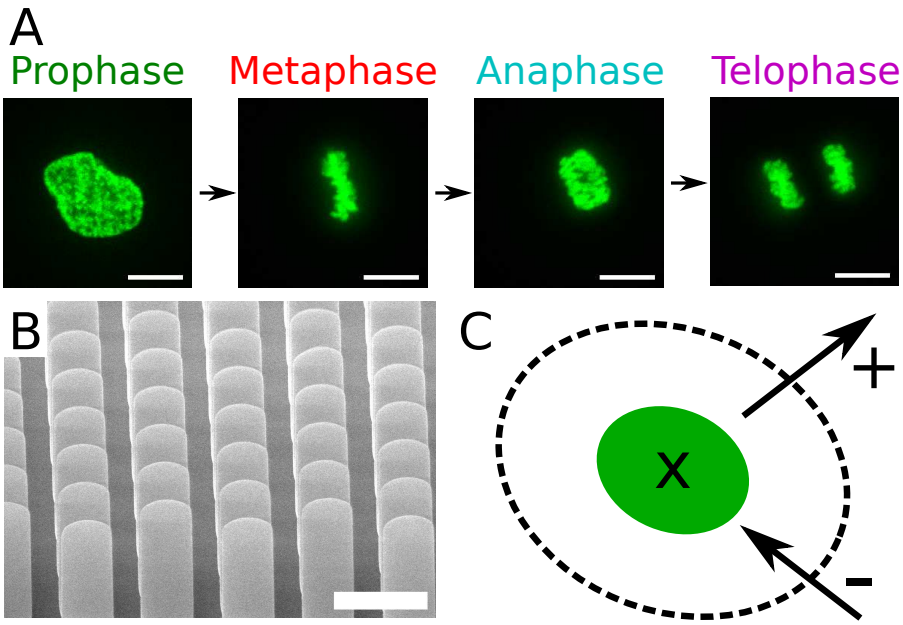

Figure 5.1
Quantification of cellular forces during division. (A) Phases during mitosis were quantified by following a maximum z-projection of z-stacks over time of a HeLa nucleus with H2B-GFP (scalebar corresponds to 10 μm). (B) PDMS micropillars were used to measure cellular traction forces during cell division. The tops of these pillars (image taken with Scanning Electron Microscopy, SEM) were coated with Fibronectin. (Scalebar corresponds to 5 μm) (C) Radial forces were quantified relative to the nucleus center (H2B-GFP schematically depicted by green) or the center of the mitotic spindle (when tubulin-GFP was used). Positive radial forces are defined as outward forces and negative radial forces were defined as inward forces. (Dotted line marks cellular outline, x marks relative center for radial forces)

Our research question was aimed at the correlation between two dynamic processes; extracellular force exertion and cell division. A more extensive description of the methods is given in Methods. Briefly, we quantified cell division and force exertion simultaneously by performing time-lapse imaging of HeLa cells on micropillar arrays of varying stiffness. We observed the state of the cell cycle (see figure 5.1A) by labeling either alpha-tubulin or histone-core protein H2B with Green Fluorescent Protein (GFP). In both cases the cells could still complete a full cell-cycle

and seemed not to be hindered by the presence of GFP. The cell-cycle phase was quantified manually by comparing the time-lapse movies to the predicted visual state given by literature [1, 21]. The phases are consistently color-coded by green, red, magenta and purple for prophase, metaphase, anaphase and telophase, respectively. Timepoints of a given phase always denote the start of a phase.

Force exertion was quantified using micropillar arrays (see figure 5.1B), as previously described [19]. Micropillars with heights of 4.1 μm and 6.9 μm were used, both with a diameter of 2 μm. Live-cell high-resolution fluorescence microscopy was performed overnight using a spinning-disk confocal attached to a home-built microscope with a multi-positioning system and a home-built autofocus system. Z-stacks from 3 to 8 μm above the pillars were recorded with a 488 nm laser, while the pillar z-slice was imaged with a 561 nm laser (to image the Fibronectin labeled with fluorescent dye Alexa568). From the deflection map and the calibrated pillar stiffness [19], the forces cells exerted on the ECM were quantified using specifically designed algorithms and further analyzed in Matlab (Mathworks).

Finally, we noticed in our analysis that the forces exerted were primarily radially oriented relative to the nucleus center (or metaphaseplate center in the case of tubulin-GFP cells). The radial component of the force was much larger as compared to the perpendicular force (as quantified in supplemental figure S1). Upon progression through telophase, the dividing cells obtained two radial force centers. Relative to the radial force centers, inward (pulling) forces were defined as negative radial forces, while outward (pushing) forces were defined as positive forces (see figure 5.1C). For each cell, the radial forces were then summed to obtain the net radial force per cell (as given in figure 5.3 and 5.5B).

5.3.1 From pulling to pushing forces in prometaphase

It is known from previous research that cells in interphase typically exert inward pulling forces. Inward pulling forces have been observed for fibroblasts [19, 22, 23], epithelial cells [23, 24] and muscle cells [23, 25]. Similarly, we observed pulling forces exerted by HeLa cells in interphase when plated on micropillar arrays (see figure 5.2A and C, figure 5.4A and E and figure 5.5A). Pulling forces were present at the cell periphery, directed towards the cell center. The maximum force exerted was 10-50 nN per pillar, depending on the stiffness of the micropillars. Over the

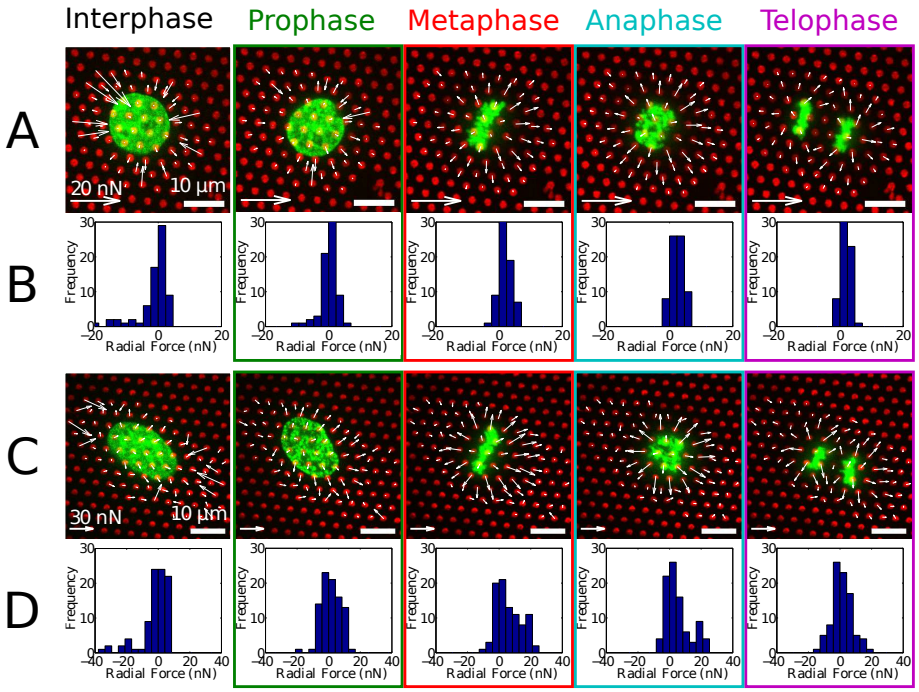

Figure 5.2
During cell division, inward pulling forces decrease and outward pushing forces increase. (A-B) Timelapse of cell division forces on low-stiffness micropillars (k_{bend} = 16.7 nN/µm). (C-D) Timelapse of cell division forces on high-stiffness micropillars (k_{bend} = 70.9 nN/µm). Phases are consistently color-coded with prophase in green, metaphase in red, anaphase in magenta and telophase in purple. Force scalebar in lower left consistent for each stiffness, fluorescence scalebar in lower right.

course of cell division, however, the pulling force decreased and the cell evolved a distinct radial outward pushing force (see figure 5.2). All experiments were performed while the micropillar array was inverted over a 100 µm coverslip, as described in [19] and in Methods.

We investigated force exertion on micropillar arrays of different heights and thus varied the stiffness. Micropillars with a bending modulus of k_{bend}=70.9 nN/µm and k_{bend}=16.7 nN/µm were used, calibrated as previously described [19] and discussed in Methods. On both stiffnesses, we observed radial outward force exertion during progression through mitosis (see figures 5.2A and C). Histograms of radial forces in figures 5.2B and D show inward-pulling (negative radial force) in interphase, as

expected. Going into mitosis, pulling was released and outward pushing forces (positive radial force) build up. In the histograms for metaphase and anaphase it is particularly clear that a force distribution around a positive radial force of 20 nN build up (figure 5.2D). For the low-stiffness pillars a broadening of the distribution towards positive forces was observed due to outward pushing forces as observed in figure 5.2A.

To get a clear picture of the progression of radial forces over the entire cell division cycle, the radial forces were summed to obtain a net radial force per cell. Figures 5.3A and B give the time-course for the net radial force for one cell on low- and high-stiffness pillars, respectively. Cells on micropillars progressed through mitosis over the time course of 1-2 hours, without a correlation between substrate stiffness and time to divide. Markedly, on both stiffnesses the initiation of prophase as observed by chromosome condensation was always preceded 5-20 minutes by the release of contractile forces.

Throughout cell division the micropillar arrays were inverted. We thus conclude that cells were continually physically connected to the fribonectin-ECM with enough strength to keep the cell attached to the substrate counteracting gravitational forces. Fluorescence imaging of tubulin-GFP (see figure 5.4) further confirmed that the cells were continuously spread on the substrate, rounding up in a dome-like shape. Using our methodology we were able to asses that ECM-binding undergoes severe remodelling and stress throughout the cell division cycle. Importantly, release of pulling forces preceded initial chromosome condensation and build-up of pushing forces coincided with progression through prometaphase. The change in force exertion thus consistently preceeded the structural reorganization progressing into formation of the mitotic spindle.

5.3.2 Force plateau during anaphase and telophase

Chromosomes re-locate massively during cell division, but MTs guide this reorganization and the ultimate physical seperation of the daughter cells. We localized MTs by labeling them with GFP. Baculovirus transduction with tubulin-GFP enabled us to simultaneously visualize MT dynamics and extracellular force exertion (see figure 5.4). As with the H2B-labeled cells, the cells showed the inward pulling-force phenotype (figure 5.4A) in interphase.

Proceeding into metaphase, the outward pushing force increased to

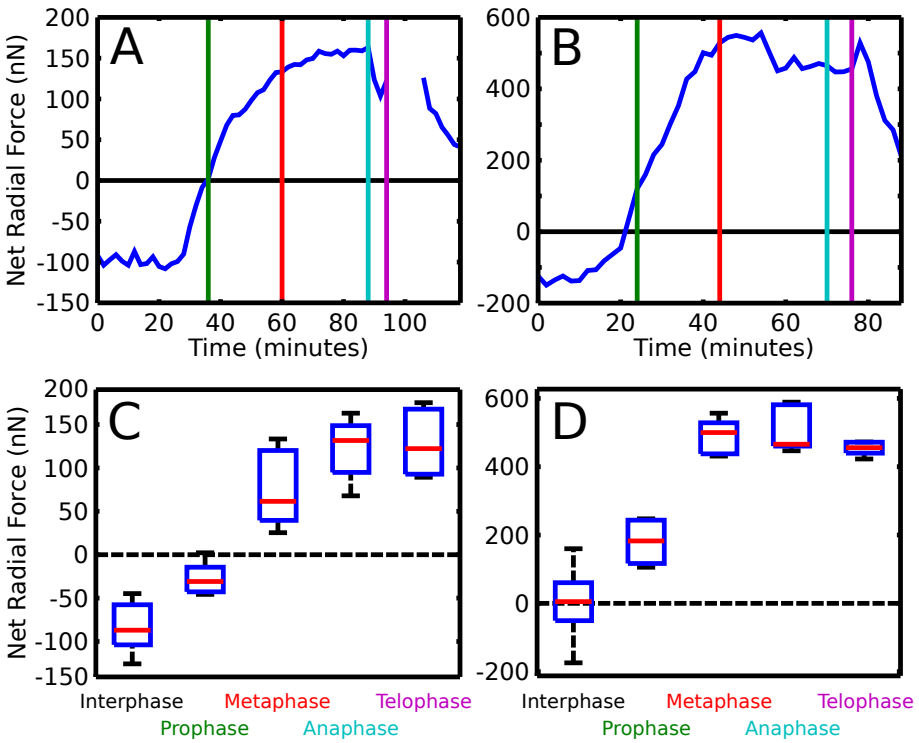

Figure 5.3
Outward pushing forces increase through mitosis. Net radial force over time on a low-stiffness substrate (A) and on a high-stiffness substrate (B) follow roughly the same trend. For multiple cells (at least 5 cells per condition) the inward pulling force is already released before prophase on both low-stiffness (C) and high-stiffness (D) micropillar arrays and a succesive outward pushing force (positive radial force) builds up.

an approximate plateau. On the lower-stiffness micropillar arrays the outward force increased gradually into anaphase at a plateau force of (120±30) nN (mean±s.d.). On the higher stiffness the plateau force was readily reached upon metaphase at (490±50) nN. Larger contractile forces on substrates with a larger stiffness were previously observed for fibroblasts and other cell types [22, 23]. The outward pushing forces during cell division also increased with increasing substrate stiffness, showing that the dividing cell also adapts to the stiffness of the environment.

Next, we noticed that in the radial force curves that were able to capture the starting point of cytokinesis, 8 out of 9 cases showed a final peak increase in outward pushing forces. Just before physical seperation of the cells, a brief additional outward pushing force was measured. Figure 5.3A shows an example of unresolved forces before force decrease, while in figure 5.3B the peak increase can be observed just before cytokinesis. Another peak in outward pushing upon cytokinesis is shown in supplemental figure S3.

Re-organization of MTs and final seperation of the chromosomes coincided with the final pushing force increase upon cytokinesis (figure 5.4B-E). The point of peak outward pushing force corresponded to figure 5.4C. This timepoint in the mitotic cycle also corresponded to the start of contraction of the cleavage furrow through actomyosin contractility. It is likely that the additional outward push is caused by the final contraction of the actomyosin ring.

Increased outward pushing forces were consistently present at the MT base in anaphase and telophase at an apporoximate plateau. Outward pushing may be a vital part of the force balance which keeps the mitotic spindle together and chromosomes aligned. As the pushing forces decreased again after the peak in figure 5.4E, mitosis was almost completed and the contractile actomyosin ring proceeded to pinch of the two daughter cells. Pushing force decreased throughout this stage, as can be observed in figure 5.3 and S3. When the cells were fully separated, they spread again, exerting inward pulling forces as observed in figure 5.4F.

5.3.3 Outward pushing is vital for succesful mitosis

During our measurements, we encountered three cases in which the mitotic spindle spontaneously became disturbed and a third centrosome was observed. Figure 5.5A shows the timecourse of MTs and force over time for such a cell undergoing a mitotic disturbance. Coincidentally,

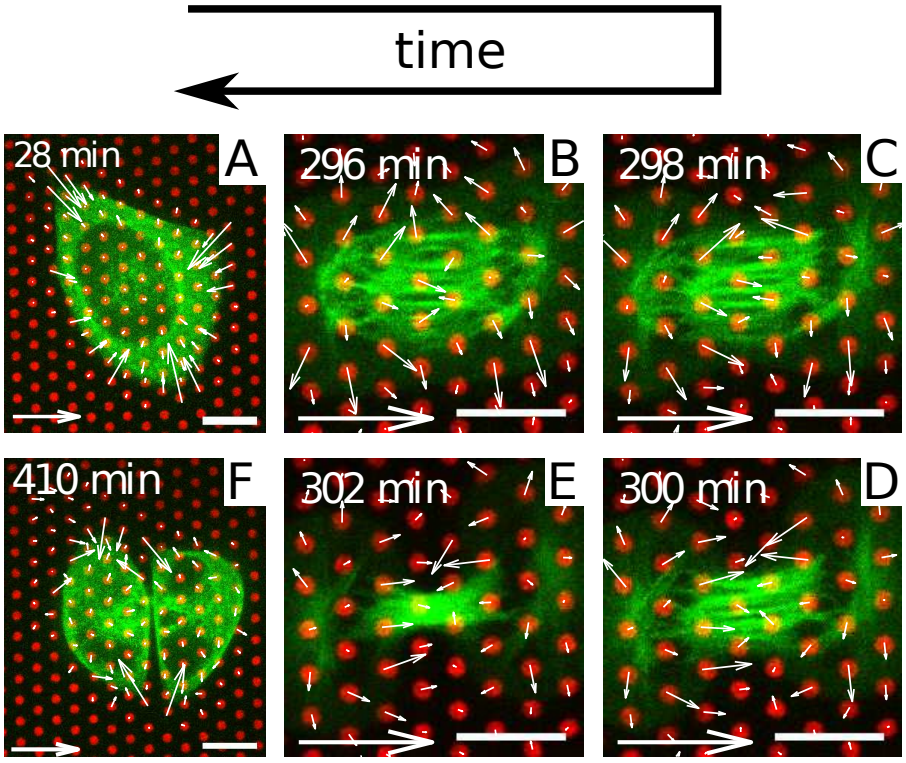

Figure 5.4
Outward pushing from two distinct bases during cytokinesis. (A) Cell in interphase with microtubules labeled with GFP (green) on fibronectin-coated micropillars (red). (B-E) During physical seperation over the time course of several minutes, two bases attach to the substrate pushed radially outward. Physical seperation of a mitotic spindle in (B) to the pinching off of two individual cells in (E) is clearly visible. Total outward pushing forces peak in (C) during physical seperation. (F) After seperation, both daughter cells spread and start exerting pulling forces at the cell periphery again. (Arrow scalebar in lower left always corresponds to 20 nN and fluorescence image scalebar in lower right to 10 μm)

we observed a striking consistent force exertion hallmark. Initially, the inward pulling forces were released before the start of prophase, as was the case in succesful division. However, upon initial spindle formation the outward pushing force did not increase immediately, but showed a delayed response. Outward pushing forces build up eventually, but could not maintain a plateau force. After several hours, the outward pushing force decreased and fluctuated around zero net radial force.

The evolution of the net radial force over time for a cell undergoing a mitotic disturbance is shown in figure 5.5B. The decrease in outward pushing force preceded the observation of one of the centrosomes splitting in two, creating a mitotic disturbance. At 166 minutes in figure 5.5A, the lack of a net outward pushing force can be seen as randomly oriented pillar deflections. The net radial force greatly fluctuated here, due to random orientation of all forces. Pillars were significantly deflected, but in a random fashion in all directions. The reason for this discrepancy became clear later when the centrosomes separated and the cell appeared to have 3 centrosomes (centrosomes duplicate in S-phase [1]). After the third centrosome seperated, the structure again stabilized and the net radial force increased again up to a plateau of $\sim$100 nN.

In another example of mitotic disturbance inward pulling was again released, but further increase in outward pushing was not visible over the full measurement of 15 hours. A tripolar spindle was again visible, but the outward pushing force again did not increase. The mitotic disturbance in figure 5.5 delayed mitosis for several hours. In the previous prophase- and metaphase force response (figure 5.2 and 5.3), the force exertion characteristics also preceded a phenotypic response. This again indicates that the force balance is a precursor for molecular rearrangement. After formation of the tripolar spindle, the cell did proceed into three daughter cells in this case, but only after another increase in outward pushing forces.

The same characteristic force plateau and peak in outward forces build up at anaphase, with ultimately again a short force peak at telophase (352 minutes), as was observed during succesful mitosis. Large outward pushing forces were again observed at the MT base (figure 5.5A), with much larger forces at the lower left base compared to the other ends of the two spindles. The same structural reorganization of the MT structure could be observed as in figure 5.4. The increased forces here can be explained by the active outward pushing of two individual mitotic spindles,

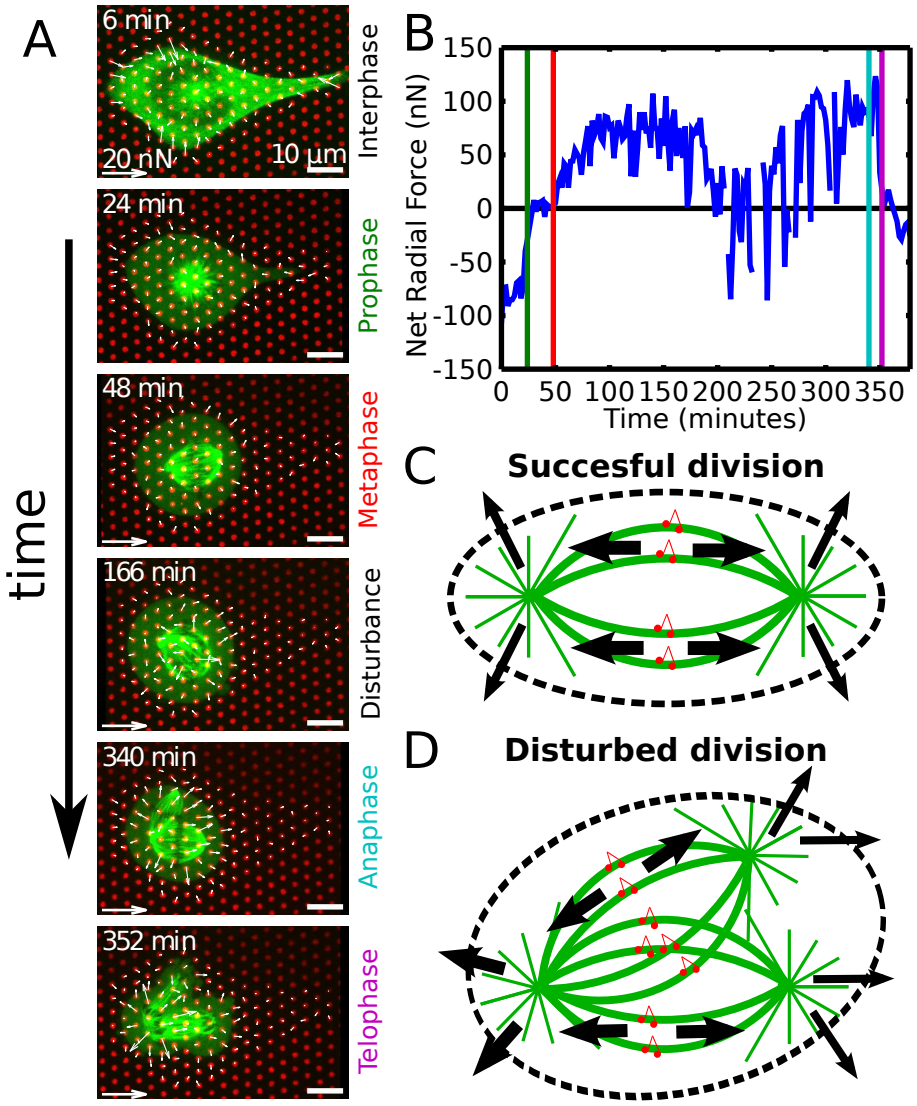

Figure 5.5
Mitotic disturbance is preceded by a lack of outward pushing forces. (A) Time-lapse microscopy of microtubules (green) and micropillars (red) on micropillars (k_{bend} = 16.7 nN/µm). (B) Net radial force over time for the cell in (A). (C-D) Schematic representation of microtubules (green), microtubule motors (kinesins, red), cell outline (dashes line) and transmission of forces (arrows). Larger arrows indicate larger forces. (C) Proposed outward pushing mechanism during succesful cell division. (D) Mitotic disturbance shows an increased outward pushing where the forces from two mitotic spindles join.

causing larger forces in the lower left compared to the two other centrosomes. In both succesful and disturbed division, the outward pushing force plateau was always present before anaphase, telophase and ultimately cytokinesis could take place. This observation provides further evidence for a spindle-mediated force balance.

Radial outward pushing forces during cell division preceded the various characteristic phases of mitosis (figure 5.3). The MT structure at the base of radial forces reorganized during a final peak of force exertion at cytokinesis (figure 5.4). A disturbance in force exertion preceded a mitotic disturbance leading to triplet division (figure 5.5A-B). We therefore propose a model describing a force balance consistent with our experimental observations in which different origins of force exertion contribute to outward pushing from the mitotic spindle to a more sparse MT network towards the cell edge (figure 5.5C-D). Forces are likely maintained by a multitude of interactions, varying from microtubule dynamics and pressure to kinesins and kinetochore complexes. The outward pushing force balance proved to be vital for mitotic spindle integrity and proper cell division.

5.4 Discussion and conclusion

The process of cell division is tightly regulated through numerous checkpoints. Here, we have shown that the mechanical integrity throughout mitosis is of vital importance to the equal division of chromosomes and proper division into two daughter cells. Using our methodology, we have shown that cells go from exerting inward pulling forces on the ECM in interphase through a progressive cycle of outward pushing forces in mitosis. Throughout this process, the cell is mechanically coupled to the ECM-coated substrate continuously. Through active force exertion throughout the division cycle, we demonstrated that the cell is not only outside-in [16, 17] but also inside-out mechanically coupled to the ECM. We measured outward force exertion build-up as the mitotic spindle organizes in prometaphase. Through anaphase and telophase outward pushing forces were needed for progression through the cell cycle. Finally, we assesed that a proper spindle-mediated force balance is crucial for succesful cell division.

Assembly of the mitotic spindle is regulated by multiple checkpoints [3]. As chromosomes and microtubules form attachments, this is heavily regulated by the KMN (KNL1, MIS12 and NDC80) network connecting centromeres to microtubules on the dynamic plus end. The increase in outward pushing force coincided with the build-up of this complex where the NDC80 complex may guide microtubule-mediated forces [2]. Outward pushing forces could be further enhanced by multiple kinesins that have proven vital for spindle formation [26, 27]. A previously quantified balance between the actin network along the cell membrane and a build-up of hydrostatic pressure would again positively correlate to the extracellular force exertion we observed [18]. Force exertion carried by many MTs with forces in the order of 3-4 pN [28] per MT for elongating MTs from the two centrosomes contribute to the idea of cohesive outward pushing during mitosis as described in figure 5.5C and D. Furthermore, the most dynamic MTs can be found at the center of the mitotic spindle as well as at the cell edge [21]. These dynamics at the KMN network [3] at the metaphase plate and the actin network [18] at the cell membrane, respectively, correspond to the locations of force transmission in our model of a changing force balance throughout mitosis.

As the cell further proceeds into metaphase, kinetochore-based activation of the Spindle Assembly Checkpoint plays an important role. The Anaphase Promoting Complex (APC, also known as Cyclosome)

triggers further mitotic progression upon phosphorylation of KNL1 [3]. Biochemically these processes are regulated by MAD1/MAD2 complexes with CDC20 activating APC/C. Incorporation of the kinase Aurora B then plays an important role [5, 29]. A gradient in phosphorylation state has been directly observed as a function of distance from the metaphase-plate, regulated by tension [30]. Such a phosphorylation gradient would fit well with our notion of a force balance, since we observed a short outward force peak upon the transition from anaphase to telophase. That peak in force could be the final pull along the chromosomes that Aurora B needed to proceed. Outward pushing forces rapidly decreased after final seperation. In previous studies it became clear that intracellular forces seem crucial for proper progression through all of these mechanisms, but the force balance with the ECM was never directly quantified.

We propose that this mechanosensitive response depends on the build-up of spindle-mediated outward pushing. If outward pushing is not build up, progression through mitosis is stalled. This is confirmed by the observation that if outward pushing was not present, centrosomes moved apart and a tripolar spindle formed. Our new methodology allowed us to quantify this force balance that couples the mitotic machinery from the inside-out to the extracellular matrix. These mechanical features related to progression through the cell cycle aid in understanding the biophysical coupling through kinetochores and checkpoints. In future work, it will be interesting to further dissect the roles of specific molecular players and their effect on force progression through mitosis.

5.5 Supplemental figures

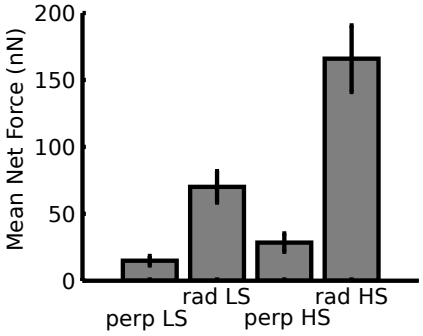

Figure S1
Radial forces compared to perpendicular forces. The mean of all measured net radial forces exerted during the various stages of mitosis are much larger as compared to the perpendicular components (bars indicate s.e.m.).

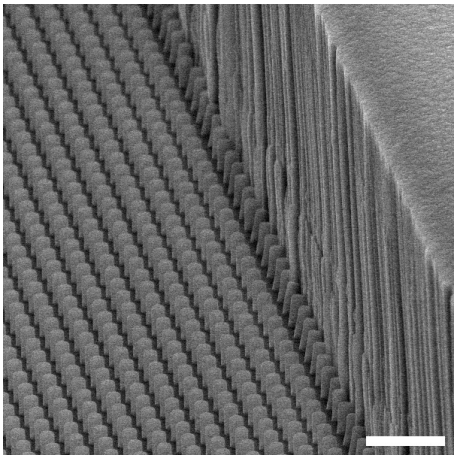

Figure S2
SEM image of spacer next to micropillar array. Micropillars (left) are shown adjacent to a 50 µm high spacer to enable the inversion of the arrays to be able to perform high-resolution imaging with a high-NA objective.

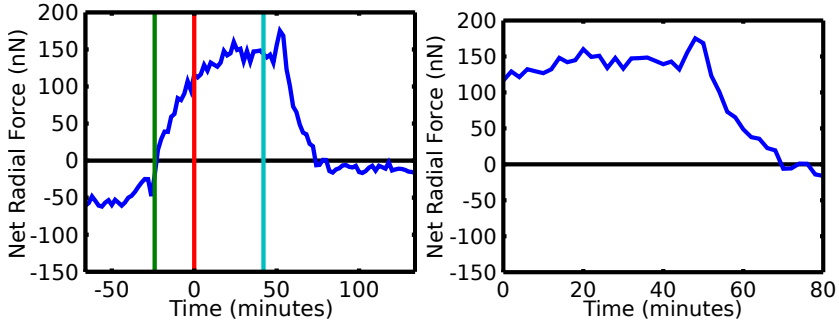

Figure S3

The peak in outward pushing just before cytokinesis. A peak in outward pushing forces is visible just before physical division at 50 minutes (time relative to metaphase).

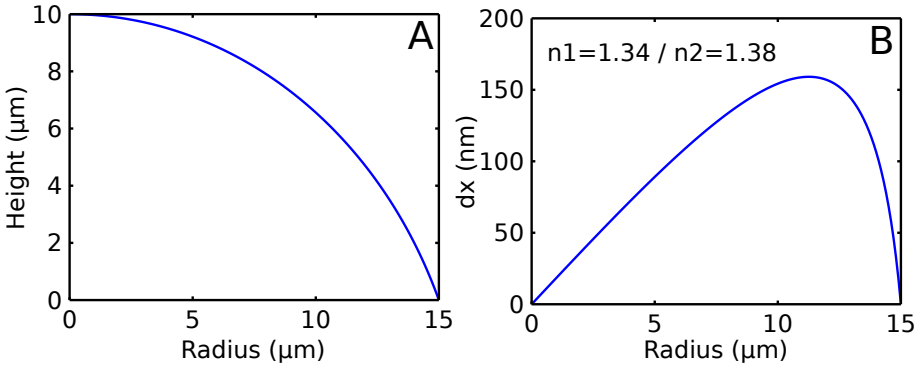

Figure S4

Lensing effect causes no more than apparent 150 nm deflection per pillar. (A) Curvature of the cell from 10 µm height along the radius of the cell. (B) When we assume a cell with refractive index of 1.38 everywhere around a medium with refractive index 1.34 this curve gives the apparent lensing effect along the radius.

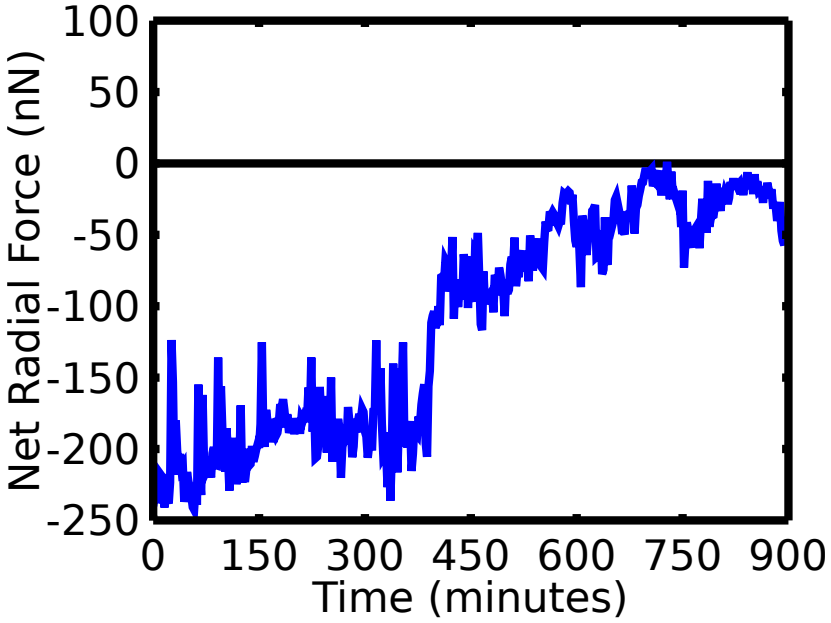

Figure S5

Build-up of outward forces does not occur when the mitotic spindle is disturbed. Inward pulling forces from interphase are released, but pushing forces are not observed. This curve of net outward force exertion corresponds to another cell where the mitotic spindle is again disturbed and a tripolar spindle forms. Until the end of the timelapse measurement (900 minutes) the cell is stuck in metaphase.

Bibliography

[1] Bruce Alberts et al. *Molecular Biology of the Cell*. 5th ed. Garland Science, 2008.

[2] Ajit P Joglekar, Kerry S Bloom, and ED Salmon. "Mechanisms of force generation by end-on kinetochore-microtubule attachments". In: *Curr. Opin. Cell. Biol.* 22.1 (2010), pp. 57–67.

[3] Emily A Foley and Tarun M Kapoor. "Microtubule attachment and spindle assembly checkpoint signalling at the kinetochore". In: *Nat. Rev. Mol. Cell Bio.* 14.1 (2013), pp. 25–37.

[4] Luying Jia, Soonjoung Kim, and Hongtao Yu. "Tracking spindle checkpoint signals from kinetochores to APC/C". In: *Trends Biochem. Sci.* 38.6 (2013), pp. 302–311.

[5] Michael A Lampson and Iain M Cheeseman. "Sensing centromere tension: Aurora B and the regulation of kinetochore function". In: *Trends Cell Biol.* 21.3 (2011), pp. 133–140.

[6] Wilma L Lingle, Kara Lukasiewicz, and Jeffrey L Salisbury. "Deregulation of the centrosome cycle and the origin of chromosomal instability in cancer". In: *Genome Instability in Cancer Development*. Springer, 2005, pp. 393–421.

[7] Juan-Manuel Schvartzman, Rocio Sotillo, and Robert Benezra. "Mitotic chromosomal instability and cancer: mouse modelling of the human disease". In: *Nat. Rev. Cancer* 10.2 (2010), pp. 102–115.

[8] Sachin Kotak and Pierre Gönczy. "Mechanisms of spindle positioning: cortical force generators in the limelight". In: *Curr. Opin. Cell. Biol.* 25.6 (2013), pp. 741–748.

[9] Nathan W Goehring and Anthony A Hyman. "Organelle growth control through limiting pools of cytoplasmic components". In: *Curr. Biol.* 22.9 (2012), R330–R339.

[10] R Bruce Nicklas. "Chromosome velocity during mitosis as a function of chromosome size and position". In: *J. Cell Biol.* 25.1 (1965), pp. 119–135.

[11] Kerry Bloom and Elaine Yeh. "Tension management in the kinetochore". In: *Curr. Biol.* 20.23 (2010), R1040–R1048.

[12] Florencia Rago and Iain M Cheeseman. "Review series: The functions and consequences of force at kinetochores." In: *J. Cell Biol.* 200.5 (2013), pp. 557–565.

[13] Jessica Ferraro-Gideon et al. "Measurements of forces produced by the mitotic spindle using optical tweezers". In: *Mol. Biol. Cell* 24.9 (2013), pp. 1375–1386.

[14] Xiaotong Li and R Bruce Nicklas. "Mitotic forces control a cell-cycle checkpoint". In: *Nature* 373.6515 (1995), pp. 630–632.

[15] R Bruce Nicklas. "How cells get the right chromosomes". In: *Science* 275.5300 (1997), pp. 632–637.

[16] Manuel Théry et al. "The extracellular matrix guides the orientation of the cell division axis". In: *Nat. Cell Bio.* 7.10 (2005), pp. 947–953.

[17] Jenny Fink et al. "External forces control mitotic spindle positioning." In: *Nat. Cell Bio.* 13.7 (2011), pp. 771–778.

[18] Martin P Stewart et al. "Hydrostatic pressure and the actomyosin cortex drive mitotic cell rounding." In: *Nature* 469.7329 (2011), pp. 226–230.

[19] Hedde van Hoorn et al. "The nanoscale architecture of force-bearing focal adhesions". In: *Nano Lett.* 14.8 (2014), pp. 4257–4262.

[20] Wonshik Choi et al. "Tomographic phase microscopy". In: *Nat. Methods* 4 (2007), pp. 717–719.

[21] Claire E Walczak, Shang Cai, and Alexey Khodjakov. "Mechanisms of chromosome behaviour during mitosis". In: *Nat. Rev. Mol. Cell Bio.* 11.2 (2010), pp. 91–102.

[22] Lea Trichet et al. "Evidence of a large-scale mechanosensing mechanism for cellular adaptation to substrate stiffness." In: *Proc. Natl. Acad. Sci. USA* 109.18 (2012), pp. 6933–6938.

[23] Sangyoon J Han et al. "Decoupling substrate stiffness, spread area, and micropost density: a close spatial relationship between traction forces and focal adhesions." In: *Biophys. J.* 103.4 (2012), pp. 640–648.

[24] Alexandre Saez et al. "Traction forces exerted by epithelial cell sheets." In: *J Phys.-Condens. Mat.* 22.19 (2010).

[25] Adrian R West et al. "Bioengineering the Lung: Molecules, Materials, Matrix, Morphology, and Mechanics: Development and characterization of a 3D multicell microtissue culture model of airway smooth muscle". In: *Am. J. Physiol.-Lung C.* 304.1 (2013), p. L4.

[26] TU Mayer et al. "Small molecule inhibitor of mitotic spindle bipolarity identified in a phenotype-based screen." In: *Science* 286.5441 (1999), pp. 971–974.

[27] Amity L Manning et al. "The kinesin-13 proteins Kif2a, Kif2b, and Kif2c/MCAK have distinct roles during mitosis in human cells". In: *Mol. Biol. Cell* 18.8 (2007), pp. 2970–2979.

[28] Marileen Dogterom and Bernard Yurke. "Measurement of the force-velocity relation for growing microtubules". In: *Science* 278.5339 (1997), pp. 856–860.

[29] Enxiu Wang, Edward R Ballister, and Michael A Lampson. "Aurora B dynamics at centromeres create a diffusion-based phosphorylation gradient". In: *J. Cell Biol.* 194.4 (2011), pp. 539–549.

[30] Brian G Fuller et al. "Midzone activation of aurora B in anaphase produces an intracellular phosphorylation gradient". In: *Nature* 453.7198 (2008), pp. 1132–1136.

Summary

Cellular forces - adhering, shaping, sensing and dividing

A cell takes many shapes and sizes in the wide variety of functions it performs. Cellular function is often directly linked to an environment that is actively deformed. In many other cases, cellular function relies on the cell's ability to deform and exert forces on its environment. Endothelial cells, for instance, are deformed when blood is pumped through the vasculature and its flow exerts an outward pressure onto these cells that line the inside of blood vessels. As muscle cells contract, they need to exert a physical force from the inside to the outside of the cell to perform their function. While muscle cells work in a multi-cellular sarcomeric unit, the ability to exert forces for individual cells is also vital. Neutrophils, for instance, need to adhere to the endothelium to exit the blood and migrate to an inflammation site. After this physical attachment as a primary immune response, they need to actively deform their membrane to engulf bacteria. Similarly, many other cell types rely on such deformations and forces for their function. Cell mechanics describes how cellular function relates to physical deformations and forces. And as such, forces, deformations and stiffnesses are ubiquitous in the functioning of cells.

Cell mechanics can roughly be divided into two types of processes. A cell can undergo force or deformation (termed outside-in, probed by active techniques) and have a biological response to that action. On the other hand, cells themselves often exert forces on their extracellular environment (often denoted by extracellular matrix, ECM) and as such push or pull on their environment (termed inside-out, probed by passive techniques). These mechanical processes take place on a stiffness that varies over five orders of magnitude throughout a (human) body.

Both inside-out and outside-in coupling between cell mechanics and biology is thus important for a multitude of biological functions. Furthermore, biological behavior changes depending on stiffness. In this thesis, I focus on understanding how cells deform their environment in relation to adhesion, cell shape, biological-mechanical adaptation through the protein p130Cas and cell division.

Chapter 2 demonstrates a new approach to probing cell mechanics. While measuring how a cell deforms its environment, high-resolution optical microscopy is crucial to understanding fundamental processes in cell mechanics. For any high-resolution optical microscopy, the use of a high-NA objective with a short working distance is essential. In particular, to enable super-resolution microscopy, single molecules need to be detected with as many photons as possible. Inverted micropillar arrays flanked by 50 μm high spacers placed micropillars and cells within the short working distance. With inverted micropillars I showed the ability to perform both live- and fixed cell measurements that quantify extracellular force exertion with simultaneous imaging of the actin cytoskeleton and focal adhesions (FAs). Further, I demonstrated the ability to perform super-resolution imaging by quantification of the nanostructure of force-bearing FAs. I showed that the stress accumulation was approximately one order of magnitude higher with the resolved sub-diffraction limited structure as compared to previous measurements.

In further experiments, I investigated specific biological processes. **Chapter 3** describes live-cell experiments of fibroblasts that express LifeAct-mCherry, a fluorophore that attaches to the actin cytoskeleton. Through direct correlation, I observed that local force exertion directs along the orientation of the actin cytoskeleton, while I also observed circular curvature along the actin cortex. *Active Solid Theory* was developed to describe a homogeneous contractile solid and I further expanded the concept of a local mechanical equilibrium along the cell cortex. I included the effect of cytoskeletal orientation attached to the circular cortex and found that this orientation influenced curvature and force exertion at the extremities of the circular arcs. The theory of a contractile solid expanded by force guidance through an oriented actin cytoskeleton corresponded well to measurements of cortex curvature and force exertion.

In **Chapter 4**, I report on the mechanosensing properties of the FA scaffolding protein p130Cas. It was previously reported that stretching of p130Cas enhances phosphorylation and influences cell migration and actin dynamics. It was never described, however, whether the mechanosensory function of p130Cas would be apparent in physiologically relevant stiffnesses nor what its effect on force exertion dynamics would be. I performed experiments on PolyAcrylamide (PA) gels and micropillars, both of varying extracellular stiffness, with cells that either expressed endogenous levels of p130Cas (Cas WT), a double mutant that did not localize to FAs (Cas ΔSH3/ΔCCH) or lacked p130Cas (Cas -/-). It became apparent that p130Cas indeed effected FA formation and localized to FAs only when the global extracellular stiffness was larger than 47.2 kPa. I further characterized the effect of stiffness-dependent localization to FAs and found that p130Cas increases extracellular force exertion and decreases the rate of force exertion. Quantification of this mechanical-biological-mechanical coupling provided insights in the function of p130Cas as a mechanosensor, which provided further clues into the physics of cancer.

Chapter 5 shows how the extracellular environment is deformed throughout cell division. In previous work, extracellular force exertion was quantified in interphase, while I observed massive cellular reorganization and a build-up of outward pushing forces through mitosis. I changed the extracellular stiffness and observed that - similar to what was observed for inward pulling forces - outward pushing increased with increasing stiffness. Radial forces relative to the cell center were predominant and amounted to 100-150 nN and 400-500 nN on micropillar arrays with a bending stiffness of 16.7 nN/μm and 70.9 nN/μm, respectively. Pulling forces towards the nucleus were released before the start of prophase and outward pushing successively increased upon chromosome alignment in metaphase. After a characteristic plateau, a peak increase in outward pushing forces coincided with telophase, after which the daughter cells pinched off and proceeded into interphase. Interestingly, outward pushing proved essential for bipolar spindle formation and ultimate division into two cells. Such a force balance likely has a direct relation to kinetochore checkpoints that can be bypassed when force exertion is absent. Furthermore, the force exertion hallmarks preceded phenotypic observations, indicating a vital role for extracellular force exertion throughout multiple stages in cell division.

Overall, in this thesis I have shown that cell mechanics plays an important role in multiple biological processes. The interplay between deformation and force exertion that is guided through extracellular stiffness impacts adhesions, cytoskeletal orientation, p130Cas localization and cell division.

Samenvatting

Cellulaire krachten - aanhechten, vormen, voelen en delen

Een cel neemt verschillende vormen en groottes aan in de grote verscheidenheid aan functies die het volbrengt. De functie van een cel is vaak direct gerelateerd aan een omgeving waarin de cel actief vervormd wordt. In veel andere gevallen hangt de functie van een cel af van de mate waarin een cel een kracht kan uitoefenen op zijn omgeving of deze kan vervormen. Endotheelcellen, bijvoorbeeld, worden vervormd als bloed door het vaatstelsel wordt gepompt en de stroming een uitwaartse druk uitoefent op de celwand aan de binnenkant van bloedvaten. Wanneer spiercellen samentrekken moeten zij ook een fysieke kracht uitoefenen van binnen in de cel naar buiten om hun functie te vervullen. Terwijl spiercellen in een multicellulaire sarcomeerstructuur functioneren is de individuele krachuitoefening van een enkele cel ook van belang. Neutrofielen moeten zich bijvoorbeeld aan endotheelcellen vastgrijpen om naar een ontstoken gebied te kunnen migreren. Na deze fysieke aanhechting als eerste imuunrespons, moeten ze vervolgens hun membraan vervormen om bacteriën te kunnen vernietigen. Op een gelijksoortige manier hangt de functie van veel andere celtypes af van vervormingen en het uitoefenen van krachten. Celmechanica omschrijft hoe cellulaire functie samenhangt met fysieke vervorming en kracht. Zodoende zijn krachten en vervormingen alomtegenwoordig in het functioneren van cellen.

Celmechanica kan grofweg in twee soorten processen worden onderverdeeld. Een cel kan een kracht of vervorming ondergaan ("outside-in" genoemd, gemeten met actieve technieken) en daar een biologische reactie op geven. Aan de andere kant oefenen cellen zelf vaak krachten uit op hun extracellulaire omgeving (ook wel "extracellular matrix", ECM, genoemd) en duwen of trekken daarmee aan hun omgeving ("inside-out"

genoemd, gemeten met passieve technieken). Deze mechanische processen vinden plaats over een stijfheid die vijf ordes van grootte varieert in het (menselijk) lichaam. Zowel "inside-out" als "outside-in" koppeling tussen celmechanica en biologie is dus belangrijk voor een groot aantal biologische functies. Bovendien hangt veel biologisch gedrag af van stijfheid van het ECM. In dit proefschrift heb ik me gericht op hoe cellen hun omgeving vervormen ten opzichte van hun aanhechting, vorm, mechanisch-biologische aanpassing door het eiwit p130Cas en celdeling.

Hoofdstuk 2 toont een nieuwe aanpak in het onderzoeken van celmechanica. Tegelijkertijd met een meting van hoe een cel zijn omgeving vervormt is hoge-resolutie optische microscopie cruciaal om de fundamentele processen in celmechanica te begrijpen. Voor iedere vorm van hoge-resolutie microscopie is het gebruik van een hoog-NA objectief met een korte werkafstand essentieel. In het bijzonder, om super-resolutie microscopie mogelijk te maken, moeten enkele moleculen met zoveel mogelijk fotonen gedetecteerd worden. Omgekeerde patronen van micropilaren met 50 µm hoge afstandshouders plaatsten de pilaren en cellen binnen de korte werkafstand. Met deze geïnverteerde micropilaren heb ik aangetoond dat het mogelijk is om van zowel levende- als gefixeerde cellen extracellulaire krachten te meten en gelijktijdig het actinecytoskelet en focal adhesions (FAs) in beeld te brengen. Bovendien demonstreerde ik de mogelijkheid om super-resolutie microscopie uit te voeren door de nanostructuur van krachtdragende FAs te kwantificeren. Ik liet zien dat de ophoping van stress ongeveer één orde grootte hoger was in de structuur onder de diffractielimiet in vergelijking met eerdere metingen.

In verdere experimenten onderzocht ik specifieke biologische processen. **Hoofdstuk 3** omschrijft experimenten op levende fibroblastcellen die LifeAct-mCherry tot expressie brengen, een fluorescerend eiwit dat hecht aan het actinecytoskelet. Door een directe correlatie observeerde ik dat de lokale uitoefening van krachten correleerde aan het actinecytoskelet, terwijl ik ook een cirkelvormige actinewand aan de celcortex heb waargenomen. *Active Solid Theory* werd ontwikkeld om een homogeen samentrekkende vaste stof te omschrijven en ik heb dit concept met een lokaal mechanisch equilibrium langs de celcortex verder ontwikkeld. Ik heb het effect van orientatie van het cytoskelet dat zich hecht aan de celcortex uitgewerkt en gezien dat deze orientatie inderdaad een invloed heeft op de kromming en de krachtuitoefening aan de uiteindes van deze bogen. De theorie van een samentrekkende vaste stof

is zodoende uitgebreid met geleiding van krachten door het actinecytoskelet en komt goed overeen met metingen van de boogkromming en krachtuitoefening.

In **Hoofdstuk 4** weid ik uit over de mechanogevoelige eigenschappen van het FA eiwit p130Cas. Het was eerder al gemeld dat uitrekking van p130Cas fosforylering kan verhogen en een invloed heeft op celmigratie en de dynamica van actine. Het was echter nog nooit beschreven of de mechanogevoelige functie van p130Cas ook waarneembaar zou zijn in een fysiologisch relevant stijfheidsgebied of wat het effect op de uitoefening van krachten zou zijn. Ik heb experimenten uitgevoerd op PolyAcrylamide (PA) gels en micropilaren, beide met gevarieerde extracellulaire stijfheid, met cellen die endogene niveaus van p130Cas (Cas WT), een dubbele mutant die niet naar FAs lokaliseert (Cas ΔSH3/ΔCCH) of een compleet gebrek aan p130Cas (Cas -/-) expressie hadden. Het werd duidelijk dat p130Cas inderdaad FA vorming veranderde en alleen werd opgenomen in FAs als de globale extracellulaire stijfheid hoger dan 47.2 kPa was. Verder heb ik de stijfheidsafhankelijke lokalisatie naar FAs gekarakteriseerd en ontdekt dat de extracellulaire kracht groter en de snelheid van krachtuitoefening lager werd bij lokalisatie van p130Cas. Kwantificatie van deze mechanisch-biologisch-mechanische koppeling toont de functie van p130Cas als mechanosensor, wat belangrijke inzichten geeft in de fysica van kanker.

Hoofdstuk 5 toont hoe de extracellulaire omgeving vervormd wordt gedurende celdeling. In eerder werk is de extracellulaire krachtuitoefening gekwantificeerd in interfase, terwijl ik grootschalige reorganisatie in de cel en een opbouw van uitwaartsgerichte duwkrachten observeerde gedurende mitose. Ik veranderde de extracellulaire stijfheid en observeerde dat - gelijksoortig aan wat geobserveerd was voor inwaartse krachten - uitwaarts duwen toenam met toenemende stijfheid. Radiële krachten ten opzichte van het middelpunt van de cel waren overheersend en bedroegen in totaal 100-150 nN en 400-500 nN op micropilaren met buigingsstijfheden van respectievelijk 16.7 nN/μm en 70.9 nN/μm. Trekkrachten richting de celkern werden losgelaten voor de start van profase en uitwaartse duwkrachten namen toe terwijl chromosomen zich op een lijn plaatsten in metafase. Na een karakteristiek plateau werd een piek in de uitwaartse duwkrachten geobserveerd in telofase, waarna de dochtercellen werden afgeknepen en interfase in gingen. Het was verwonderlijk om te zien dat uitwaartse krachten noodzakelijk waren voor de vorm-

ing van een bipolaire spindel en uiteindelijk deling in twee cellen. Een dergelijke krachtbalans heeft waarschijnlijk een directe relatie met oriëntatiepunten in de kinetochoren die overgeslagen kunnen worden als de kracht niet aanwezig is. Bovendien was de karakteristieke krachtuitoefening telkens voorafgaand aan de fenotypische waarnemingen, hetgeen indicatief is voor de essentiële rol van extracellulaire krachtuitoefening gedurende opeenvolgende stadia in celdeling.

Samenvattend heb ik in dit proefschrift laten zien dat celmechanica een belangrijke rol speelt in verscheidene biologische processen. De wisselwerking tussen vervorming en krachtuitoefening die door extracellulaire krachten wordt geleid heeft een invloed op aanhechting, oriëntatie van het cytoskelet, lokalisatie van p130Cas en celdeling.

Publications

1. "A closer look at cellular force exertion - inversion improves resolution"
   H. van Hoorn, T. Schmidt
   in preparation

2. "Outward force exertion is crucial for mitosis"
   H. van Hoorn, M. de Valois, C. Backendorf, T. Schmidt
   in preparation

3. "Orientation of the actin cytoskeleton determines cell shape and directed force exertion"
   H. van Hoorn, W. Pomp, T. Schmidt
   in preparation

4. "GFAP isoforms control intermediate filament network dynamics, cell morphology, and focal adhesions"
   M. Moeton, O.M.J.A. Stassen, H. van Hoorn, T. Schmidt, J.A. Sluijs, V. van der Meer, L.J. Kluivers, E.A.J. Reits, M.E. van Strien, E.M. Hol
   in preparation

5. "p130Cas is a mechanosensor that modulates force exertion at focal adhesions"
   H. van Hoorn[1], D.M. Donato[1], H.E. Balcioglu, E.H. Danen, T. Schmidt
   in preparation

[1] these authors contributed equally to this work

6. "Distinct cellular mechanotransduction through α5β1 and αvβ3 integrins"
   H.E. Balcioglu, H. van Hoorn, D.M. Donato, T. Schmidt, E.H. Danen
   under review at Journal of Cell Science

7. "The nanoscale architecture of force-bearing focal adhesions"
   H. van Hoorn, R. Harkes, E.M. Spiesz, C. Storm, D. van Noort, B. Ladoux, T. Schmidt
   Nano Lett., **14** (8), 4257-4262 (2014)

8. "De uitgever aan het woord 2010: de trendmonitor van de uitgeefbranche"
   T. Huibers, K. Voermans, H. van Hoorn, J. van Raak, E. Oltmans, M. de Gier
   Book published by Thaesis, Utrecht (2010)

9. "The Influence of cell shape anisotropy on the tensile behavior of open cell aluminum foam "
   E. Amsterdam, H. van Hoorn, J.T.M. de Hosson, P.R. Onck
   Adv. Eng. Mat., **10** (9), 877-881 (2008)

Curriculum vitae

Hedde van Hoorn was born on December 21, 1983 in Marum, the Netherlands. He studied Applied Physics at the University of Groningen from 2002 to 2008, specializing in Materials Science. He joined the group of Prof. Jeff de Hosson for both his bachelor's and master's degree. His bachelor's research was focussed on the material properties of Sandvik Nanoflex in collaboration with Philips Research in Drachten. For his master's research he investigated the effect of anisotropy in open-cell aluminium foam structures. His final research internship during his master's degree was in Biological Engineering in the group of Prof. Subra Suresh at the Massachusetts Institute of Technology. There, he investigated the effect of malaria infection on the stiffness of erythrocytes using atomic force microscopy.

After his graduation, Hedde was a strategy consultant in Media and Technology for Thaesis from 2008 to 2010, where he advised companies and published on his research on trends and developments in the publishing industry. In July 2010 he returned to science when he joined the Physics of Life Processes group at Leiden University as a PhD student. Under the guidance of Prof. Thomas Schmidt he worked on the development of new techniques to probe cell mechanics and apply high-resolution imaging to a range of biological questions. During his 4 years in Leiden, Hedde presented his work at numerous conferences in the Netherlands, Singapore, France, Austria and the USA. He assisted with optics experiments in the course "Experimental Physics", taught exercise classes in "Classical Mechanics" and guided 1 bachelor and 3 master students.

In October 2014, Hedde will start a postdoctoral appointment in the group of Prof. Davide Ianuzzi at VU University Amsterdam.

Acknowledgements

The road towards a PhD is a significant fraction of life, and the last four years have been valuable to me and well spent. At "Physics of Life Processes" the atmosphere was always one of healthy, scientific curiosity - the way a research group should be. It has been a pleasure and honor to be able to work in this warm environment where a helping hand was always present and extended. Numerous scientific and social explorations have enriched me as a person and an aspiring scientist. The research presented in this thesis was always a collaborative effort in that spirit and for that I am grateful to many people.
I would like to thank a few people in particular:

Thank you Thomas Schmidt for giving me the opportunity to learn and explore in the wonderful field of biophysics. Sylvie Olthuis; thanks for the assistance in cell culture and biochemistry and thanks Marcel Hesselberth and Thanasis Giannitsis for support with SEM, deposition, etching and lithography. Thanks for all other things technical to John van Egmond, Fred Kranenburg, Raymond Koehler, Arjen Geluk, Gert Koning and Kees van Oosten at the mechanical department. And thanks Yvonne Kerkhof, for always helping with all matters administrative.

Many thanks to the FvL group with in particular Rolf, Dominique, Meng, Lena and Wim for both a nice joint research effort and social life. No research can be done without wonderful colleagues and friends to participate in discussions, coffee breaks and borrels: Anna, Susanne, Freek, Laurent, Paige, Thijn, Ruth, Bram, Fan-Tso, John, Wietske, Sara, Olga, Jeremie, Doris, Artur, Kirsten and Thomas III: thank you! And of course, a special thanks to my former students Rianca, Wim, Martin and Donato for their hard work.

Many collaborations outside the group have greatly enriched the past four years. Benoit Ladoux, Danny van Noort, Man Chun Leong and Sri

Ram Krishna Vedula; thanks for introducing me to the world of micropillars in Singapore. Erik Danen and Emrah Balcioglu, who were basically adopted to FvL; thanks for all your mechanobio-input. Kees Storm and Ewa Spiesz, thanks for your theoretical insights and simulations. Claude Backendorf; thanks for your ideas and input on cell division forces. Christine Mummery, Robert Passier and Marcelo Ribeiro; thanks for your keen interest in forces and cardiomyocytes. Elly Hol and Oscar Stassen; thanks for bringing us into the world of the brain, Astrocytes and GFAP. And of course many thanks to the rest of the Mechanobiology NL consortium for stimulating meetings and discussions.

Last but not least I would like to thank my family and friends who have always been there and have evolved as I have during my PhD track: Michiel, Ulka, Rogier, Anne-Laura, David, Eliza, Anais, Matthias, Andrija, Marika, Tom (praeses h.t.), Mark, Rudy, Peynacker, Sander, Pelle, Jasper, Jakko. This thesis is dedicated to my family: Bart, Melissa, Inez and Peter. And to the only one who combines the roles of friend, family and the love of my life: Vivian.